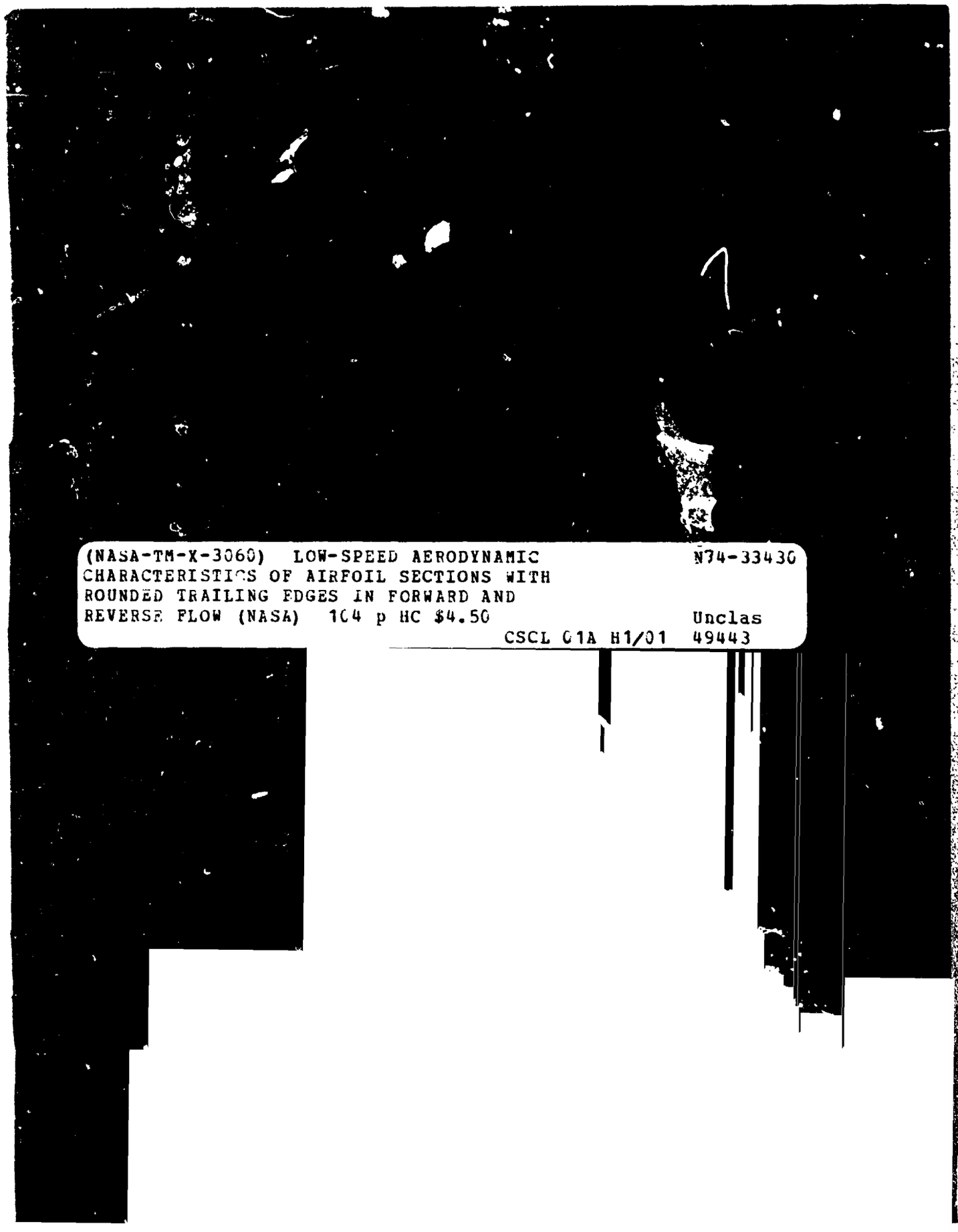

1. Report No.	2. Government Accession No.	3. Recipient's Catalog No.
NASA TM X-3060		

4. Title and Subtitle	5. Report Date
LOW-SPEED AERODYNAMIC CHARACTERISTICS OF AIRFOIL SECTIONS WITH ROUNDED TRAILING EDGES IN FORWARD AND REVERSE FLOW	September 1974
	6. Performing Organization Code
7. Author(s)	8. Performing Organization Report No.
William D. Beasley and Robert J. McGhee	L-9327
	10. Work Unit No.
9. Performing Organization Name and Address	760-17-01-11
NASA Langley Research Center Hampton, Va. 23665	11. Contract or Grant No.
	13. Type of Report and Period Covered
12. Sponsoring Agency Name and Address	Technical Memorandum
National Aeronautics and Space Administration Washington, D.C. 20546	14. Sponsoring Agency Code

15. Supplementary Notes

16. Abstract

Low-speed wind-tunnel tests have been conducted to determine the two-dimensional aerodynamic characteristics of 6-, 12-, and 18-percent-thick airfoil sections with rounded trailing edges in both forward and reverse flow. The shapes incorporated camber with both the leading and trailing edges rounded to provide reasonable aerodynamic performance with either edge directed toward the free-stream flow. The tests were conducted with the airfoils in both normal and reverse orientations relative to the free stream. The Mach number was varied from 0.16 to 0.36 and the angle of attack was varied from -10° to 24°. Reynolds number, based on the airfoil chord, was varied from about 1.0×10^6 to 12.0×10^6.

17. Key Words (Suggested by Author(s))	18. Distribution Statement
Rounded trailing-edge airfoils Rotorcraft airfoils Low-speed aerodynamics Reynolds number effect Forward and reverse flow	Unclassified – Unlimited STAR Category 01

19. Security Classif. (of this report)	20. Security Classif. (of this page)	21. No. of Pages	22. Price*
Unclassified	Unclassified	102	$4.50

*For sale by the National Technical Information Service, Springfield, Virginia 22151

LOW-SPEED AERODYNAMIC CHARACTERISTICS OF AIRFOIL SECTIONS WITH ROUNDED TRAILING EDGES IN FORWARD AND REVERSE FLOW

By William D. Beasley and Robert J. McGhee
Langley Research Center

SUMMARY

An investigation was conducted in the Langley low-turbulence pressure tunnel to determine the low-speed two-dimensional characteristics of 6-, 12-, and 18-percent-thick airfoil sections (cambered with both leading and trailing edges rounded). Tests in both forward and reverse flow were conducted with each section oriented in the wind tunnel with the leading or trailing edge directed toward the free stream. The data were obtained over a Mach number range from 0.16 to 0.36 and an angle-of-attack range from -10° to 24°. Reynolds number, based on the airfoil chord, was varied from about 1.0×10^6 to 12.0×10^6.

Each airfoil section exhibited nonlinear variations in section lift and pitching-moment coefficients with angle of attack in forward and reverse flow at low Reynolds numbers. Increasing the Reynolds number or forcing boundary-layer transition by applying roughness near the leading edge essentially removed these nonlinear variations. These results are attributed to delayed flow separation on the lower surface near the rounded trailing edge. Boundary-layer flow separation was present near the rounded trailing edges at all test conditions. Thus, the wake survey measurements used to determine the section profile drag resulted in erratic drag data, particularly for the thicker sections in the reversed orientation. The largest maximum section lift coefficient in the normal orientation was about 1.8 for the 12-percent-thick airfoil. In the reverse orientation, the 18-percent-thick airfoil produced the largest maximum section lift coefficient of about 1.5.

INTRODUCTION

Historically, helicopter rotor blades have been comprised of conventional symmetrical airfoil sections, for example NACA 0012, which have shown generally good rotor performance. However, helicopters operate with portions of the rotor disk subjected to both forward and reverse flow fields. The extent of the reverse flow, which occurs over the retreating portion of the rotor disk, is a function of vehicle forward flight speed and

rotor rotational speed. In general, helicopter rotor sections operate within these reverse regions producing negative lift, which consequently contributes to limiting performance in high-speed forward flight.

One approach to overcome the penalities incurred with reverse flows over a conventional rotor is to design a rotor that can effectiveiy perform in both forward and reverse flow fields. Unusual airfoil shapes may be required for such rotors; consequently, two-dimensional aerodynamic data would be desirable over a large speed range on such shapes.

Exploratory low-speed wind-tunnel tests have been conducted to examine the basic behavior and aerodynamic trends on three cambered airfoil sections with rounded trailing edges and ratios of maximum thickness to chord of 6, 12, and 18 percent. All three airfoils were tested with both the leading and trailing edges alternately directed toward the free-stream flow; thus, both conventional aerodynamic characteristics and the characteristics of the airfoil in steady reversed flow were obtained. The investigation was performed in the Langley low-turbulence pressure tunnel over a Mach number range from 0.16 to 0.36 (test Mach number was constrained by the operational limits of the facility) for an angle-of-attack range from about -10° to 24°. The Reynolds number, based on airfoil chord, varied from 1.0×10^6 to 12.0×10^6.

SYMBOLS

Values are given in both SI and U.S. Customary Units. The measurements and calculations were made in U.S. Customary Units.

C_p pressure coefficient, $\frac{p_\ell - p_\infty}{q_\infty}$

c airfoil chord, 45.72 cm (18 in.)

c_c section chord-force coefficient, $\int_{\substack{\text{forward} \\ (t/c)_{max}}} C_p \, d\left(\frac{z}{c}\right) - \int_{\substack{\text{aft} \\ (t/c)_{max}}} C_p \, d\left(\frac{z}{c}\right)$

c_d section profile-drag coefficient determined from wake measurements, $\int_{\text{wake}} c_d' \, d\left(\frac{h}{c}\right)$

c_d' point drag coefficient, $2\left(\frac{\rho_1}{\rho_2}\right)^{1/2}\left(\frac{q_1}{q_\infty}\right)^{1/2}\left[\left(\frac{\rho_2}{\rho_\infty}\right)^{1/2} - \left(\frac{q_2}{q_\infty}\right)^{1/2}\right]$

c_ℓ section lift coefficient, $c_n \cos \alpha - c_c \sin \alpha$

c_m section pitching-moment coefficient about quarter-chord point: referenced from point on model that serves as leading edge,

$$\int_{l.s.} C_p\left(0.25 - \frac{x}{c}\right)d\left(\frac{x}{c}\right) - \int_{u.s.} C_p\left(0.25 - \frac{x}{c}\right)d\left(\frac{x}{c}\right)$$

c_n section normal-force coefficient, $\int_{l.s.} C_p\, d\left(\frac{x}{c}\right) - \int_{u.s.} C_p\, d\left(\frac{x}{c}\right)$

h vertical distance in wake profile from top total-pressure tube, cm (in.)

M free-stream Mach number

p static pressure, N/m^2 (lb/ft^2)

Δp_t total-pressure loss in wake, N/m^2 (lb/ft^2)

q dynamic pressure, N/m^2 (lb/ft^2)

R Reynolds number based on free-stream conditions and airfoil chord

t airfoil maximum thickness, cm (in.)

x airfoil abcissa, cm (in.)

z airfoil ordinate, cm (in.)

z_c mean-line ordinate, cm (in.)

α geometric angle of attack, deg

ρ density, kg/m^3 ($slugs/ft^3$)

Subscripts:

ℓ local point on airfoil

max maximum

∞ free-stream conditions

t mean thickness

1 tunnel station 1.65c downstream of model

2 tunnel station downstream of model where static pressure equals free-stream static pressure and total pressure assumed equal to total pressure at station 1

Abbreviations:

l.s. lower surface

u.s. upper surface

L.E. leading edge

T.E. trailing edge

APPARATUS AND PROCEDURE

Wind Tunnel and Model Support

The Langley low-turbulence pressure tunnel (ref. 1) is a closed-throat single return tunnel which is normally operated at stagnation pressures from 101.3 to 1013 kN/m^2 (1 to 10 atm) for which the maximum Mach numbers of the empty test section vary from 0.46 to 0.23. The test section is 91.44 cm (3 ft) wide by 228.6 cm (7.5 ft) high. Circular end plates provide attachments for the two-dimensional models. The end plates are 101.6 cm (40 in.) in diameter and are flush with the tunnel wall. They are hydraulically rotated to provide for model angle-of-attack changes. The models were mounted so that the center of rotation of the circular plates was at 0.33c on the model chord line. The air gaps at the tunnel walls were sealed with flexible sliding metal seals.

Models

The airfoil coordinates for the three airfoils are presented in table I. The 12- and 18-percent-thick models were machined from aluminum and the 6-percent-thick model was machined from steel to minimize deflections near maximum lift conditions. All models were polished to provide smooth aerodynamic surfaces. The models had a 45.72 cm (18 in.) chord and completely spanned the width of the tunnel. Figure 1 shows a sketch of each airfoil section shape and also illustrates the thickness and camber distributions. The maximum mean camber of the 6-, 12-, and 18-percent-thick models was located at 0.40c and was approximately 1.3-, 2.5-, and 3.7-percent chord as shown in figure 1(b).

Figure 2 is a photograph of the 18-percent-thick model mounted in the wind tunnel. The metal seals shown in the photograph have been partially disassembled. The models were equipped with both upper and lower surface orifices which were drilled perpendicular to the surface with a drill diameter of 0.0813 cm (0.032 in.) and were located at the chord stations indicated in tables II to IV.

Wake Survey Rake

A fixed wake survey rake (fig. 3) was mounted on the tunnel sidewall and located 1.65c aft of the trailing edge of the airfoil model. The wake rake utilized 91 total-pressure tubes and 5 static-pressure tubes 0.1524 cm (0.060 in.) in diameter. The total-pressure tubes were flattened to 0.1016 cm (0.040 in.) for a distance of 0.61 cm (0.24 in.) from the tips of the tubes in order to minimize total-pressure tube displacement effects. The rake static tubes had four flush orifices drilled 90° apart and located eight tube diameters from the tip of the tube and in the plane of the total-pressure tubes.

Instrumentation

Measurements of the static pressures on the airfoil surfaces, tunnel sidewalls, and the wake rake pressures were made by an automatic pressure-scanning system utilizing variable capacitance-type precision transducers. Basic tunnel pressures were measured with precision quartz manometers. Angle of attack was measured with a calibrated potentiometer with a pinion gear and rack attached to the circular plates. Data were obtained by a high-speed data acquisition system and recorded on magnetic tape.

TEST AND METHODS

The airfoil models were tested at Mach numbers from 0.16 to 0.36. Reynolds number, based on the airfoil chord, was varied from about 1.0×10^6 to 12.0×10^6, primarily by varying the tunnel stagnation pressure. The geometric angle of attack varied from about -10° to 24°. The airfoils were tested smooth (natural boundary-layer transition); however, for several test conditions, boundary-layer transition strips sized according to reference 2 (nominal grit diameter of 0.0211 cm (0.0083 in.) at $R = 2.5 \times 10^6$) were installed on both upper and lower surfaces. The transition strips were 0.25 cm (0.10 in.) wide. The grit was sparsely spaced and attached to the surface with lacquer. For several test runs, tufts were attached to the models and to the adjacent tunnel walls with plastic tape in order to investigate the stall patterns and to observe any regions of local flow separation.

The static-pressure measurements at the airfoil surface were reduced to standard pressure coefficients and machine integrated to obtain section normal-force and

chord-force coefficients and section pitching-moment coefficients about the quarter-chord point (referenced from the point on the model that serves as the leading edge).

Previous tests with the existing wake rake have indicated that the static pressures measured by the rake static-pressure probes were influenced by the rake body and flow angularities resulting from airfoil-generated downwash. Therefore, the static pressures used to compute the section profile-drag coefficients were measured at three sidewall static-pressure orifices. The orifices were alined in a vertical row at the same longitudinal station as the rake total-pressure tubes. One static-pressure orifice was located on the vertical center line of the tunnel and the other orifices were 0.44c above and below the vertical center line. The section profile-drag coefficient was computed by the method of reference 3 and a typical wake profile is shown in figure 4 for the 12-percent-thick airfoil section.

An estimate of the standard low-speed wind-tunnel boundary corrections, as calculated by the method of reference 4, indicated that these corrections are within the accuracy of the data and have not been applied.

PRESENTATION OF RESULTS

The results of this investigation have been reduced to coefficient form and are presented in the following figures:

DISCUSSION OF RESULTS

6-Percent-Thick Airfoil Section – Leading Edge Forward

Reynolds number effect.- The effect of Reynolds number on the aerodynamic characteristics is shown in figure 5 for the 6-percent-thick section with the leading edge forward (forward flow). Increasing the Reynolds number resulted in a decrease in the s-shape nonlinear nature of the lift curve and an increase in maximum lift coefficient (figs. 5(a) and 11). In the low Reynolds number range, the lift coefficient data indicate nonlinear variation with angle of attack which becomes more pronounced as the airfoil thickness is

increased, as discussed later. Maximum lift coefficients increased from only about 1.0 to 1.10 as the Reynolds number was increased from about 1.0×10^6 to 12.0×10^6 (fig. 11). Figure 5(a) indicates that the stall characteristics depend on the Reynolds number. In the low Reynolds number range, the stall characteristics are gradual; however, in the higher Reynolds number range, the airfoil section reaches maximum lift coefficient and then levels out with increasing angle of attack (fig. 5(a)). Tuft data obtained at $R = 7.7 \times 10^6$ indicate that the stall characteristics are of the typical thin airfoil types; that is, the stall is characterized by flow separation from the leading edge with subsequent reattachment further downstream. With increase in angle of attack, the point of reattachment moves progressively toward the trailing edge. Stall occurs when the flow reattachment point occurs approximately at the trailing edge.

Increasing the Reynolds number had two effects on the pitching-moment data as indicated by figure 5(a). At the highest test Reynolds number, the nonlinear variation of c_m with α is eliminated up to $\alpha = 12^\circ$ and the slope of the pitching-moment curve is positive.

The profile-drag data (fig. 5(b)) indicate considerable scatter and are the results of drag measurements in an unsteady wake that exists behind an airfoil where flow separation is present. Increasing the Reynolds number eliminated the laminar drag bucket that occurred at the low Reynolds number and increased the range of lift coefficient over which low values of c_d occurred.

Typical pressure distributions for this airfoil at $R = 2.50 \times 10^6$ are shown in figure 12. Approximately flat pressure distribution over the airfoil chord are shown near $\alpha = 0^\circ$. At $\alpha = 8^\circ$, most of the airfoil loading is distributed over the forward region of the airfoil.

Roughness effect.- The effect of installing roughness near the leading edge of the airfoil is shown in figure 6. At $R = 0.93 \times 10^6$ (fig. 6(a)), the roughness had no effect on the maximum lift coefficient; however, a decrease in the s-shaped nonlinearities of the lift curve was measured. Increasing the Reynolds number to about 2.5×10^6 (fig. 6(b)) resulted in a decrease in both the lift-curve slope and the maximum lift coefficient, compared with the smooth-model results. This observed decrease in the lift-curve slope with the addition of roughness is similar to the Reynolds number effect with the smooth model as discussed earlier.

The effect of roughness on the pitching-moment data (fig. 6(b)) was to reduce the nonlinear variation of c_m with α over the range of low drag coefficients and to change the sign of the pitching-moment curve slope.

Utilizing roughness on the airfoil resulted in eliminating the laminar bucket which was observed at low test Reynolds numbers (fig. 6(a)) and decreased the range of c_l over which low values of c_d occurred (fig. 6(b)).

Mach number effects.- The effect of Mach number on the aerodynamic characteristics for the 6-percent-thick airfoil section is essentially negligible as shown in figure 7 for the Mach number range from 0.16 to 0.35.

6-Percent-Thick Airfoil Section – Trailing Edge Forward

Reynolds number effect.- The effect of Reynolds number on the lift characteristics of the 6-percent-thick section (fig. 8(a)) with the trailing edge directed forward to the free stream to serve as the leading edge (reverse flow) is very similar to the results for this airfoil with the leading edge forward. Maximum lift coefficients (fig. 11) increased only slightly (from about 1.0 to 1.03) as the Reynolds number was increased from about 1.0×10^6 to 7.7×10^6; however, the angle of attack for $c_{l,max}$ increased about 6^o (fig. 8(a)). The stall characteristics indicate that the airfoil in the reverse flow (fig. 8(a)) is very similar to the airfoil in the forward flow (fig. 5(a)); that is, they are gradual at low Reynolds numbers and, at the higher Reynolds number ($R = 7.7 \times 10^6$), the stall characteristics are of the typical thin airfoil type. Figure 11 indicates that in the low Reynolds number range, the maximum lift coefficient was slightly higher with the trailing edge forward than with the leading edge forward.

The effect on the pitching-moment data due to directing the trailing edge forward is shown by comparing figures 5(a) and 8(a). Generally, a small negative increment in c_m is shown for the trailing edge forward. Figure 13 illustrates typical pressure data at a Reynolds number of 2.60×10^6. Comparison of the pressure data of figure 12 (leading edge forward) and figure 13 (trailing edge forward) at $\alpha \approx 8^o$ illustrates the reduced upper-surface pressure peaks and change in airfoil loading due to directing the trailing edge forward.

Comparison of figures 5(b) and 8(b) illustrates the effect on c_d as a result of directing the trailing edge forward. The lift coefficient range where low values of c_d occurred is reduced, and the laminar bucket at $R = 0.93 \times 10^6$, measured with the leading edge forward, is eliminated.

Roughness effect.- Generally, the effect of roughness on the aerodynamic characteristics with the trailing edge forward is the same as with the leading edge forward. (Compare figs. 6 and 9.) One additional Reynolds number, 7.7×10^6, was investigated with roughness for the trailing edge forward (fig. 9(c)). These data indicate that the effect of roughness observed at the lower test Reynolds numbers is essentially removed.

Mach number effect.- Figure 10 shows that the effect of Mach number on the aerodynamic characteristics for this section in reverse flow are small for Mach numbers from 0.16 to 0.35. However, a slightly higher maximum lift coefficient is shown for M = 0.26.

12-Percent-Thick Airfoil Section – Leading Edge Forward

Reynolds number effect.- The nonlinear variations of both c_l and c_m with α in the low Reynolds number range become more pronounced for the 12-percent-thick section than for the 6-percent-thick section as shown by comparing figures 5(a) and 14(a). Increasing the Reynolds number above 7.60×10^6 (fig. 14(a)) essentially removes these effects on c_l and c_m. Maximum lift coefficients increase from about 1.26 to 1.81 as the Reynolds number was increased from about 1.0×10^6 to 8.0×10^6 and decreased slightly at higher Reynolds numbers (fig. 20). The lift data (fig. 14(a)) indicate that this section reached higher angles of attack before stall than the 6-percent-thick section (fig. 5(a)). With increasing Reynolds number the lift characteristics displayed are typical of those of a conventional section with this thickness ratio. The stall characteristics (fig. 14(a)) are of the trailing-edge type; that is, the lift curves characteristically display a decrease in lift-curve slope near maximum lift and a well-rounded lift curve at stall. Tuft data obtained on this section also indicate the stall was of the trailing-edge type.

At low Reynolds numbers and small positive and negative angles of attack, increases in lift coefficient and a negative increment in pitching-moment coefficient are indicated when compared with the high Reynolds number data (fig. 14(a)). For example, at $\alpha = 2^\circ$, a decrease in c_l of about 0.2 occurs when the Reynolds number is increased from 0.93×10^6 to 11.65×10^6. In order to gain some insight for this behavior of the section data at low Reynolds numbers, selected pressure data are presented in figure 21. At low Reynolds number (fig. 21(a)) flow separation is indicated near the airfoil trailing edge by the approximately constant values of C_p on the airfoil lower surface. Increasing the Reynolds number to 11.65×10^6 reduces the extent of separation on the lower surface near the rounded trailing edge. Large changes in the lower surface pressure coefficient for this region indicate higher velocity flow around the curved surface. This delayed separation results in a decrease in circulation over the airfoil which accounts for the observed changes in lift and pitching-moment coefficients as affected by Reynolds number. Figure 21(b) illustrates pressure distributions near maximum lift coefficient for this airfoil at the same two Reynolds numbers. Flow separation is present near the airfoil trailing edge on both upper and lower surfaces at the low Reynolds number and a large decrease in the upper surface pressure peak is indicated.

The profile-drag data of figure 14(b) show, at moderate lift coefficients, the expected decrease in c_d with increases in Reynolds number. This drag reduction is

associated with the related decrease in boundary-layer thickness and accompanying reduction in skin-friction drag.

Roughness effect.- The effect of roughness on the aerodynamic characteristics (fig. 15) is essentially the same as for the 6-percent-thick airfoil section.

Mach number effect.- While the 6-percent-thick section indicated negligible effects of Mach number on maximum lift coefficients (fig. 7), figure 16(a) illustrates a substantial effect of Mach number on maximum lift coefficient for this section. Increasing the Mach number from 0.16 to 0.35, at $R = 2.50 \times 10^6$, decreases the maximum lift coefficient from about 1.62 to 1.40.

12-Percent-Thick Airfoil Section – Trailing Edge Forward

Reynolds number effect.- Directing the trailing edge of the airfoil to the oncoming free-stream flow generally results in the same type of nonlinear variations of c_l and c_m with α (fig. 17(a)) as observed for the airfoil with the leading edge forward (fig. 14(a)). In addition, the lift coefficient at $\alpha = 0^\circ$ decreases from about 0.36 to 0.20 as the Reynolds number increases from about 0.96×10^6 to 7.60×10^6. This is now understood to be due to the decrease in separation over the lower surface near the rounded trailing edge discussed previously. The effect of Reynolds number on maximum lift coefficient is almost negligible as shown by comparing figures 17(a) and 20. Maximum section lift coefficients are considerably reduced and reach only a value of 1.17 at $R = 7.60 \times 10^6$ compared with 1.80 for the airfoil with the leading edge forward. (See fig. 20.) Some flow separation is present on the airfoil near the aft region as observed by tufts and indicated by the pressure distribution data of figure 22. Figure 22(c) illustrates the pressure distribution over the airfoil chord at maximum lift coefficient ($\alpha \approx 12^\circ$) for $R = 0.96 \times 10^6$ and 7.60×10^6. At the lower test Reynolds number, both leading- and trailing-edge flow separations are indicated by the approximately constant values of C_p. The observed reduction in maximum lift coefficient for this section in reverse flow is attributed to the interaction of local laminar separation near the leading edge and turbulent separation near the trailing edge. It is of interest to note that the nature of the lift curves near stall shown in figure 17(a) appears to be the same as the 6-percent-thick section at low Reynolds numbers shown in figure 8(a).

The profile-drag data of figure 17(b) indicate an increase in c_d as the Reynolds number is increased from 2.50×10^6 to 7.60×10^6. This result is attributed to the large suction region on the lower surface (fig. 22(b)) near the airfoil rounded trailing edge caused by delayed flow separation at $R = 7.60 \times 10^6$.

Roughness effect.- The effect of applying roughness (fig. 18) generally results in the same type of variations of c_l and c_m with α as previously discussed. However,

figure 18(a) indicates a decrease in c_d near $c_l = 0$ when roughness is utilized at $R = 0.96 \times 10^6$. The wake profiles for this test condition are also sketched in the figure. With the grit off, large regions of flow separation are suspected as illustrated by the much broader wake profile. The pressure distribution data at this same lift coefficient and Reynolds number are shown in figure 23. Favorable pressure gradients are shown over much of the airfoil upper surface and laminar flow separation is suspected over the aft region of the airfoil. Utilizing roughness near the leading edge results in a turbulent boundary layer over most of the airfoil chord and, hence, less flow separation and lower values of c_d. It is of interest to compare the pressure data of figure 22(a) for $c_l \approx 0$ and $R = 7.60 \times 10^6$ for the smooth model with figure 23 for $c_l \approx 0$ and $R = 0.96 \times 10^6$ with roughness. Either increasing Reynolds number with the smooth model or applying roughness at low Reynolds numbers produce similar pressure distributions over the airfoil chord.

Mach number effect.- Whereas the results of the 12-percent-thick section with leading edge forward indicated a substantial effect of Mach number on maximum lift coefficient (fig. 16(a)), directing the trailing edge forward resulted in a negligible effect (fig. 19(a)).

12-Percent-Thick Airfoil Section – Rounded and Sharp Trailing Edges

The aerodynamic differences of the cambered 12-percent-thick rounded trailing-edge airfoil of this test and a symmetrical sharp trailing-edge airfoil in both forward and reverse flow at similar test conditions are illustrated in figures 24 and 25. In forward flow, the most predominate aerodynamic effect is the large increase in c_d for the rounded trailing edge compared with the sharp trailing edge (fig. 24). In reverse flow, the sharp trailing edge (serving as leading edge) induces complete flow separation at all angles of attack except near 0^o and large changes in c_m and c_d occur (fig. 25).

18-Percent-Thick Airfoil Section – Leading Edge Forward

Reynolds number effect.- The nonlinear variation of c_l and c_m with α in the low Reynolds number range is also present for this airfoil section as shown by figure 26(a). Increasing the Reynolds number to 7.6×10^6 removes this nonlinear effect. The pressure data of figure 33(a) illustrate that increasing Reynolds number results in decreased flow separation on the airfoil lower surface near the trailing edge and results in a pronounced decrease in the lift coefficient. This effect is attributed to a decrease in circulation around the airfoil at the higher Reynolds number (discussed earlier for the 12-percent-thick airfoil). Maximum lift coefficients increase from 1.38 to 1.73 as the Reynolds number increases from 1.0×10^6 to about 8.0×10^6 and, at higher Reynolds numbers the maximum lift coefficient decreases somewhat (fig. 32). Tuft studies indicate that the

stall characteristics are of the trailing-edge type. Figure 33(b) illustrates the pressure distribution over the airfoil chord at maximum lift coefficient for $R = 0.94 \times 10^6$ and 11.80×10^6. Comparisons of the pressure data near maximum lift coefficient for the 12-percent-thick airfoil (fig. 21(b)) and the 18-percent-thick airfoil (fig. 33(b)) illustrate the reduction in upper surface leading-edge pressure peaks for the 18-percent-thick airfoil associated with the larger leading-edge radius.

Roughness effect.- The effect of roughness near the leading edge of the airfoil (fig. 27) is generally the same as that observed for the 6- and 12-percent-thick sections (figs. 6 and 15, respectively). Comparisons of the pressure data of figures 33(a) and 34(a) (at $\alpha = 4^o$) indicate that increasing Reynolds number or applying roughness at low Reynolds number produce similar effects; that is, lower surface separation is reduced as well as a reduction in lift coefficient.

Mach number effect.- The effect of Mach number on maximum lift coefficient for this 18-percent-thick section is considerably less than that for the 12-percent-thick section (compare figs. 16(a) and 28(a)); for example, increasing the Mach number from 0.16 to 0.35 only decreased maximum lift coefficient from 1.48 to 1.43. Figure 28(b) simultaneously indicates that increases in section drag coefficient are observed as the Mach number is increased from 0.16 to 0.35.

18-Percent-Thick Airfoil Section – Trailing Edge Forward

Reynolds number effect.- The effect of Reynolds number on the aerodynamic characteristics for this airfoil in reverse flow is generally of the same nature, and even magnified under certain conditions, as observed for the 12-percent-thick airfoil. However, large differences in the nature of the lift characteristics for these airfoils near maximum lift coefficient are observed. (Compare figs. 17(a) and 29(a).) The results of the 12-percent-thick section indicates little effect of Reynolds number on maximum lift coefficient (fig. 20), whereas the result for the 18-percent-thick airfoil indicate a substantial effect (fig. 32). For example, maximum lift coefficients increase from about 1.23 to 1.53 as the Reynolds number is increased from about 1.0×10^6 to 7.7×10^6. This improvement in maximum lift coefficient for the 18-percent-thick airfoil can be explained by comparison of the pressure data for the 12-percent-thick airfoil near maximum lift (fig. 22(c)) with the pressure data for the 18-percent-thick airfoil near maximum lift (fig. 35(b)). The 18-percent-thick airfoil does not display the loss in upper surface leading-edge pressure peak that was observed for the 12-percent-thick airfoil. This result is believed to be a reduction in leading-edge flow separation associated with the larger leading-edge radius for the 18-percent-thick airfoil. The stall characteristics for the 18-percent-thick airfoil are of the trailing-edge type as indicated by the lift data shown in figure 29(a) and observed by a tuft study at $R = 7.7 \times 10^6$.

The low Reynolds number data for this airfoil near $\alpha = 4^{o}$ indicate what appears to be a local region of flow separation with reattachment occurring at a higher angle of attack (fig. 29(a)). The lift coefficient reaches a value of about 1.0 and then decreases, the pitching-moment coefficient indicates a sudden nose-up change, and the drag coefficient (fig. 29(b)) indicates a rapid increase. Figure 35(a) presents the pressure data for these test conditions. Flow separation at the low Reynolds number is indicated on the airfoil near the trailing edge, and in particular on the lower surface near the large rounded base. In addition, some local upper surface leading-edge flow separation is suspected. Increasing the Reynolds number to 7.70×10^{6} results in delayed separation on the lower surface near the rounded trailing edge as indicated by the large suction pressure peak (fig. 35(a)). A reduction in lift coefficient (fig. 29(a), $\alpha = 4^{o}$) of about twice that observed for the 12-percent-thick airfoil in reverse flow (fig. 17(a), $\alpha = 2^{o}$) occurs. This result is similar to that which occurs by an up flap deflection for a conventional airfoil.

Figure 29(b) indicates large erratic variations in the profile-drag coefficient at positive lift coefficients. This result might be expected because of the large region of flow separation present on the airfoil, particularly at the lower test Reynolds numbers.

Roughness effect.- The effect of roughness on the aerodynamic characteristics for this section is shown in figure 30. Generally, the effect is the same as discussed for the 12-percent-thick section. Comparison of the pressure data of figure 35 (smooth model) and figure 36 (grit on) illustrates that both increasing the Reynolds number or applying roughness at a low Reynolds number produce similar pressure distributions. This result is associated with the delayed separation on the airfoil lower surface near the rounded trailing edge.

Mach number effect.- The effect of Mach number (fig. 31(a)) on maximum lift coefficient is also more pronounced than was observed on the 12-percent-thick section (fig. 19(a)). For example, figure 31(a) indicates a decrease in maximum lift coefficient from about 1.47 to 1.30 by increasing the Mach number from 0.16 to 0.35. In addition, at $\alpha = 2^{o}$, a large Mach number effect on the aerodynamic characteristics is observed on this 18-percent-thick section (fig. 31) which was not observed on the 6- and 12-percent-thick sections (figs. 10 and 19, respectively). This Mach number effect is analogous to the Reynolds number effect previously discussed; that is, an increase in Mach number results in a decrease in c_{ℓ} and c_{m}. The effect on c_{d} is to reduce the lift coefficient at which a sudden drag increase occurs and to increase c_{d} at lower lift coefficients. These results are attributed to changes in flow separation on the airfoil lower surface near the rounded trailing edge.

CONCLUDING REMARKS

An investigation was conducted in the Langley low-turbulence pressure tunnel to determine the low-speed two-dimensional aerodynamic characteristics of 6-, 12-, and 18-percent-thick airfoil sections (cambered with both leading and trailing edges rounded) in forward and reverse flow. The airfoils were tested in the wind tunnel with the leading edge and the trailing edge directed toward the free stream. The data were obtained with the airfoils in both orientations over a Mach number range from 0.16 to 0.36 and an angle-of-attack range from -10° to 24°. Reynolds number, based on the airfoil chord, was varied from about 1.0×10^6 to 12.0×10^6.

All three airfoil sections exhibited nonlinear variations in section lift and pitching-moment coefficients with angle of attack in a normal or reverse flow at low Reynolds numbers. Increasing the Reynolds number or forcing boundary-layer transition by applying roughness near the leading edge of the airfoils essentially removed these nonlinear variations. These results are attributed to delayed flow separation on the lower surface near the rounded trailing edge.

At all test conditions, some flow separation was present near the rounded trailing edges of the airfoils. Thus the wake rake measurements used in determining the section profile drag for the airfoils resulted in erratic drag data, particularly for the thicker sections in the reverse orientation.

The largest maximum section lift coefficient in the normal orientation was about 1.8 for the 12-percent-thick airfoil. In the reverse orientation, the 18-percent-thick airfoil produced the largest maximum section lift coefficient of about 1.5.

Langley Research Center,
National Aeronautics and Space Administration,
Hampton, Va., June 17, 1974.

REFERENCES

1. Von Doenhoff, Albert E.: and Abbott, Frank T., Jr.: The Langley Two-Dimensional Low-Turbulence Pressure Tunnel. NACA TN 1283, 1947.

2. Braslow, Albert L; and Knox, Eugene C.: Simplified Method for Determination of Critical Height of Distributed Roughness Particles for Boundary-Layer Transition at Mach Numbers From 0 to 5. NACA TN 4363, 1958.

3. Baals, Donald D.; and Mourhess, Mary J.: Numerical Evaluation of the Wake-Survey Equations for Subsonic Flow Including the Effect of Energy Addition. NACA WR L-5, 1945. (Formerly NACA ARR L5H27.)

4. Allen, H. Julian; and Vincenti, Walter G.: Wall Interference in a Two-Dimensional-Flow Wind Tunnel, With Consideration of the Effect of Compressibility. NACA Rep. 782, 1944. (Supersedes NACA WR A-63.)

5. Loftin, Laurence K., Jr.; and Smith, Hamilton A.: Aerodynamic Characteristics of 15 NACA Airfoil Sections at Seven Reynolds Numbers From 0.7×10^6 to 9.0×10^6. NACA TN 1945, 1949.

6. Critzos, Chris C.; Heyson, Harry H.; and Boswinkle, Robert W., Jr.: Aerodynamic Characteristics of NACA 0012 Airfoil Section at Angles of Attack From 0° to 180°. NACA TN 3361, 1955.

TABLE I.- MEASURED COORDINATES FOR AIRFOIL MODELS

x/c	6-percent thickness		12-percent thickness		18-percent thickness	
	$(z/c)_{u.s.}$	$(z/c)_{l.s.}$	$(z/c)_{u.s.}$	$(z/c)_{l.s.}$	$(z/c)_{u.s.}$	$(z/c)_{l.s.}$
0.0	0.0	0.0	0.0	0.0	0.0	0.0
.0010	.00336	-.00305	.00663	-.00629	.00858	-.00867
.0020	.00466	-.00426	.00914	-.00854	.01245	-.01173
.0030	.00571	-.00525	.01103	-.01029	.0153-	-.01414
.0050	.00731	-.00653	.01386	-.01272	.01996	-.01768
.0100	.01006	-.00814	.01904	-.01677	.02814	-.02387
.0150	.01207	-.00928	.02300	-.01961	.03440	-.02809
.0200	.01375	-.01028	.02633	-.02165	.03964	-.03136
.0250	.01524	-.01111	.02933	-.02328	.04419	-.03396
.0300	.01658	-.01181	.03219	-.02468	.04827	-.03609
.0350	.01781	-.01243	.03475	-.02590	.05209	-.03792
.0400	.01894	-.01296	.03709	-.02693	.05557	-.03947
.0450	.02002	-.01341	.03924	-.02782	.05885	-.04081
.0500	.02105	-.01386	.04126	-.02862	.06190	-.04202
.0550	.02203	-.01422	.04314	-.02928	.06476	-.04311
.0600	.02295	-.01453	.04492	-.02988	.06748	-.04412
.0650	.02383	-.01477	.04663	-.03042	.07009	-.04501
.0700	.02466	-.01499	.04829	-.03091	.07257	-.04581
.0750	.02547	-.01519	.04986	-.03133	.07493	-.04652
.0800	.02622	-.01536	.05135	-.03172	.07721	-.04714
.0850	.02695	-.01551	.05281	-.03208	.07933	-.04770
.0900	.02767	-.01564	.05417	-.03239	.08138	-.04822
.0950	.02836	-.01576	.05551	-.03267	.08335	-.04869
.1000	.02900	-.01587	.05680	-.03293	.08525	-.04908
.1100	.03027	-.01606	.05917	-.03339	.08885	-.04983
.1200	.03144	-.01622	.06135	-.03378	.09213	-.05044
.1300	.03251	-.01636	06337	-.03411	.09513	-.05098
.1400	.03349	-.01653	.06524	-.03438	.09799	-.05142
.1900	.03744	-.01706	.07281	-.03518	.10958	-.05276
.2400	.04008	-.01711	.07811	-.03534	.11752	-.05307
.2900	.04186	-.01703	.08162	-.03538	.12273	-.05321
.3400	.04283	-.01703	.08352	-.03538	.12570	-.05323
.3900	.04324	-.01708	.08424	-.03542	.12679	-.05332
.4400	.04311	-.01720	.08394	-.03543	.12632	-.05330
.4900	.04244	-.01716	.08267	-.03544	.12462	-.05309
.5400	.04143	-.01692	.08060	-.03526	.12162	-.05270
.5900	04028	- 01694	.07782	-.03474	.11732	-.05204
.6400	.03839	-.01678	.07426	-.03399	.11182	-.05077
.6900	.03638	-.01647	.06997	-.03296	.10512	-.04902
.7400	.03416	-.01619	.06481	-.03157	.09701	-.04678
.7900	.03143	-.01597	.05850	-.03003	.08723	-.04377
.8400	.02799	-.01542	.05103	-.02775	.07555	-.03998
.8900	.02383	-.01432	.04157	-.02486	.06149	-.03511
.9200	.02059	-.01338	.03481	-.02244	.05138	-.03122
.9450	.01736	-.01210	.02808	-.01964	.04143	-.02704
.9700	.01287	-.01014	.01959	-.01535	.02913	-.02109
.9950	.00460	-.00494	.00638	-.00720	.01128	-.00944
1.0000	.0	-.00001	.00001	.0	.0	-.00001

TABLE II.- ORIFICE LOCATIONS FOR 6-PERCENT-THICK AIRFOIL MODEL

Upper surface		Lower surface	
x/c	z/c	x/c	z/c
0.0	0.00051		
.00298	.00586	0.00185	-0.00427
.00539	.00769	.00566	-.00673
.00868	.00959	.00886	-.00786
.01571	.01251	.01609	-.00956
.01927	.01367	.02009	-.01031
.02441	.01517	.02477	-.01106
.03686	.01828	.03743	-.01267
.04959	.02100	.04970	-.01382
.07438	.02556	.07512	-.01519
.09973	.02922	.09999	-.01586
.14980	.03437	.15008	-.01655
.19993	.03806	.20044	-.01699
.24954	.04046	.25017	-.01699
.29977	.04208	.30033	-.01695
.39989	.04325	.40017	-.01696
.49982	.04228	.50022	-.01699
.60055	.03970	.59967	-.01658
.70023	.03594	.69969	-.01637
.75035	.03361	.74980	-.01606
.80002	.03081	.79995	-.01581
.85020	.02727	.84972	-.01511
.89987	.02292	.89998	-.01400
.92493	.02009	.92483	-.01305
.95020	.01656	.94994	-.01158
.96235	.01436	.96184	-.01069
.97531	.01150	.97584	-.00923
.98018	.01017	.97967	-.00871
.98561	.00842	.98554	-.00767
.99036	.00666	.98998	-.00658
.99519	.00447	.99529	-.00472
.99859	.00029		

TABLE III.- ORIFICE LOCATIONS FOR 12-PERCENT-THICK AIRFOIL MODEL

Upper surface		Lower surface	
x/c	z/c	x/c	z/c
0.0	0.00096		
.00298	.01069	0.00308	-0.01019
.00533	.01410	.00567	-.01333
.00904	.01801	.00903	-.01610
.01602	.02354	.01572	-.01990
.02029	.02645	.02055	-.02191
.02487	.02924	.02571	-.02362
.03728	.03560	.03774	-.02766
.05015	.04107	.04985	-.02879
.07461	.04958	.07500	-.03156
.10017	.05673	.10019	-.03308
.14897	.06674	.15052	-.03472
.19933	.07392	.20007	-.03537
.24985	.07882	.25029	-.03552
.29879	.08197	.30019	-.03554
.39895	.08421	.40099	-.03558
.49973	.08228	.50057	-.03560
.59860	.07718	.60107	-.03473
.69962	.06899	.70074	-.03284
.74992	.06356	.75067	-.03142
.79993	.05698	.80089	-.02977
.84908	.04931	.85056	-.02751
.89910	.03947	.90100	-.02433
.92411	.03361	.92599	-.02216
.94933	.02664	.95060	-.01917
.96194	.02248	.96293	-.01706
.97487	.01738	.97606	-.01421
.97944	.01536	.98123	-.01282
.98520	.01247	.98566	-.01146
.98978	.00982	.99051	-.00964
.99511	.00603	.99471	-.00737
.99934	.00131		

TABLE IV.- ORIFICE LOCATIONS FOR 18-PERCENT-THICK AIRFOIL MODEL

Upper surface		Lower surface	
x/c	z/c	x/c	z/c
0.0	0.00044		
.00296	.01548	0.00304	-0.01402
.00579	.02159	.00579	-.01858
.00902	.02665	.00893	-.02247
.01601	.03527	.01564	-.02831
.02002	.03941	.01981	-.03096
.02503	.04406	.02492	-.03363
.03752	.05372	.03736	-.03833
.04997	.06172	.04982	-.04169
.07502	.07484	.07488	-.04616
.09992	.08515	.09938	-.04870
.15002	.10055	.14969	-.05131
.19946	.11128	.19968	-.05238
.24987	.11870	.24986	-.05266
.29986	.12343	.29942	-.05276
.39973	.12674	.39934	-.05288
.49992	.12410	.49987	-.05258
.59987	.11623	.59972	-.05133
.69984	.10358	.69979	-.04819
.74977	.09516	.74970	-.04582
.80006	.08491	.79974	-.04261
.84960	.07293	.84985	-.03868
.89974	.05844	.90006	-.03357
.92489	.04957	.92433	-.03022
.94873	.03977	.94951	-.02577
.96217	.03329	.96233	-.02283
.97469	.02634	.97492	-.01914
.97994	.02306	.98024	-.01719
.98483	.01969	.98494	-.01518
.98989	.01577	.98984	-.01273
.99488	.01126	.99443	-.00941
.99995	.0		

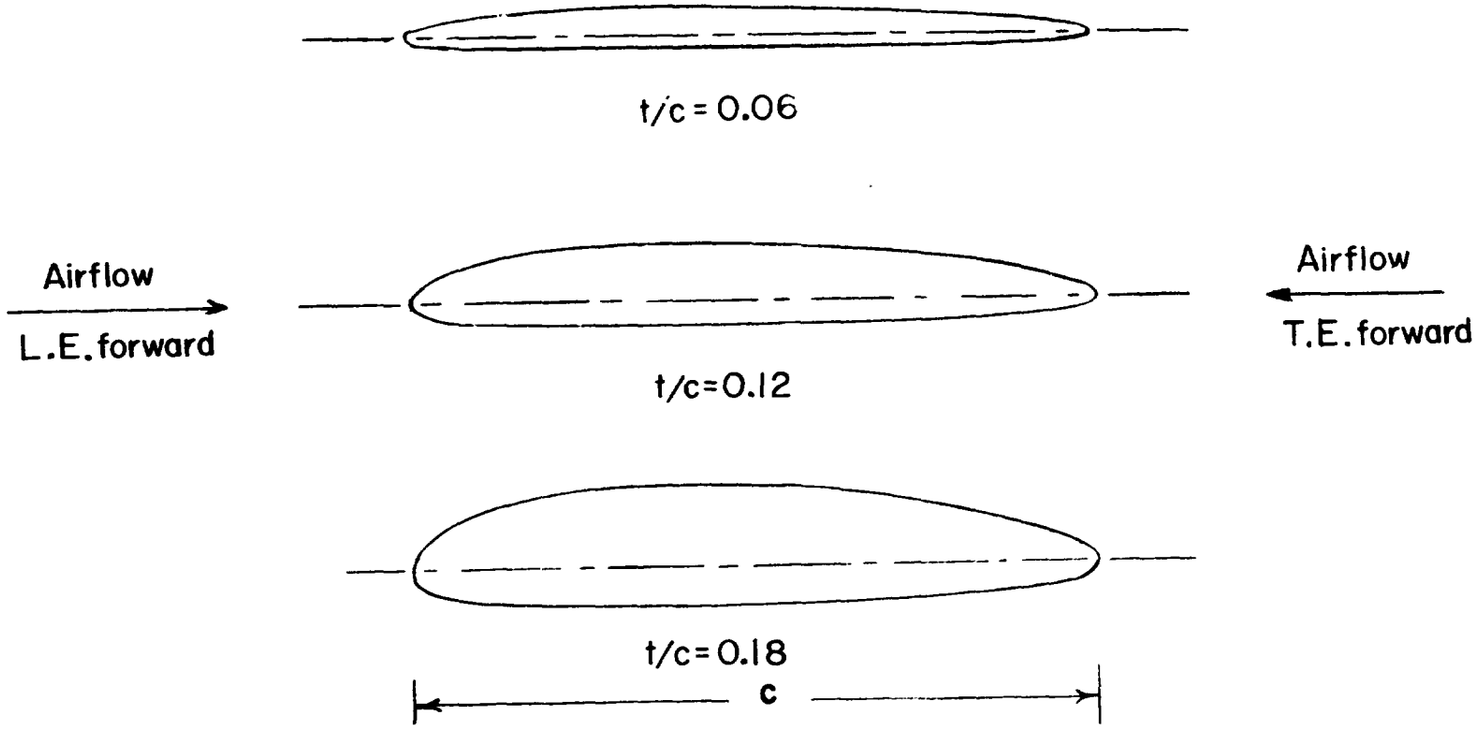

(a) Section shapes; c = 45.72 cm (18 in.).

Figure 1.- Airfoil shapes and distributions of thickness and camber.

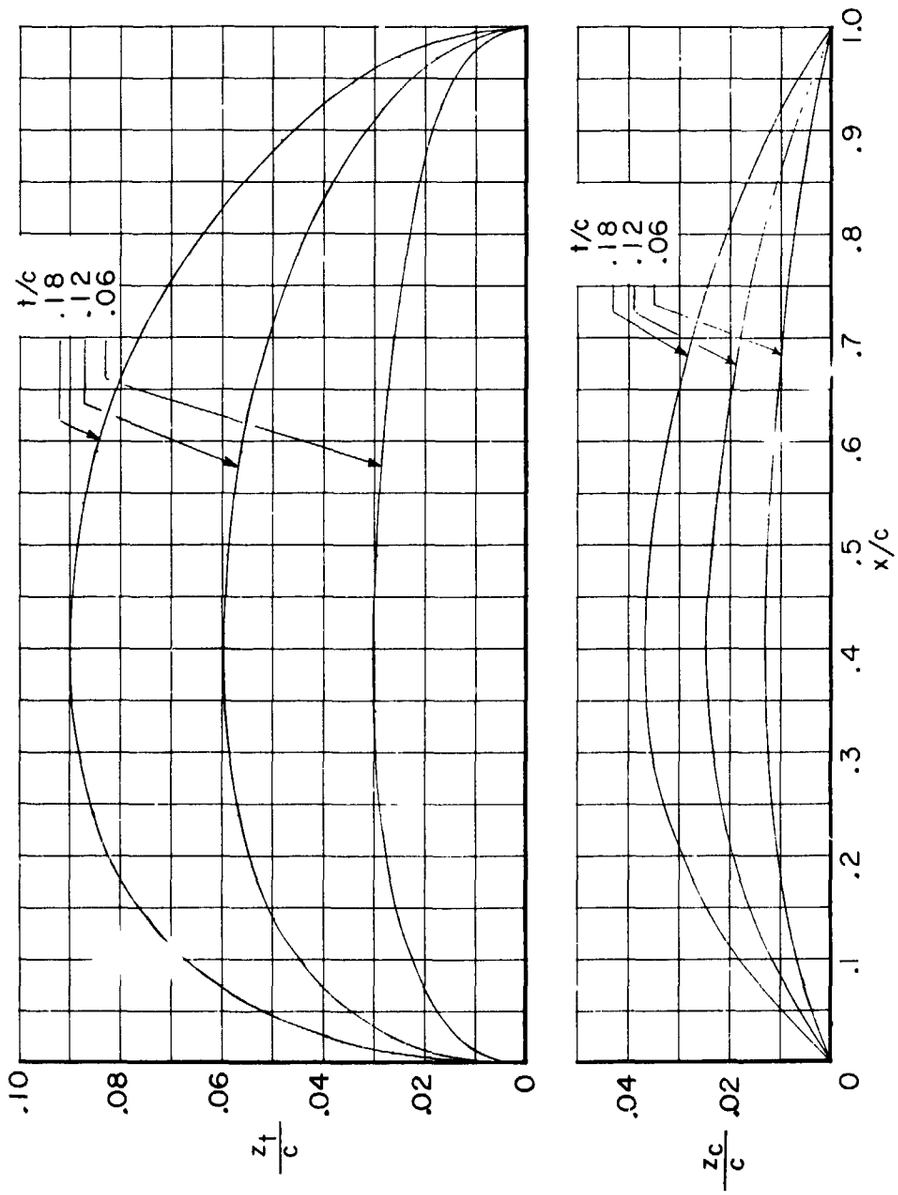

(b) Distributions of thickness and camber.

Figure 1.- Concluded.

L-72-5981

Figure 2.- 18-percent-thick airfoil mounted in wind tunnel with trailing edge forward.

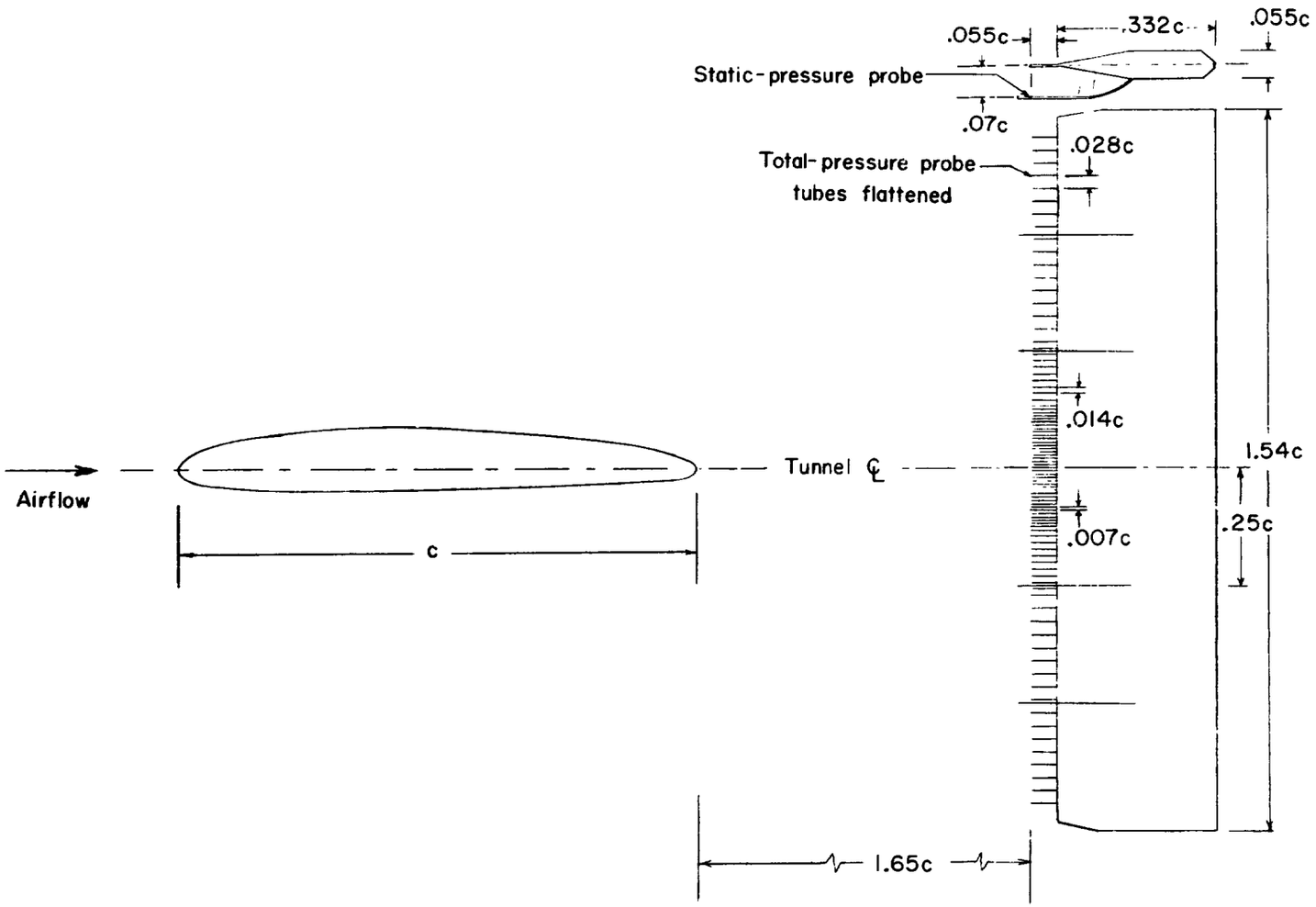

Figure 3.- Typical airfoil installation and wake rake. c = 45.72 cm (18 in.).

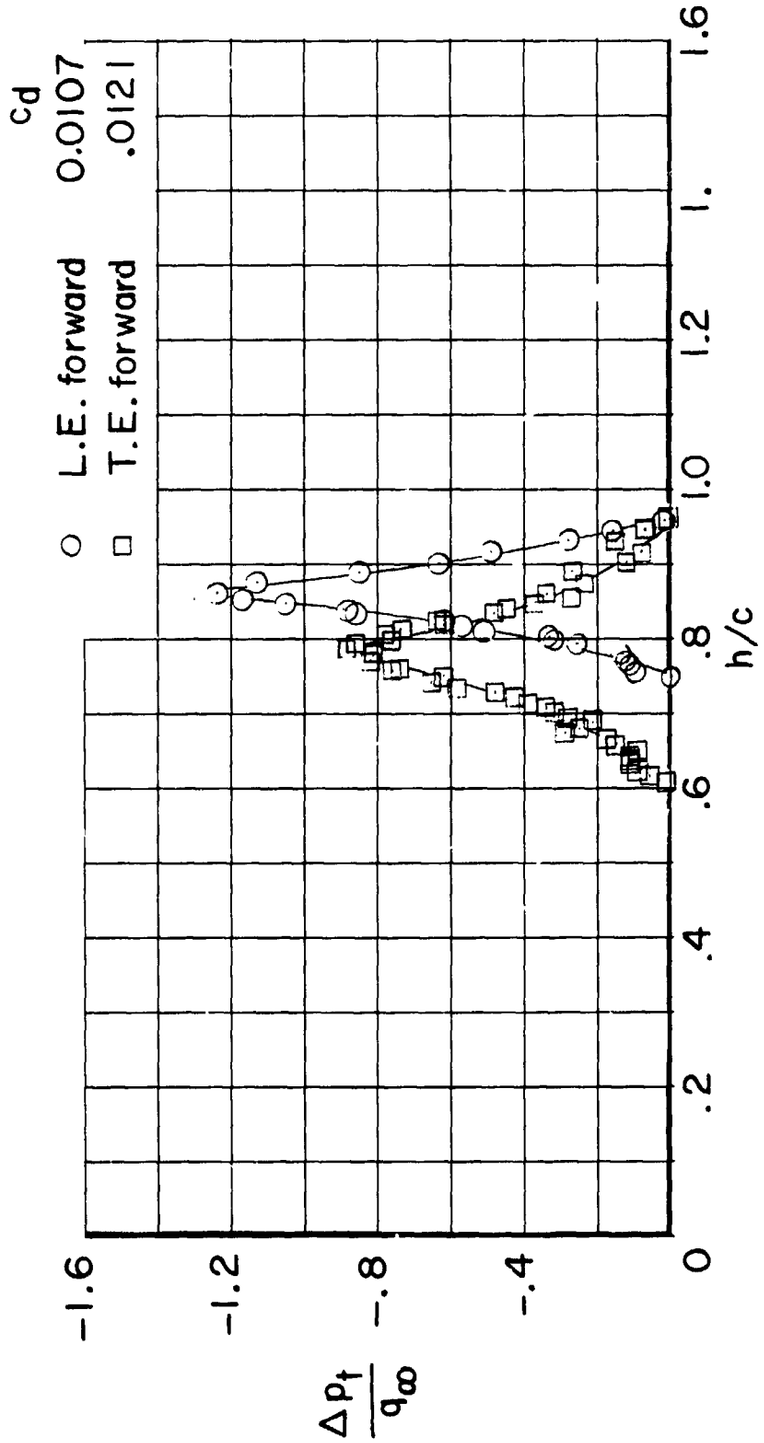

Figure 4.- Typical wake profiles for 12-percent-thick airfoil.
M = 0.26; $\alpha = 4^o$; R = 2.50×10^6.

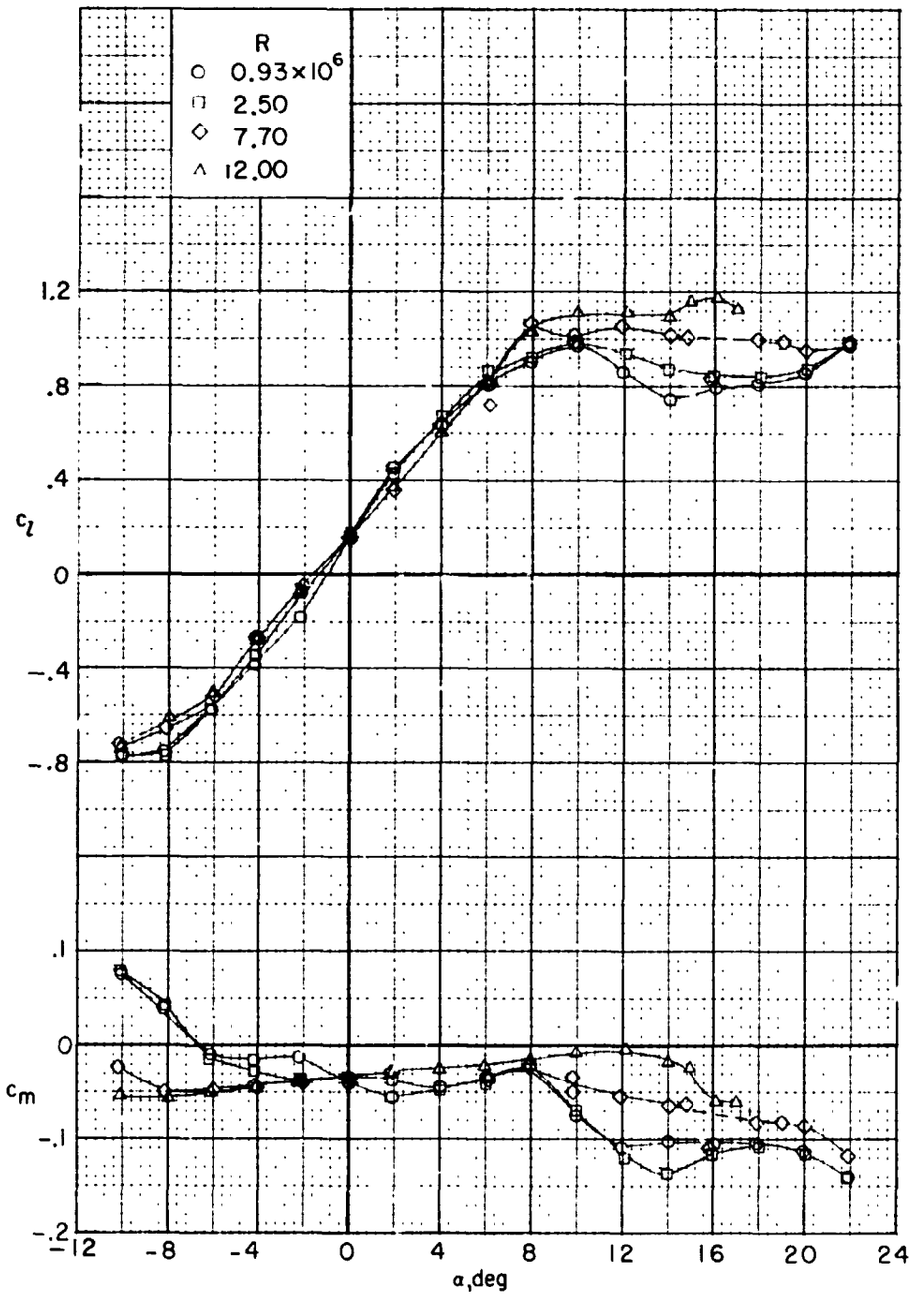

(a) c_l and c_m as a function of α.

Figure 5.- Effect of Reynolds number on section characteristics for 6-percent-thick airfoil with leading edge forward. M = 0.26; smooth model.

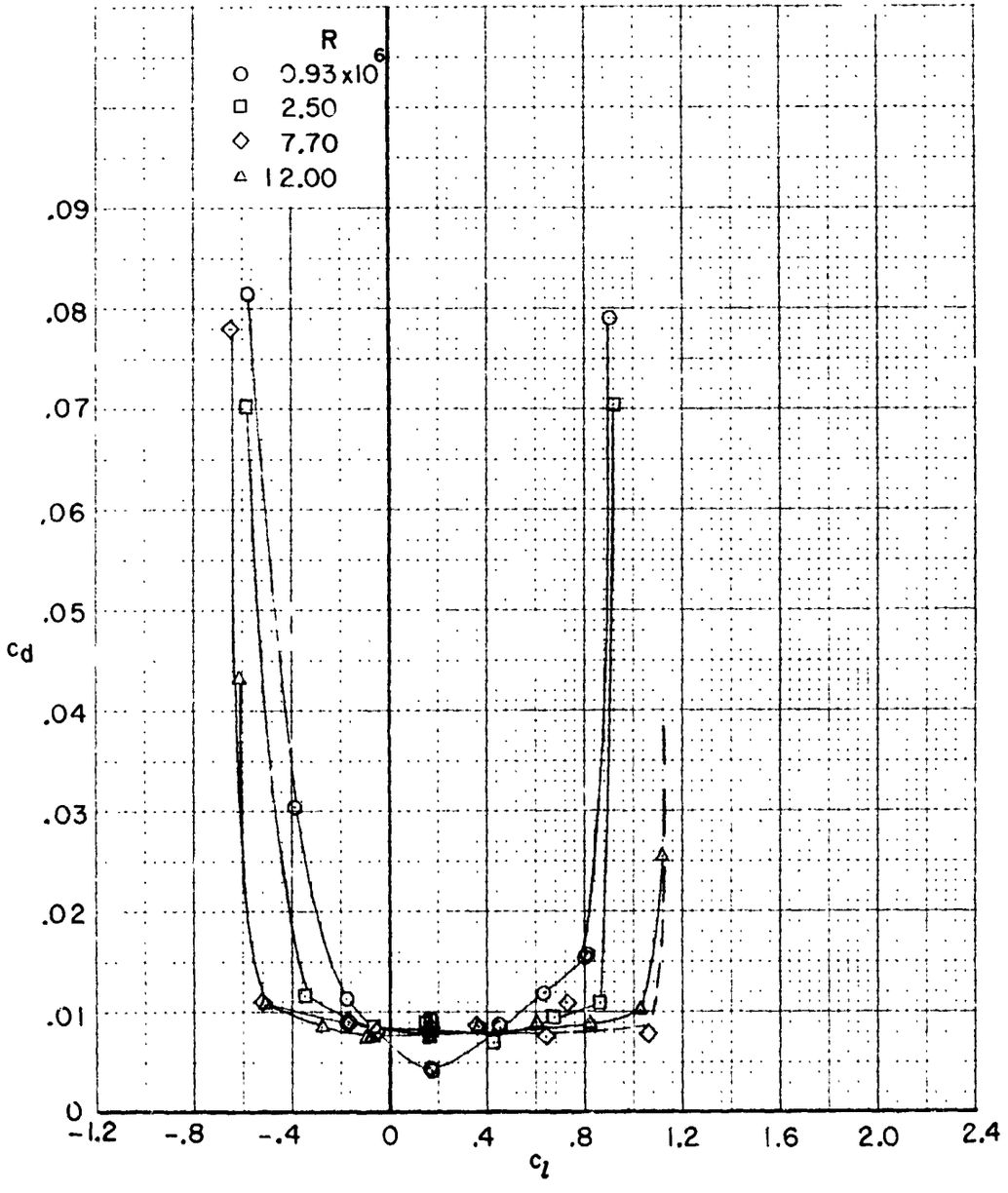

(b) c_d as a function of c_l.

Figure 5.- Concluded.

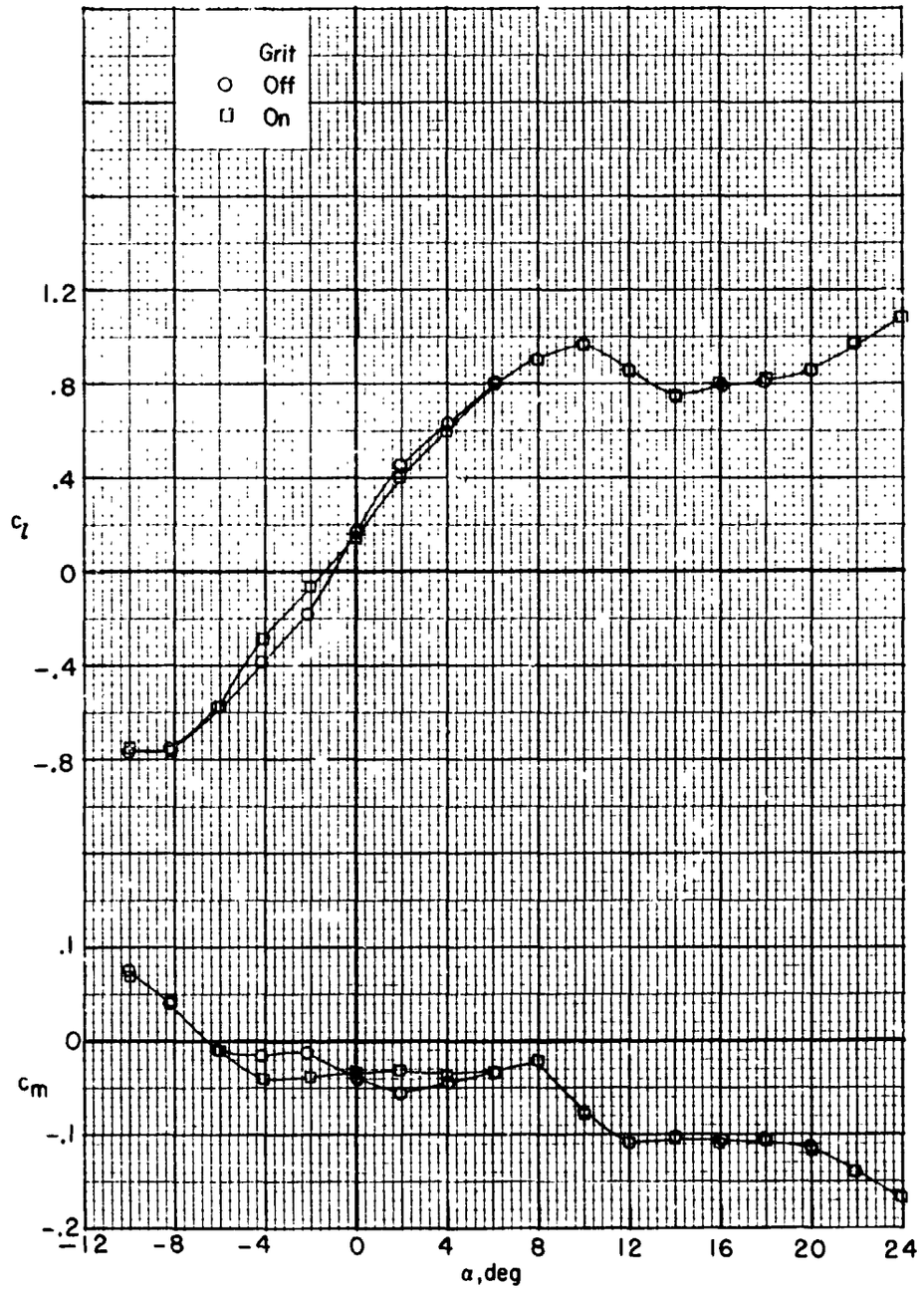

(a) $R = 0.93 \times 10^6$.

Figure 6.- Effect of roughness on section characteristics for 6-percent-thick airfoil with leading edge forward. Grit located at 0.05c; M = 0.26.

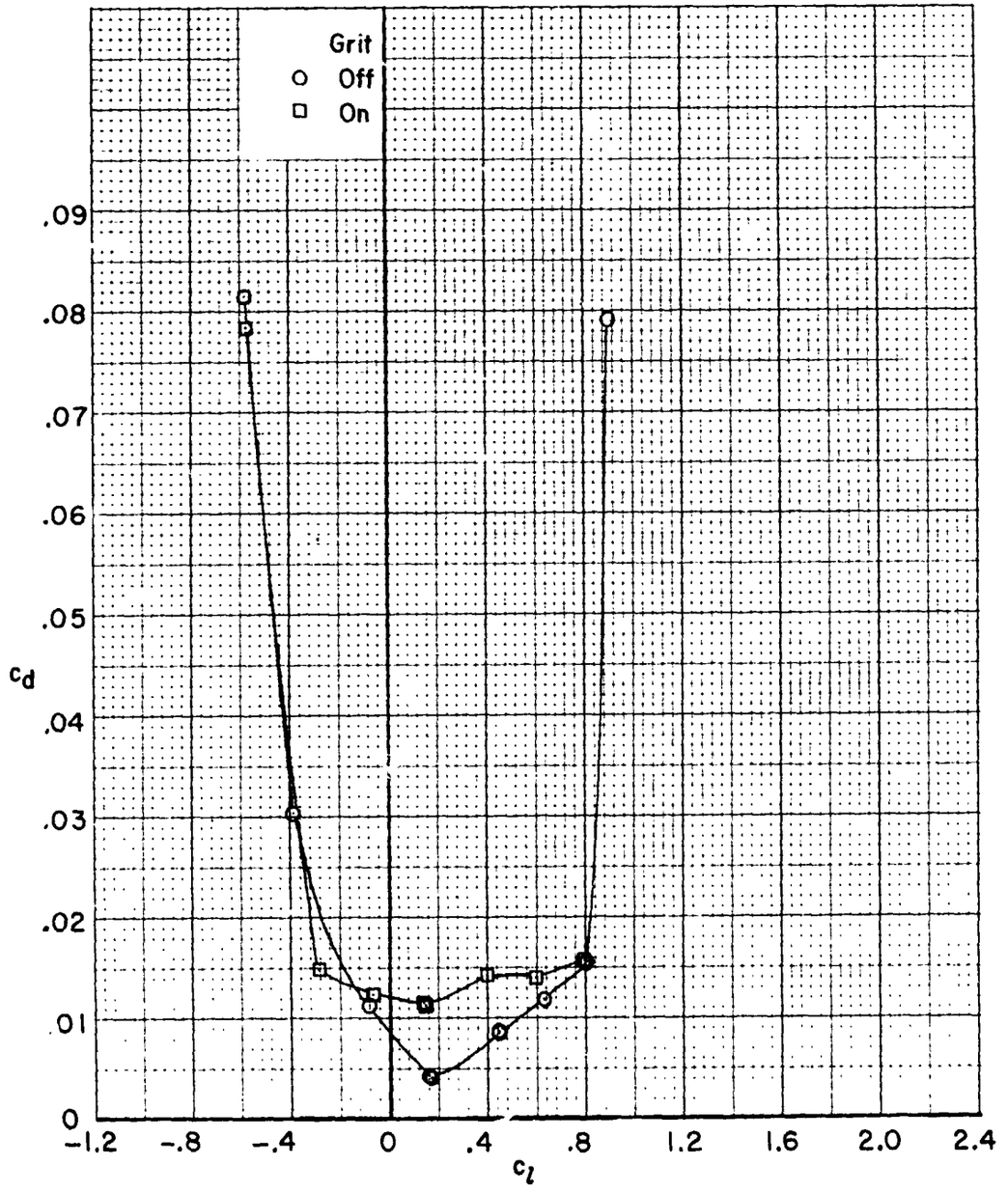

(a) R = 0.93×10^6. Concluded.

Figure 6.- Continued.

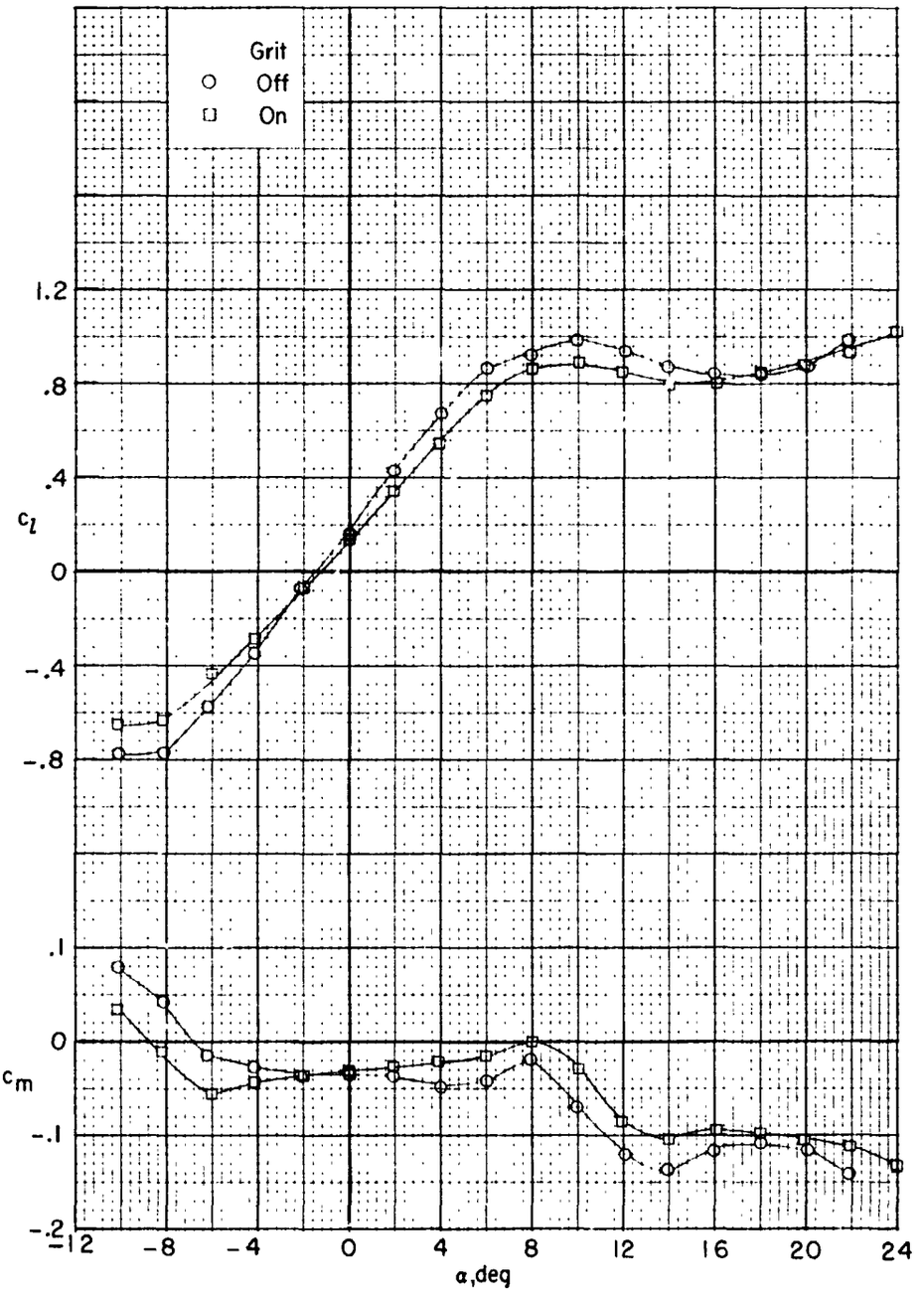

(b) $R \approx 2.50 \times 10^6$.

Figure 6.- Continued.

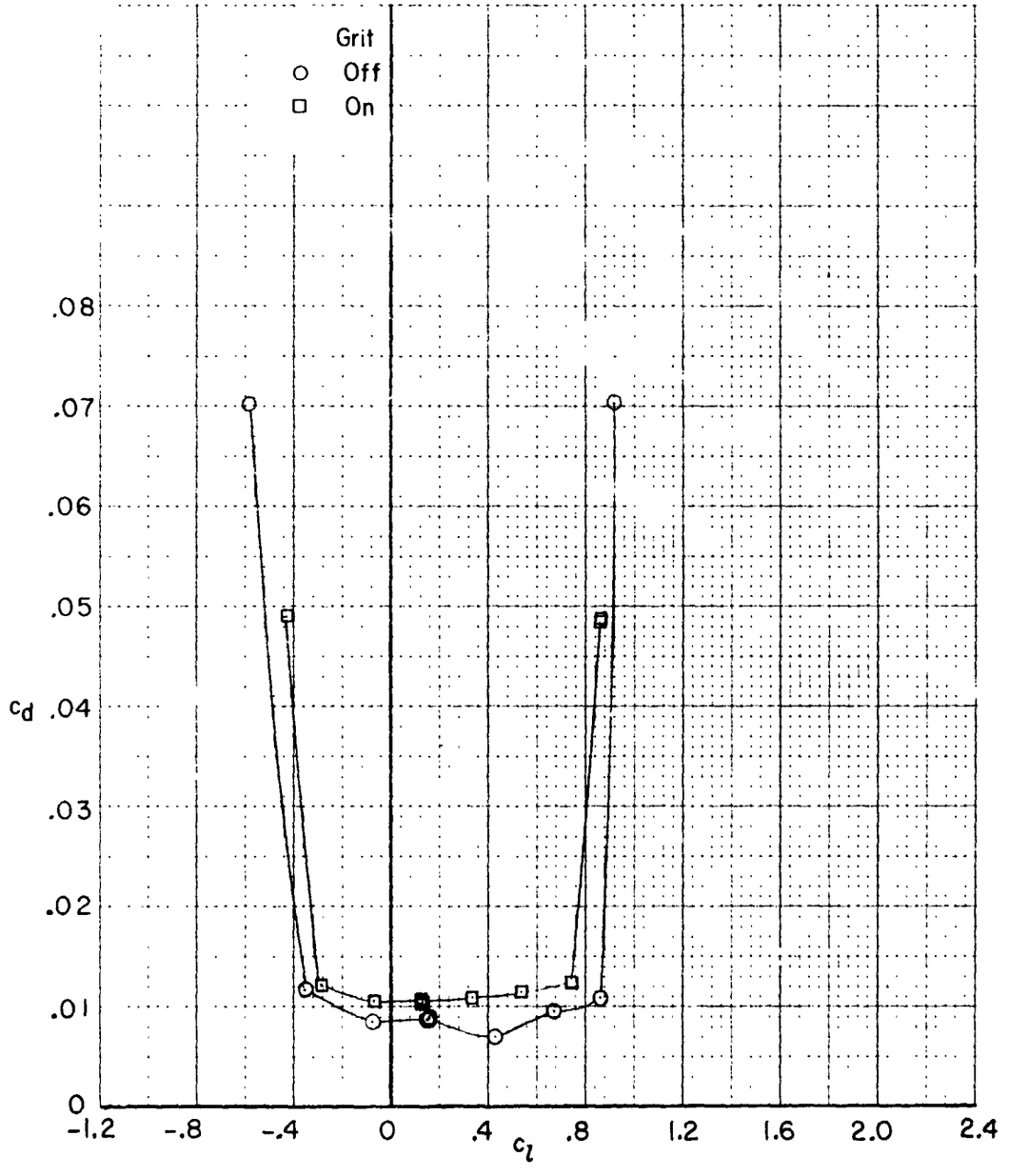

(b) $R \approx 2.50 \times 10^6$. Concluded.

Figure 6.- Concluded.

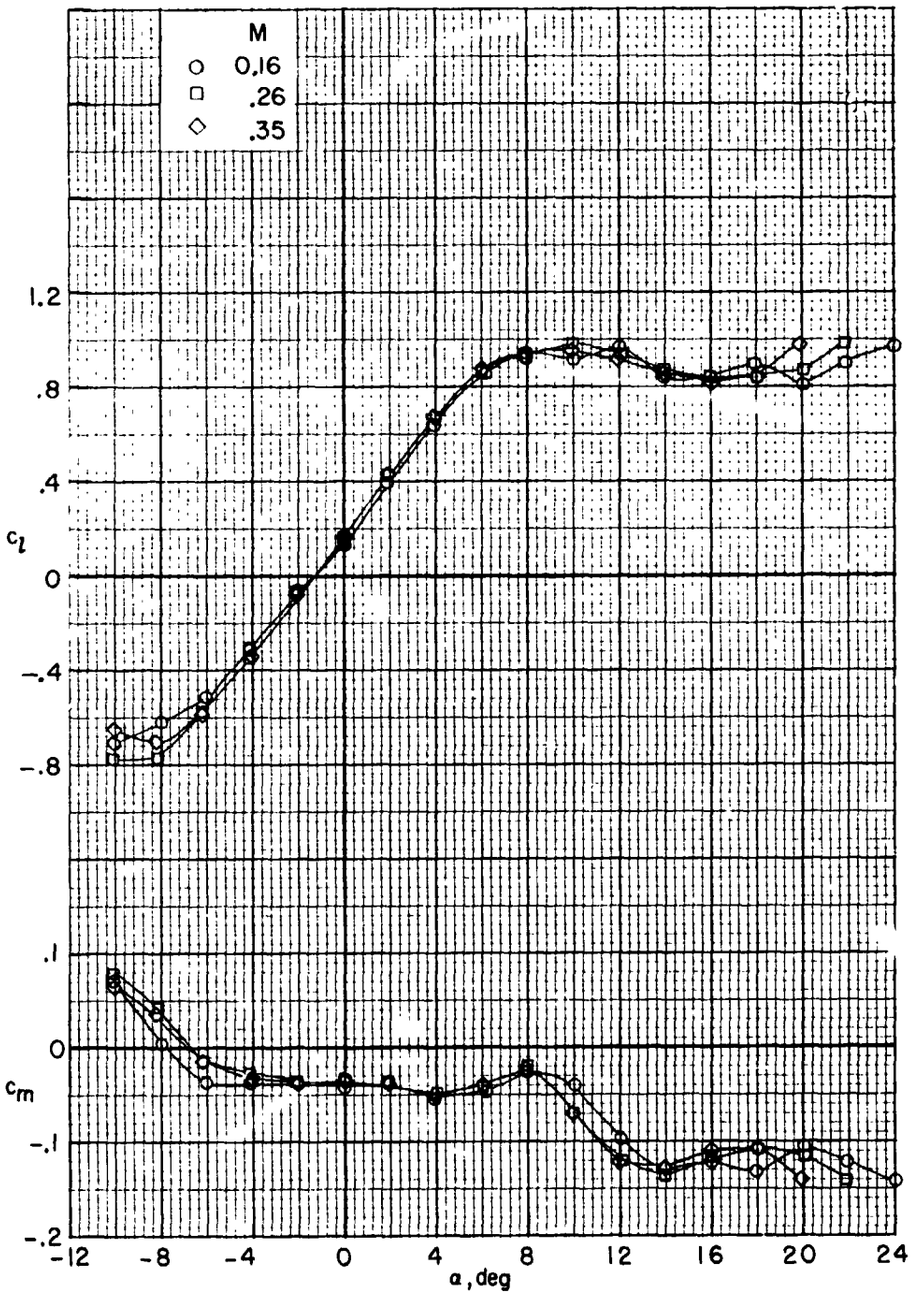

(a) c_l and c_m as a function of α.

Figure 7.- Effect of Mach number on section characteristics for 6-percent-thick airfoil with leading edge forward. $R \approx 2.50 \times 10^6$; smooth model.

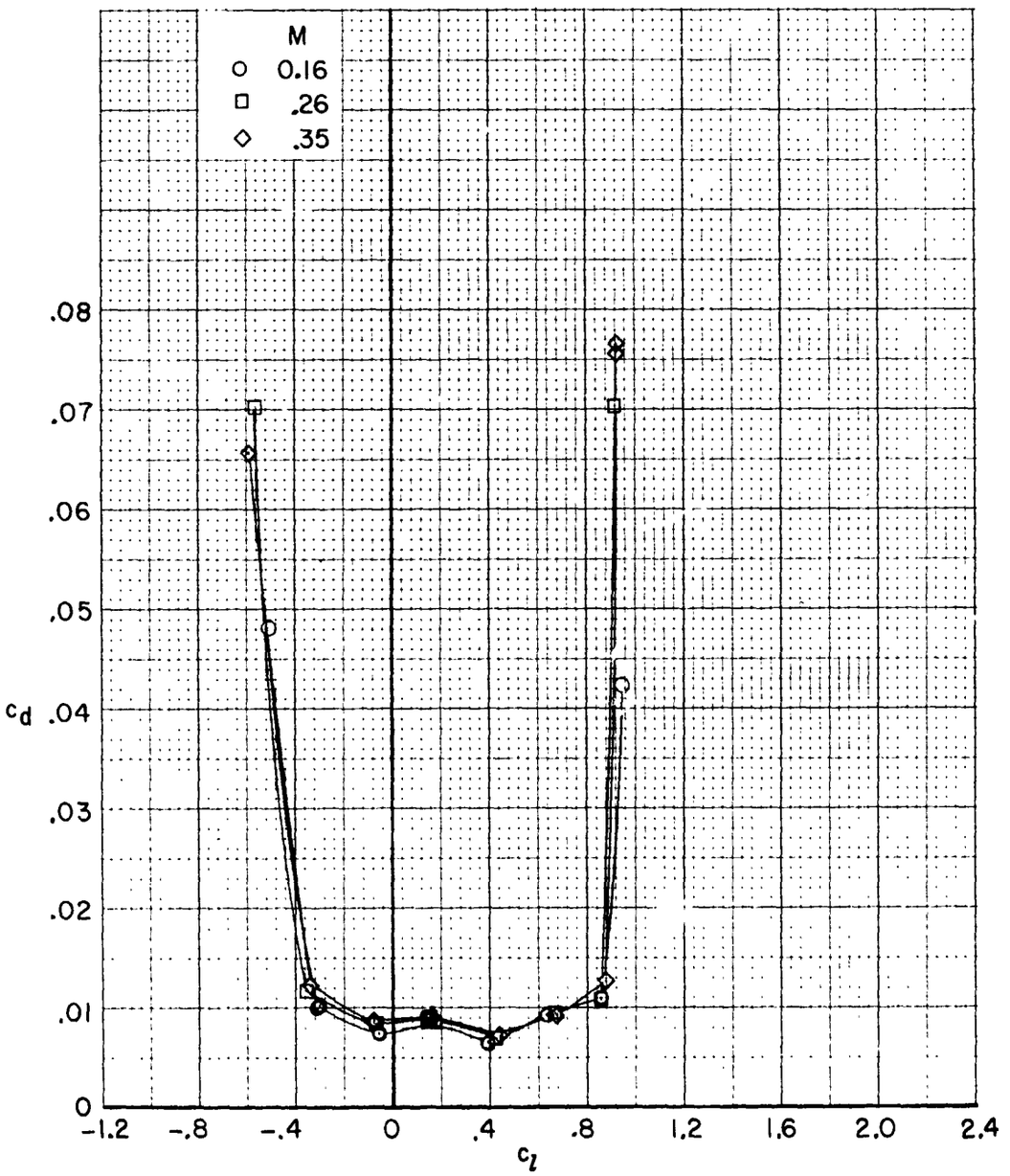

(b) c_d as a function of c_l.

Figure 7.- Concluded.

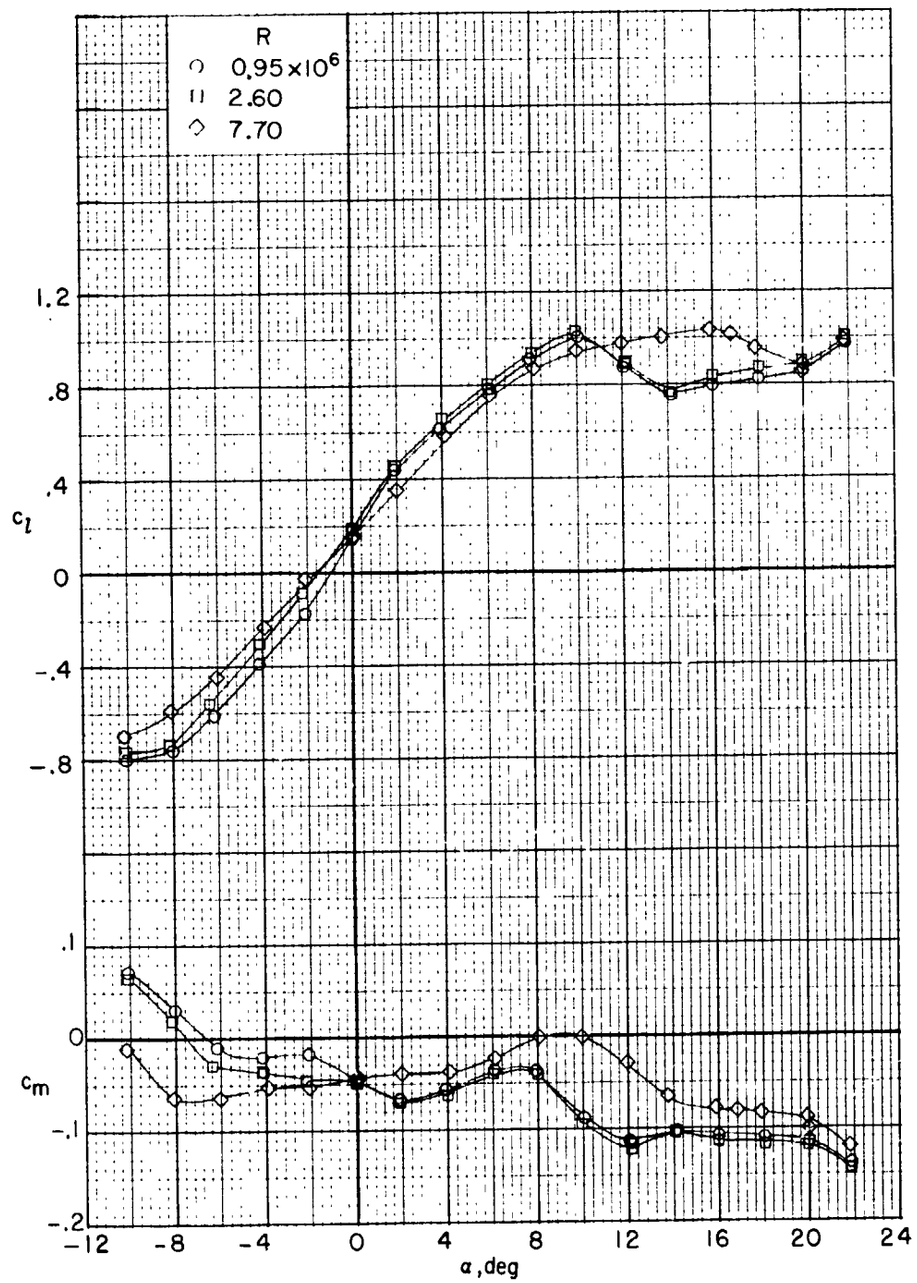

(a) c_l and c_m as a function of α.

Figure 8.- Effect of Reynolds number on section characteristics for 6-percent-thick airfoil with trailing edge forward. M = 0.26; smooth model.

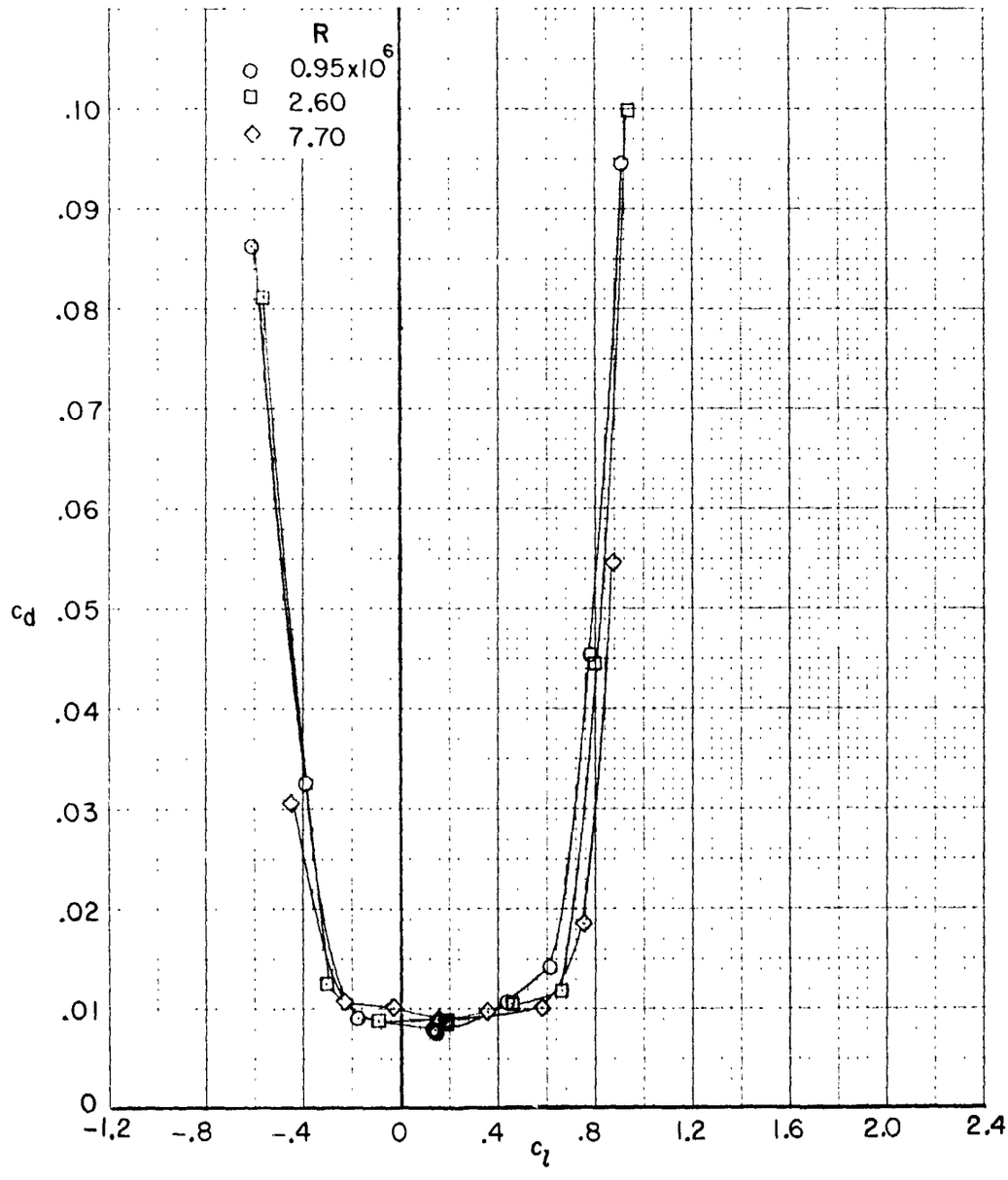

(b) c_d as a function of c_l.

Figure 8.- Concluded.

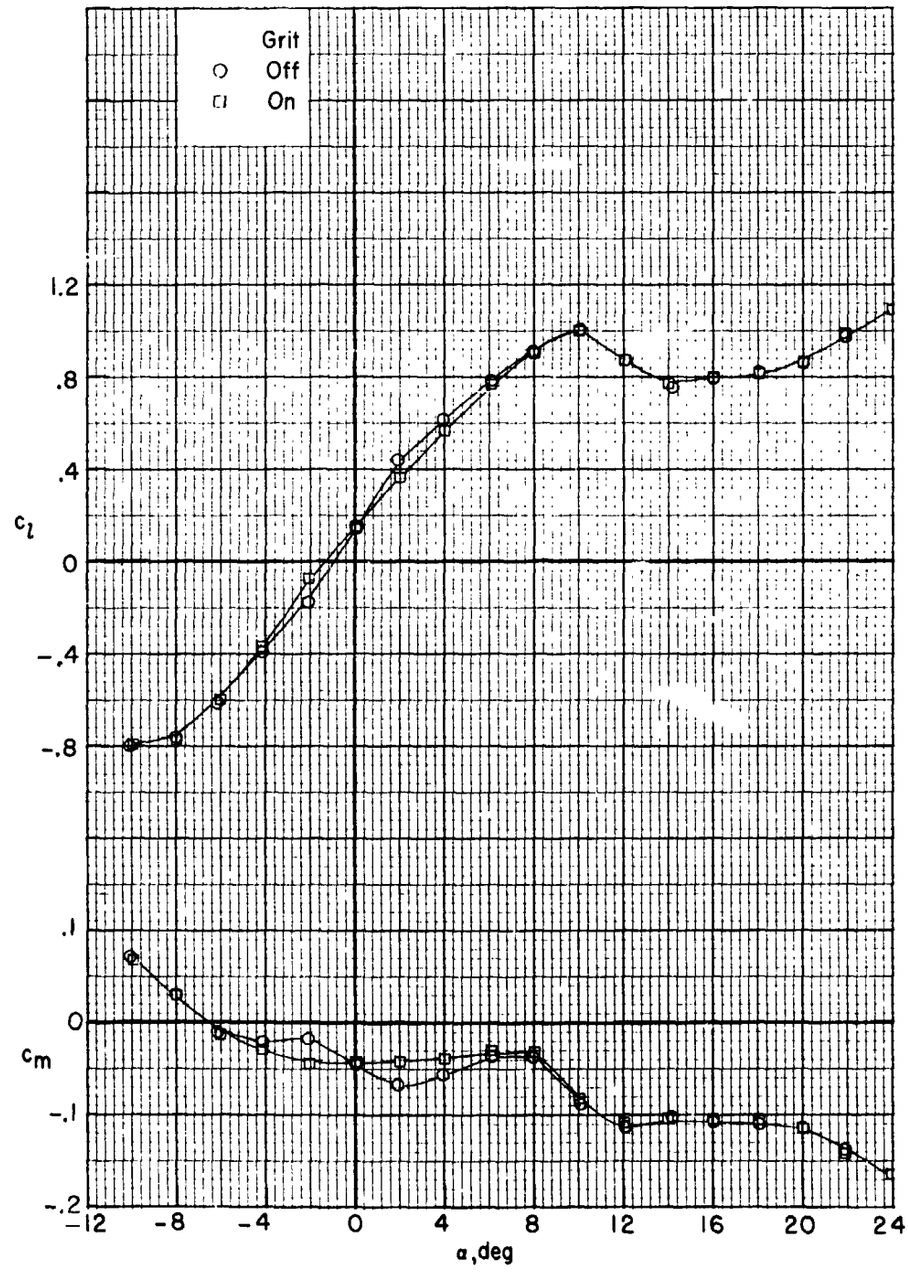

(a) $R = 0.93 \times 10^6$.

Figure 9.- Effect of roughness on section characteristics for 6-percent-thick airfoil with trailing edge forward. Grit located at 0.05c; M = 0.26.

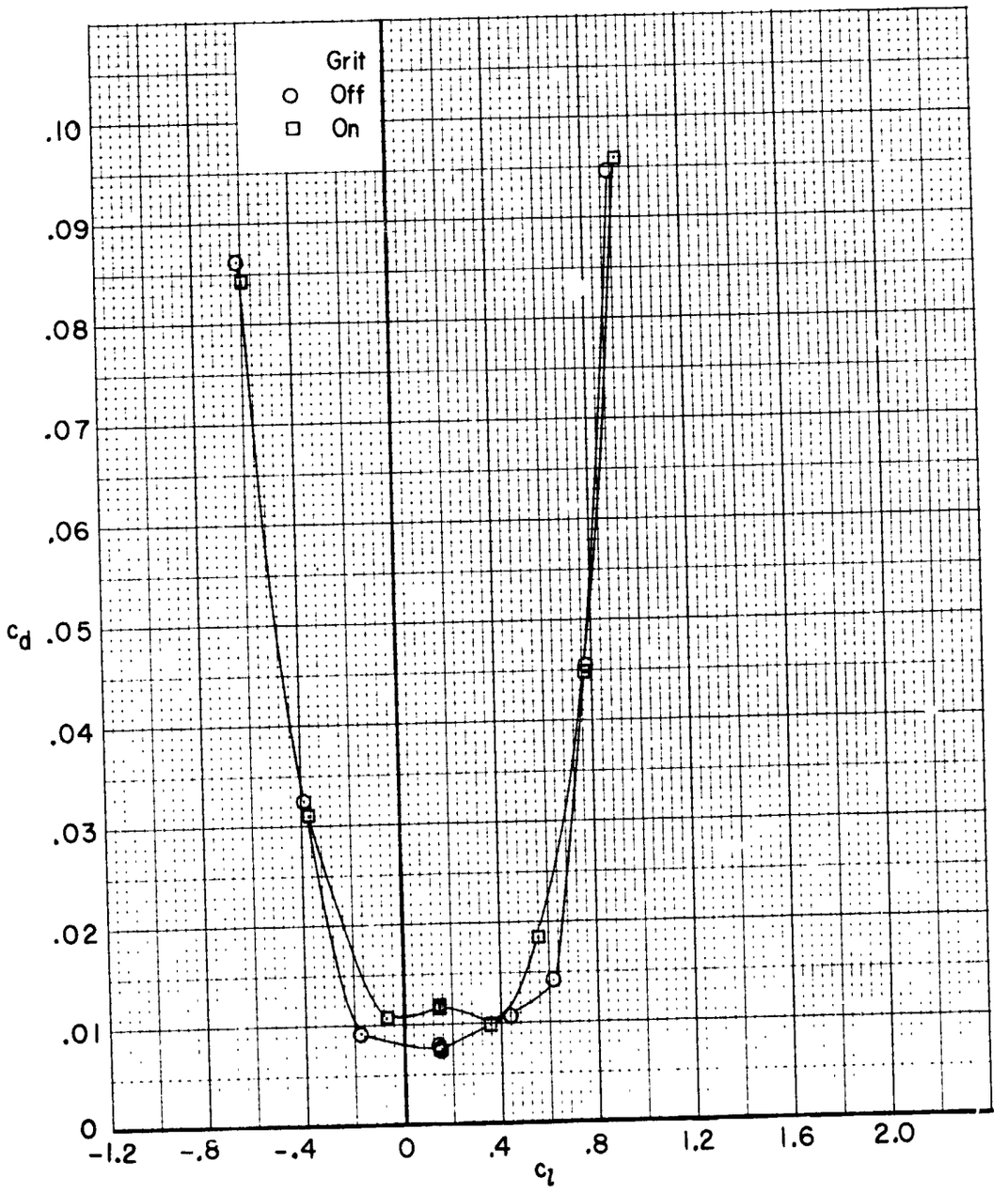

(a) $R = 0.93 \times 10^6$. Concluded.

Figure 9.- Continued.

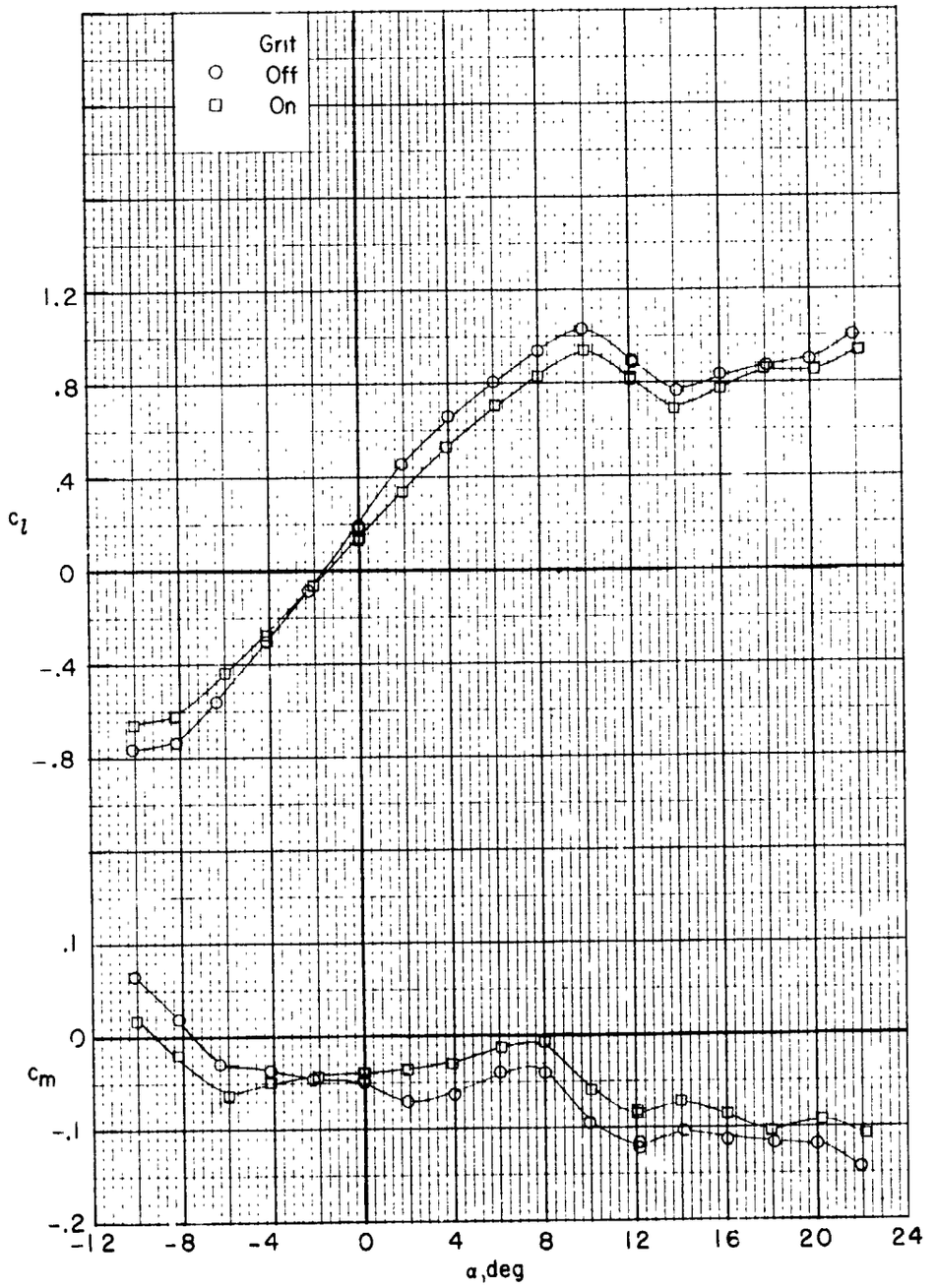

(b) $R = 2.60 \times 10^6$.

Figure 9.- Continued.

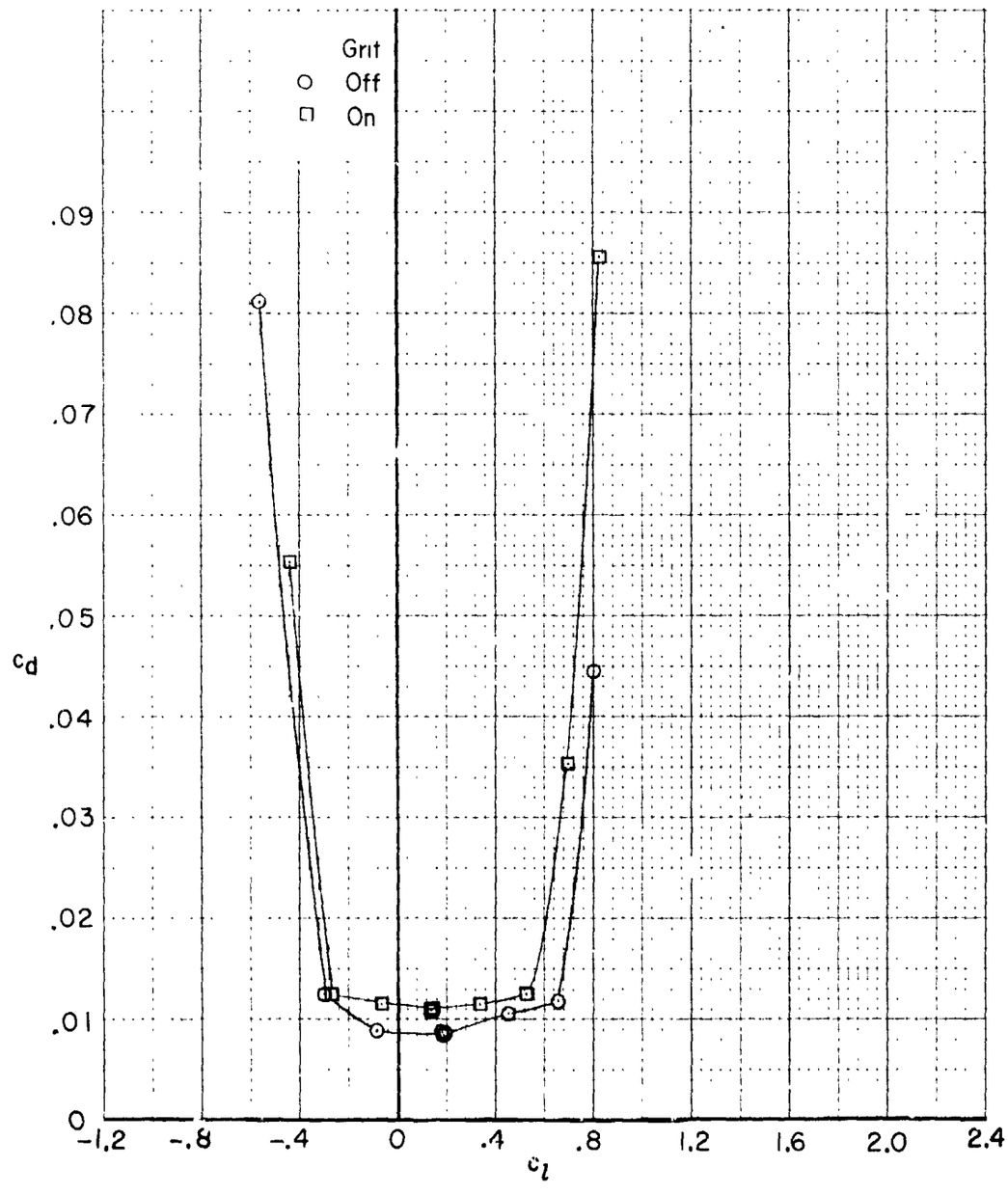

(b) R = 2.60×10^6. Concluded.

Figure 9.- Continued.

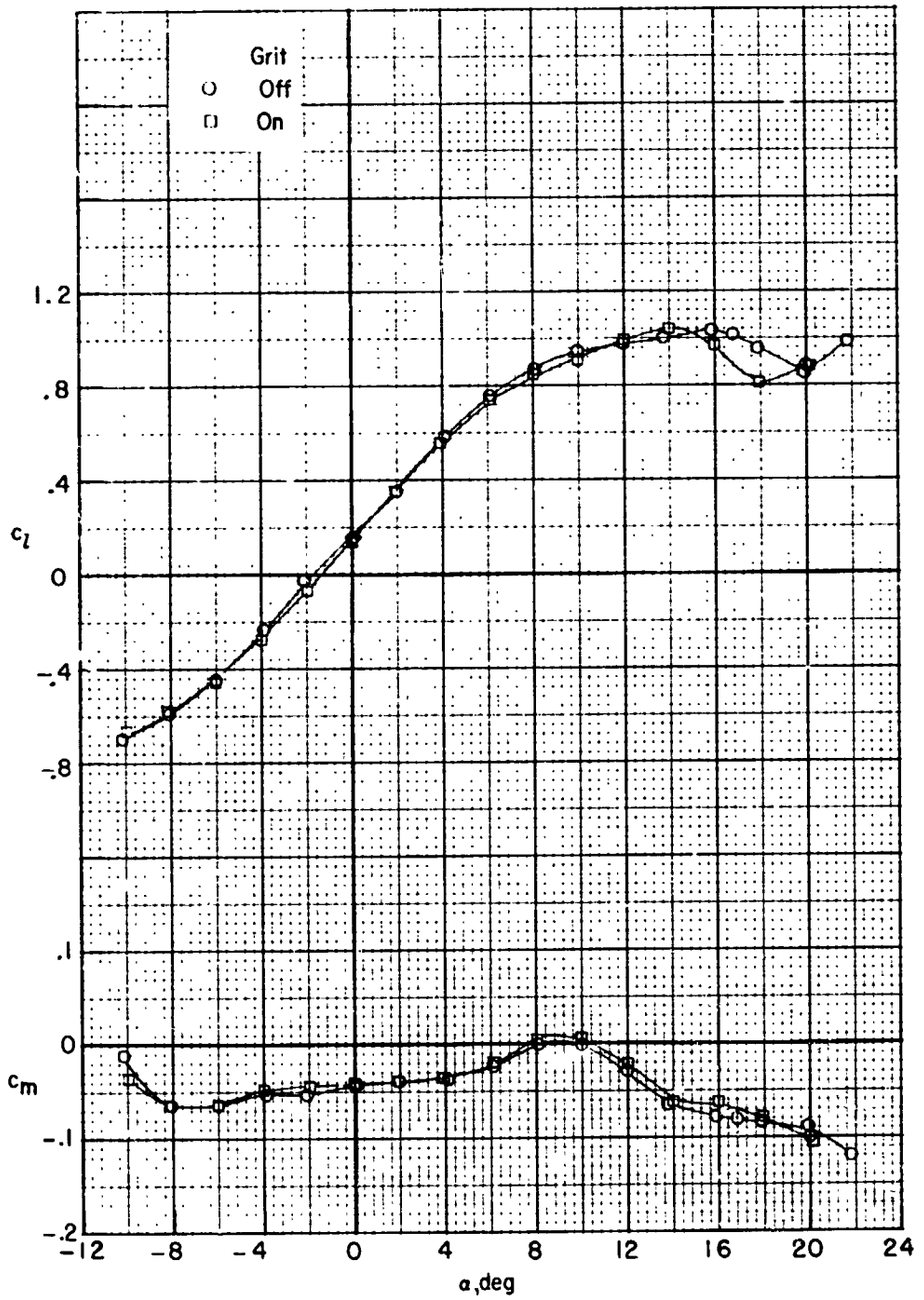

(c) R = 7.70×10^6.

Figure 9.- Continued.

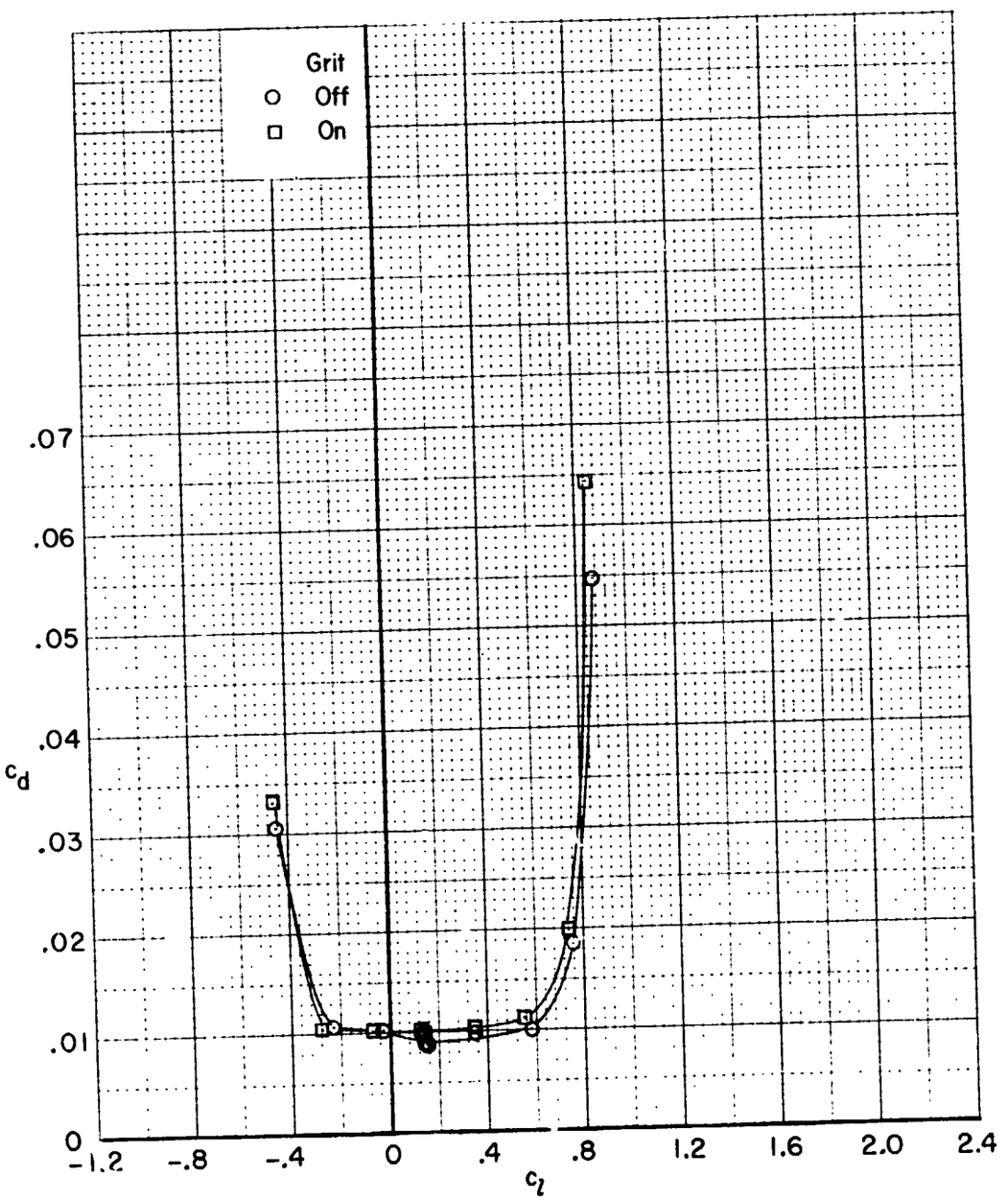

(c) R = 7.70×10^6. Concluded.

Figure 9.- Concluded.

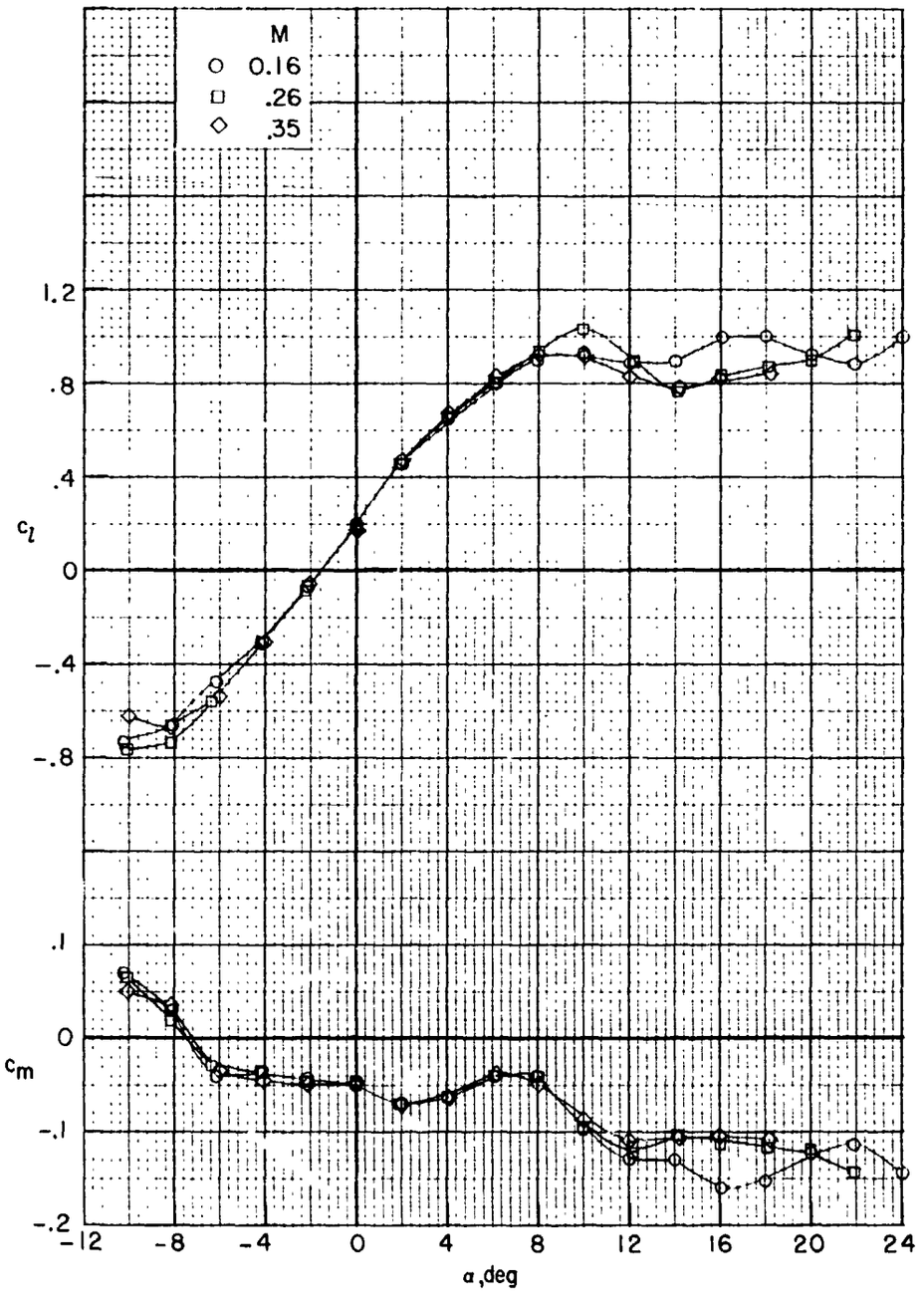

(a) c_l and c_m as a function of α.

Figure 10.- Effect of Mach number on section characteristics for 6-percent-thick airfoil with trailing edge forward. $R = 2.60 \times 10^6$; smooth model.

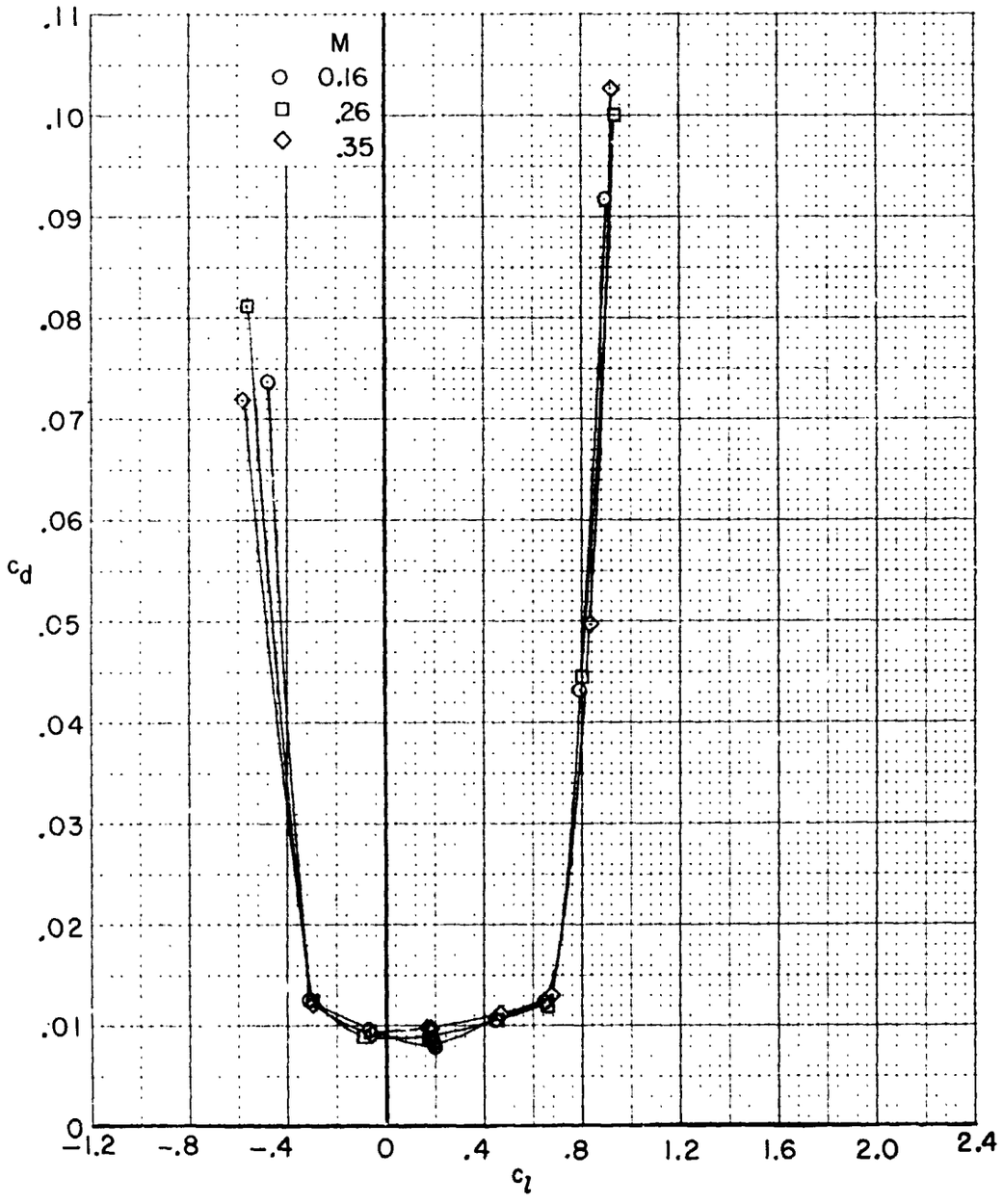

(b) c_d as a function of c_l.

Figure 10.- Concluded.

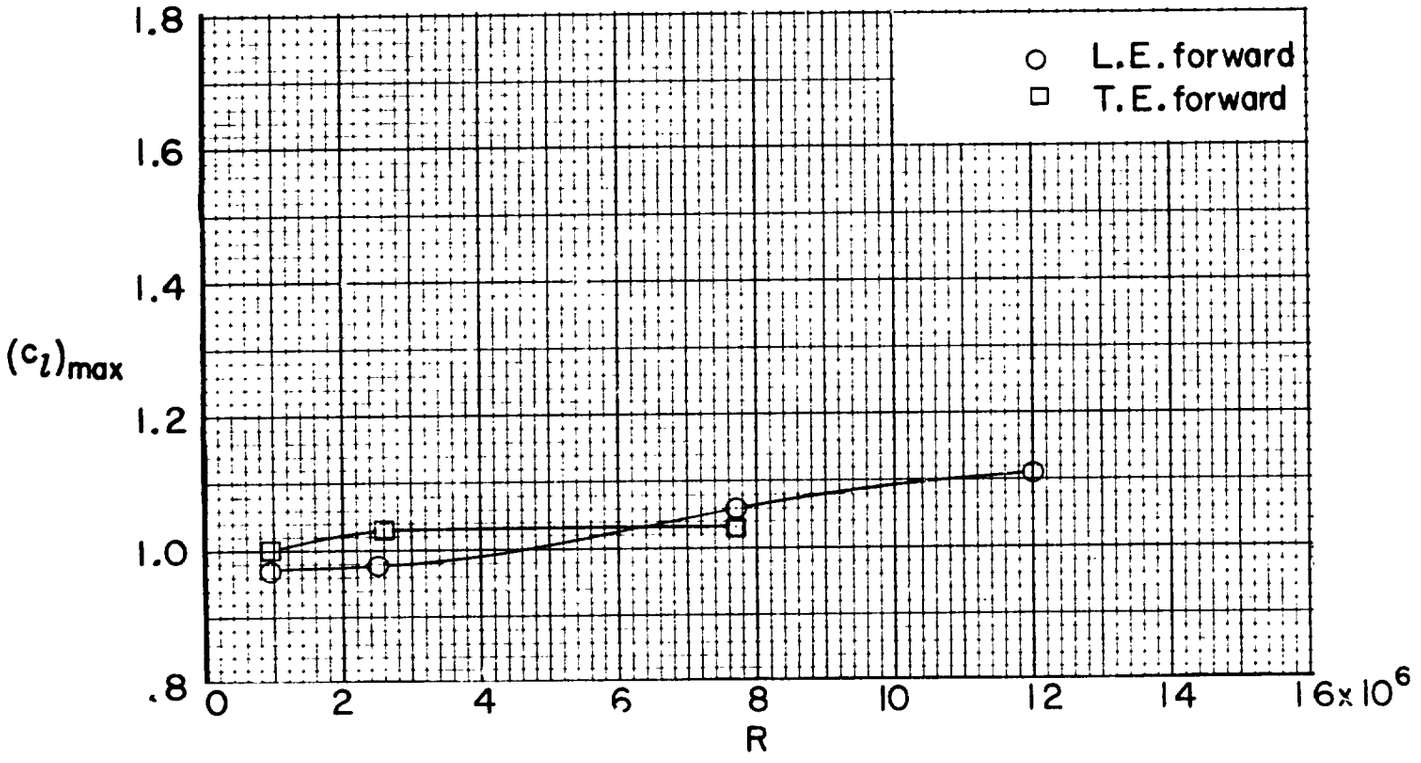

Figure 11.- Variation of maximum section lift coefficient with Reynolds number for 6-percent-thick airfoil. M = 0.26; smooth model.

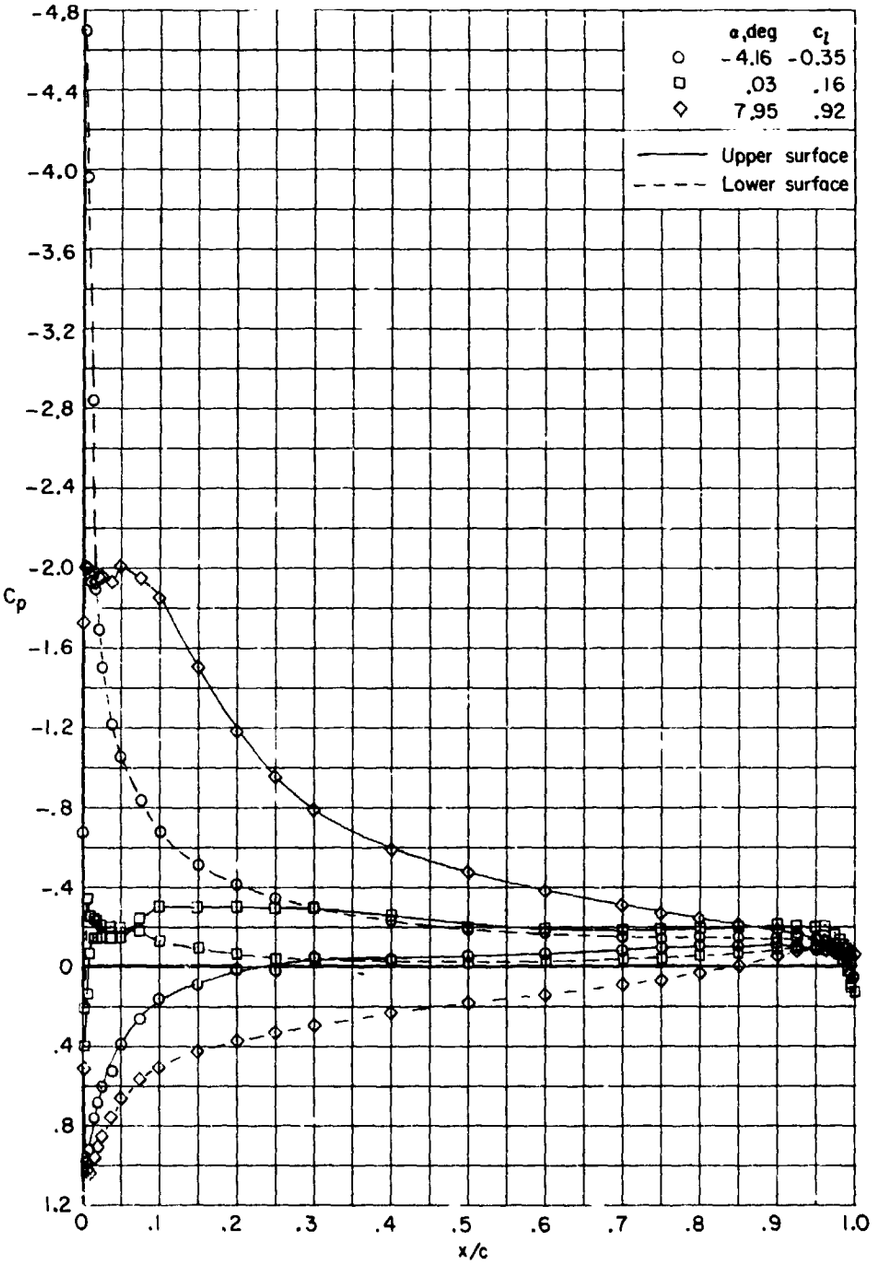

Figure 12.- Effect of angle of attack on pressure distributions for 6-percent-thick airfoil with leading edge forward. M = 0.26; R = 2.50 × 10^6; smooth model.

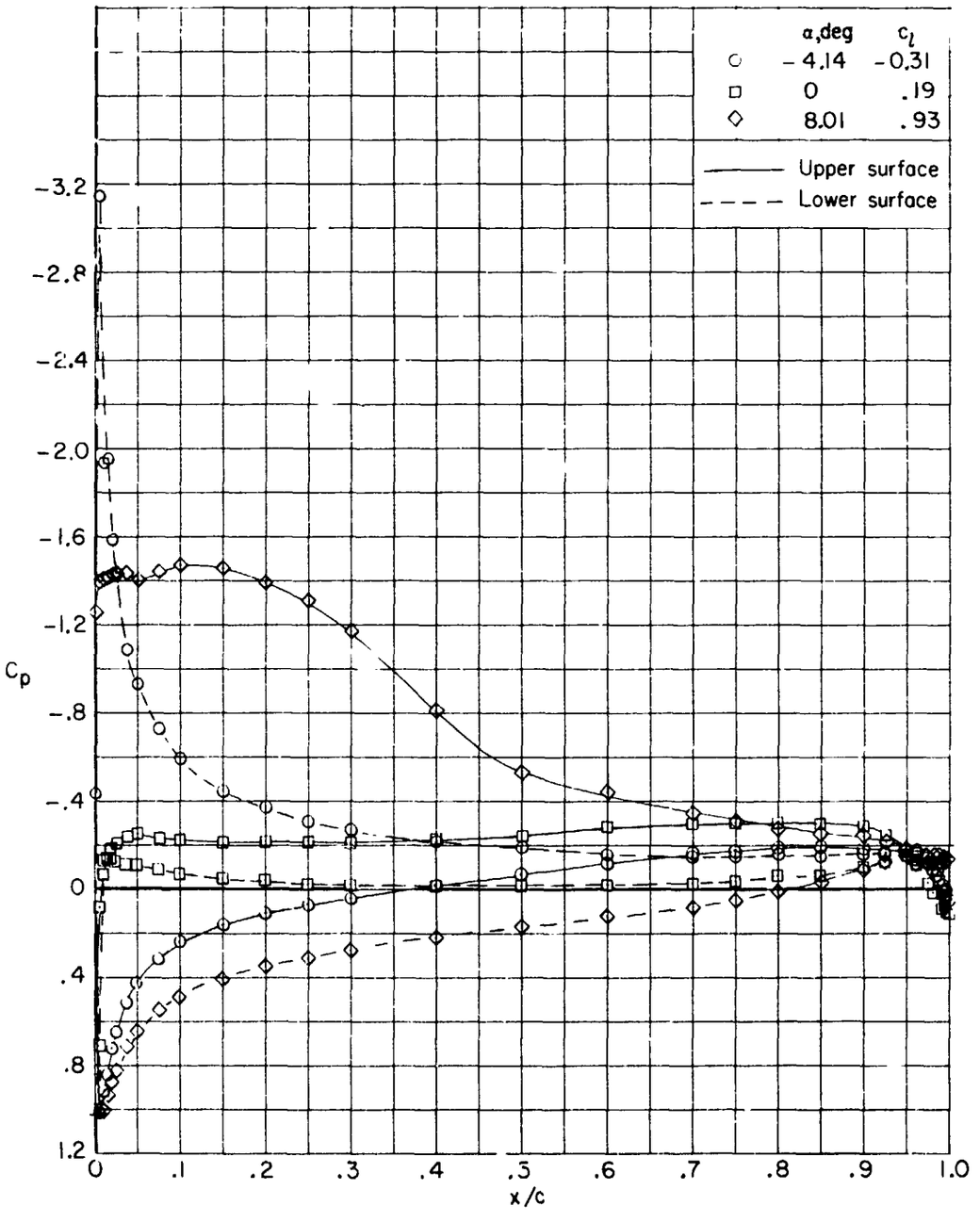

Figure 13.- Effect of angle of attack on pressure distributions for 6-percent-thick airfoil with trailing edge forward. $M = 0.26$; $R = 2.60 \times 10^6$; smooth model.

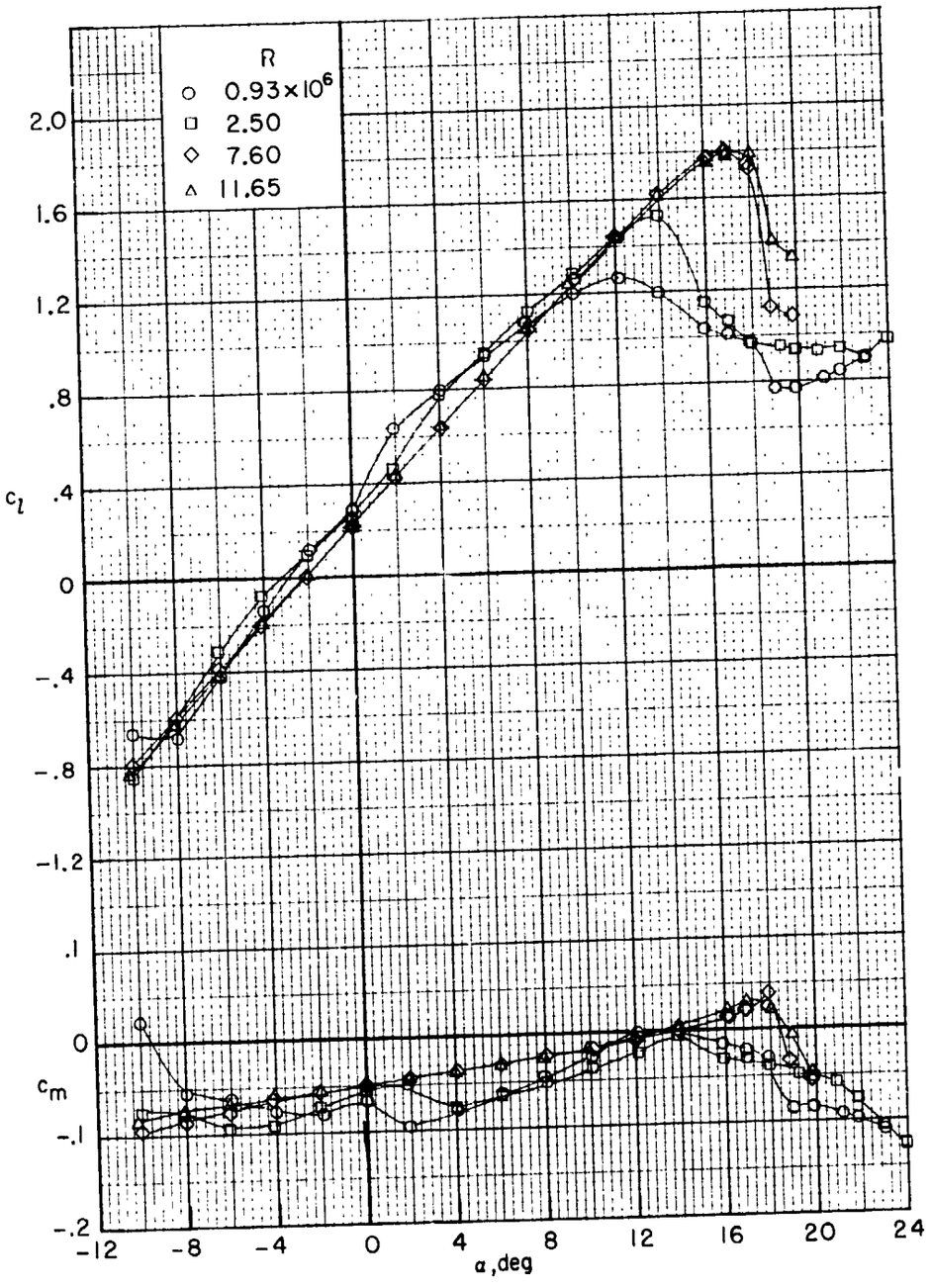

(a) c_l and c_m as a function of α.

Figure 14.- Effect of Reynolds number on section characteristics for 12-percent-thick airfoil with leading edge forward. M = 0.26; smooth model.

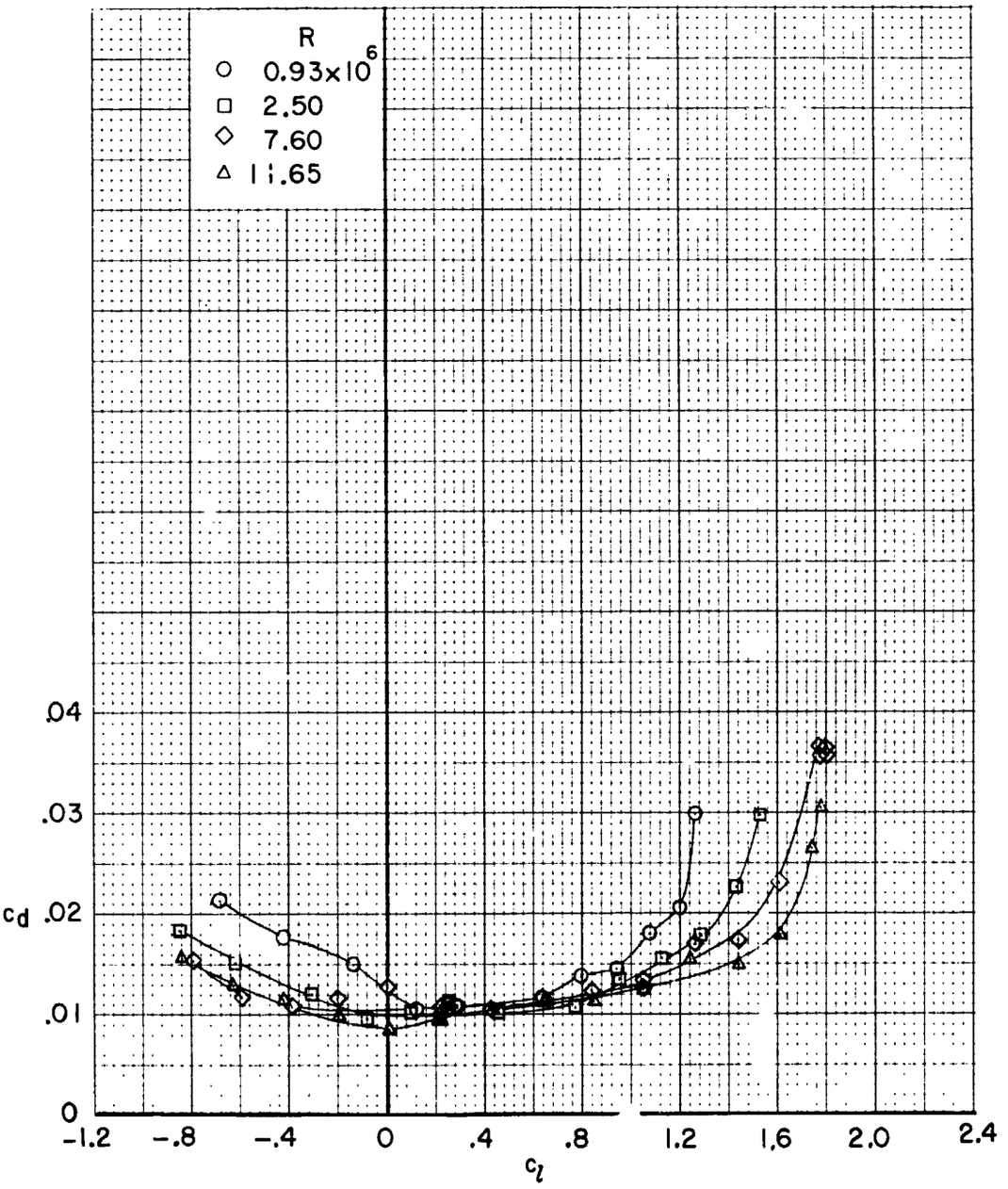

(b) c_d as a function of c_l.

Figure 14.- Concluded.

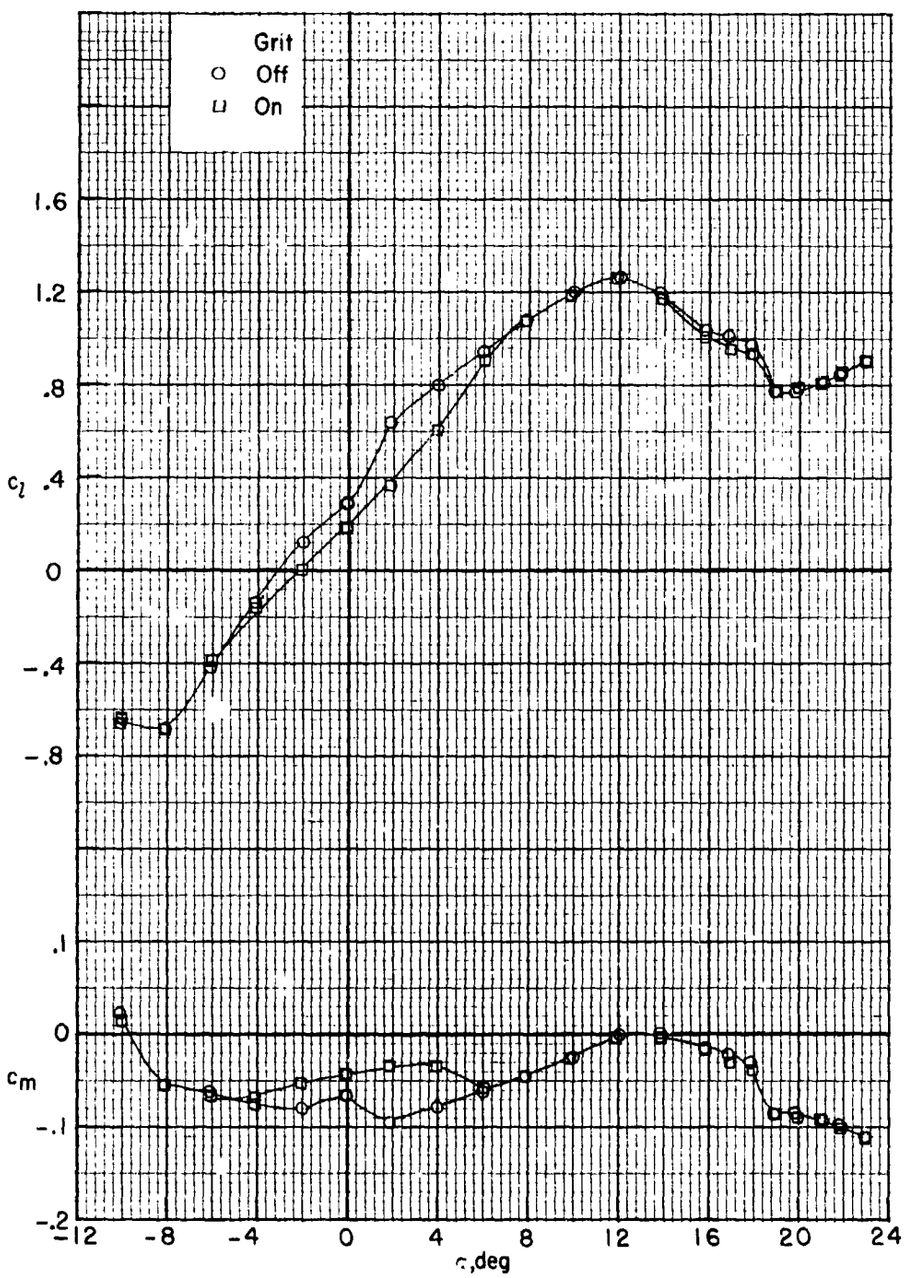

(a) $R = 0.93 \times 10^6$.

Figure 15.- Effect of roughness on section characteristics for 12-percent-thick airfoil with leading edge forward. Grit located at 0.05c; M = 0.26.

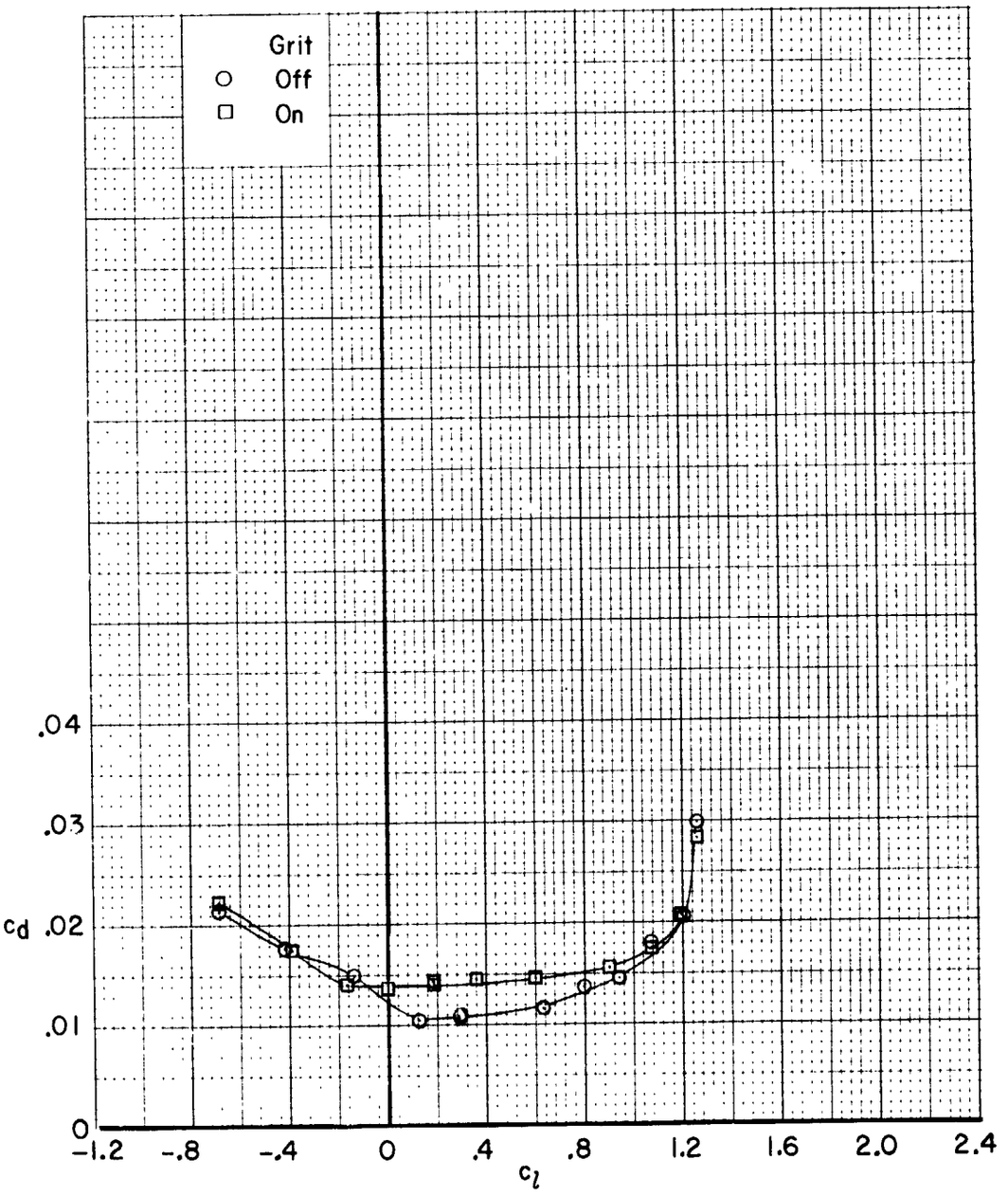

(a) $R = 0.93 \times 10^6$. Concluded.

Figure 15.- Continued.

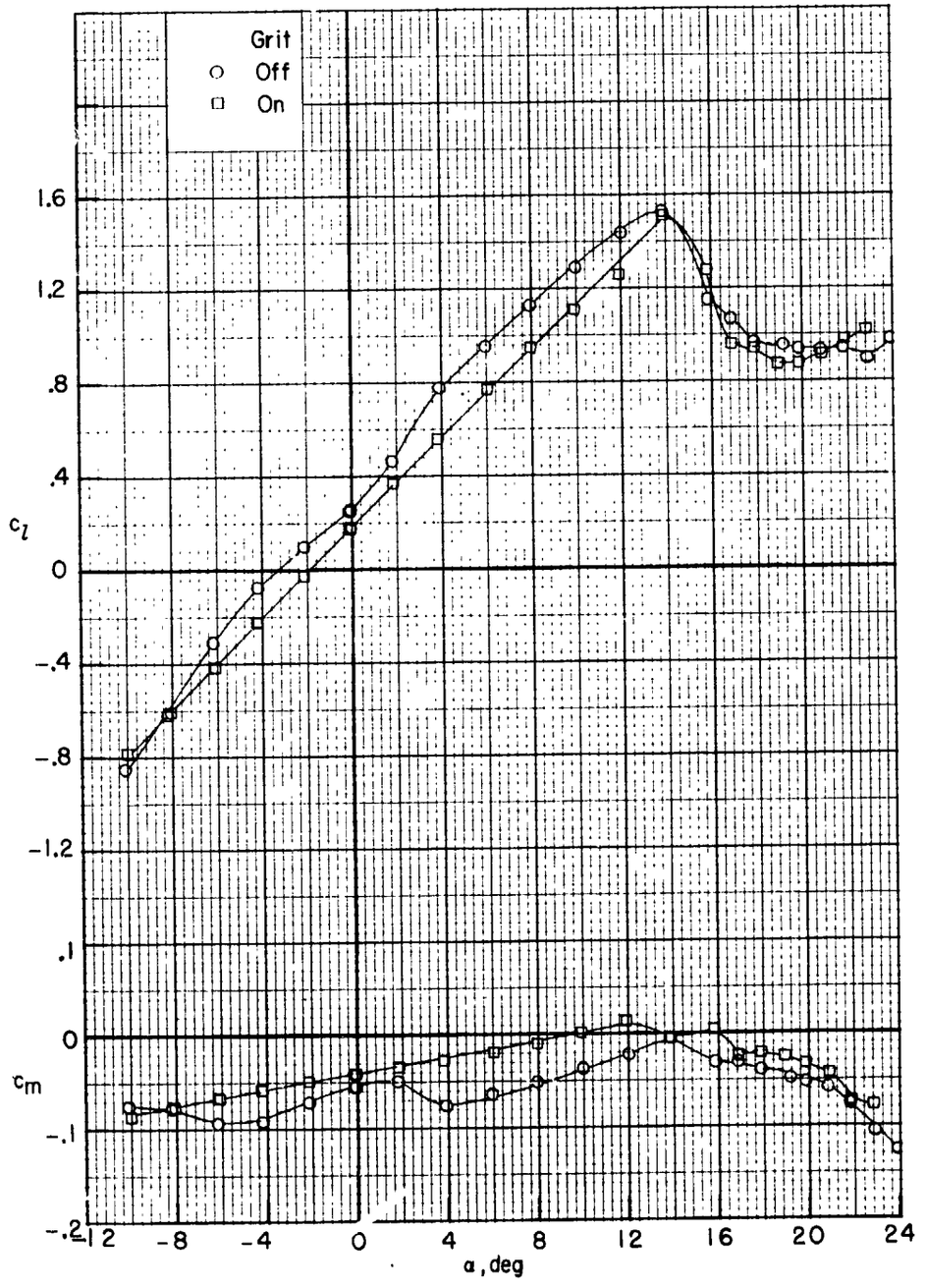

(b) $R = 2.50 \times 10^6$.

Figure 15.- Continued.

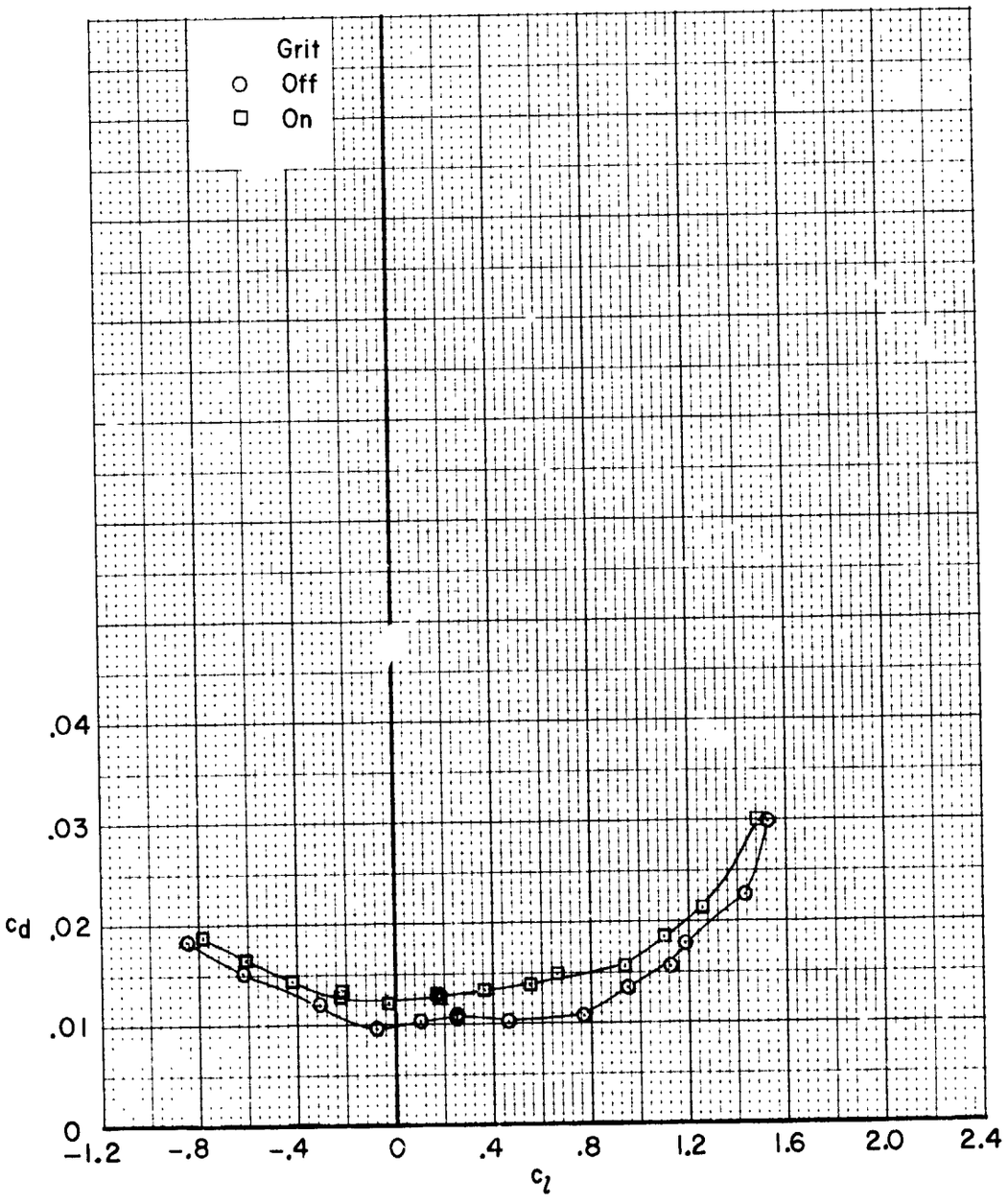

(b) $R = 2.50 \times 10^6$. Concluded.

Figure 15.- Continued.

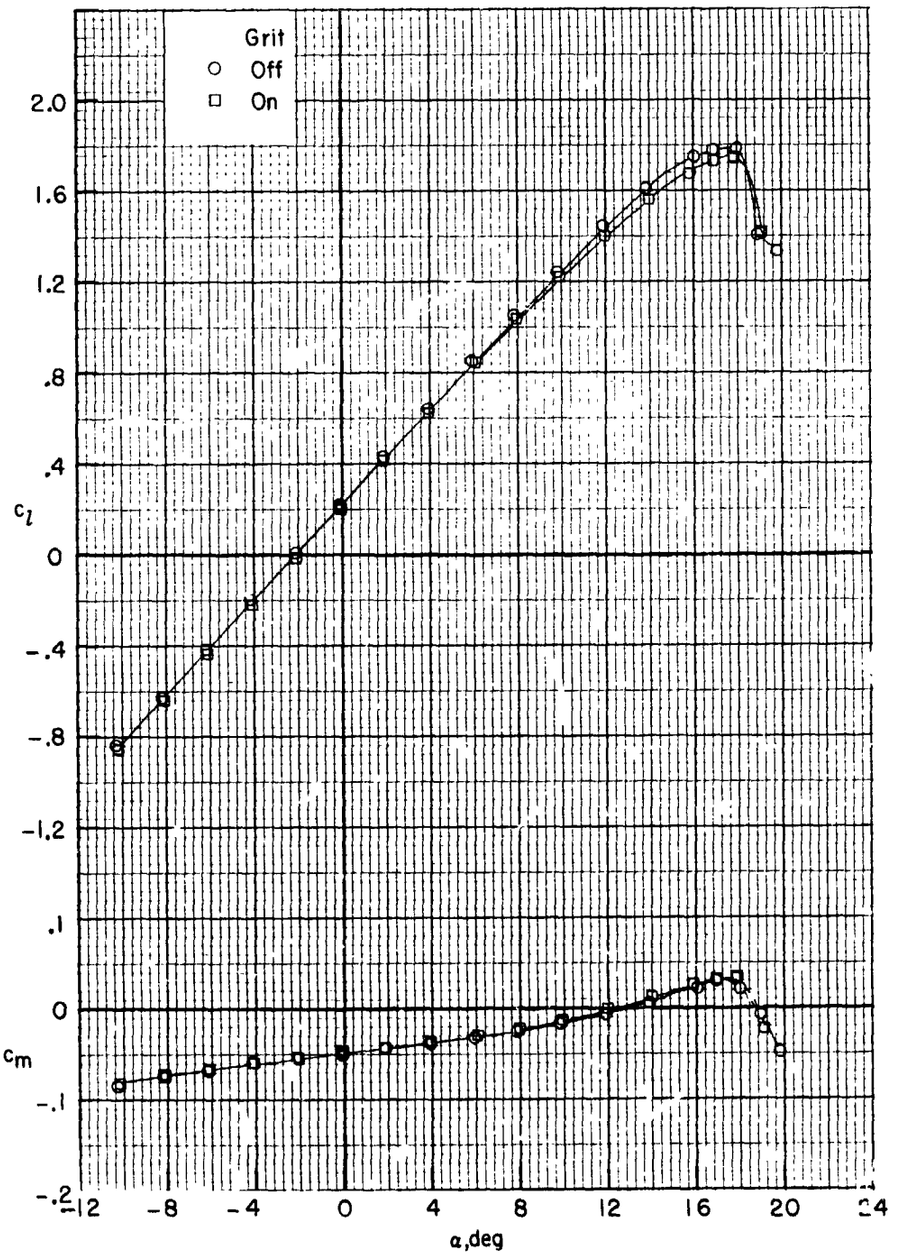

(c) $R = 11.65 \times 10^6$.

Figure 15.- Continued.

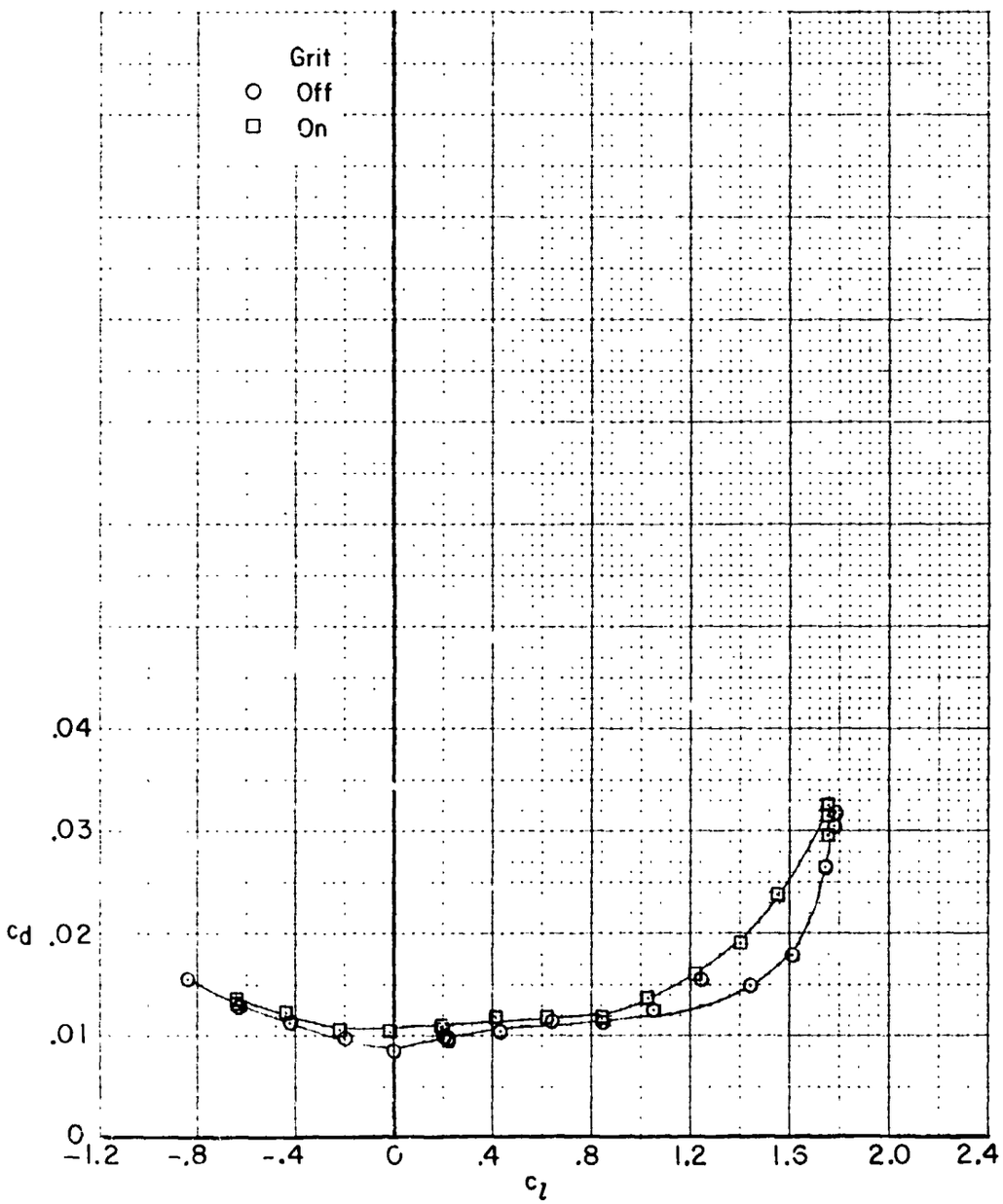

(c) R = 11.65×10^6. Concluded.

Figure 15.- Concluded.

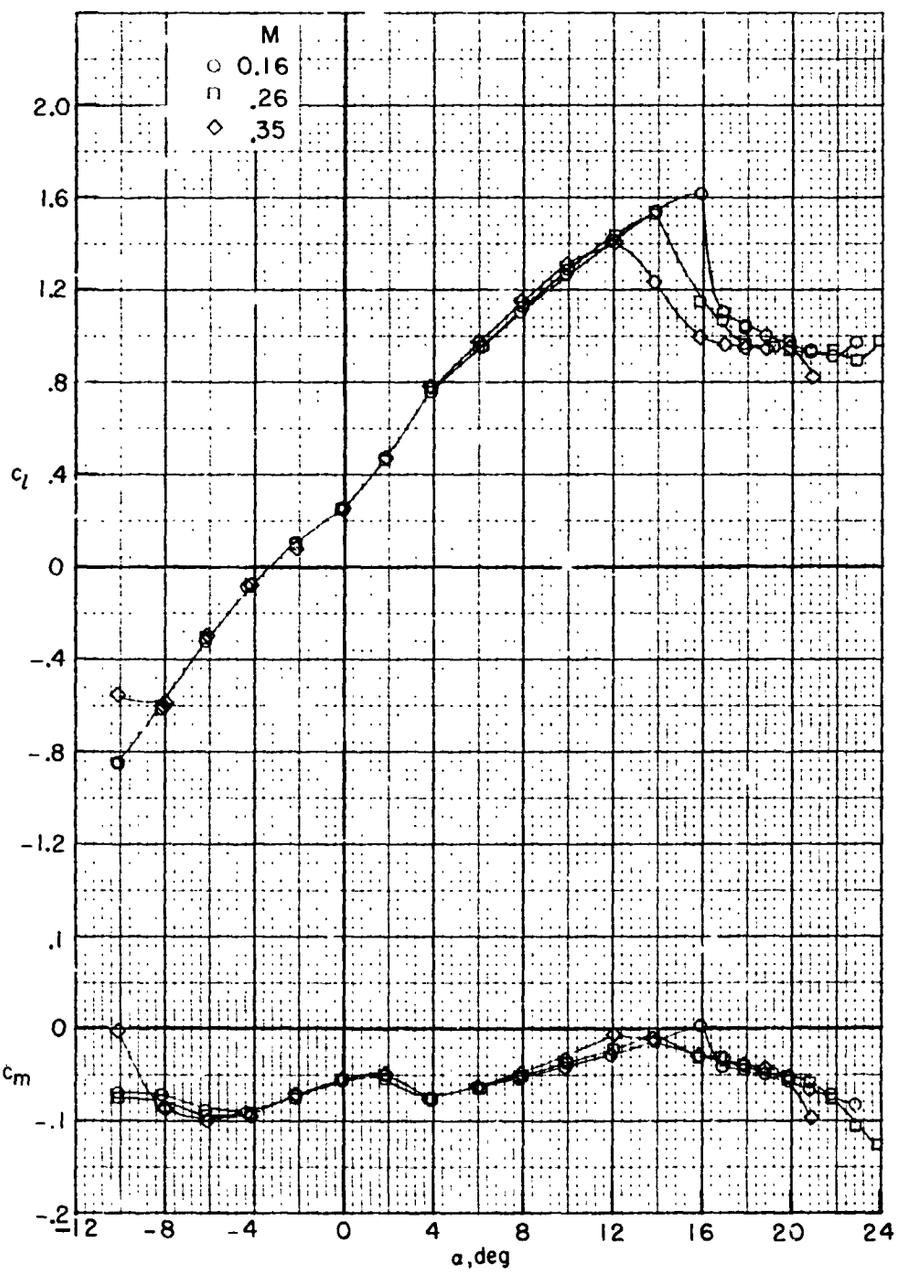

(a) c_l and c_m as a function of α.

Figure 16.- Effect of Mach number on section characteristics for 12-percent-thick airfoil with leading edge forward. $R = 2.50 \times 10^6$; smooth model.

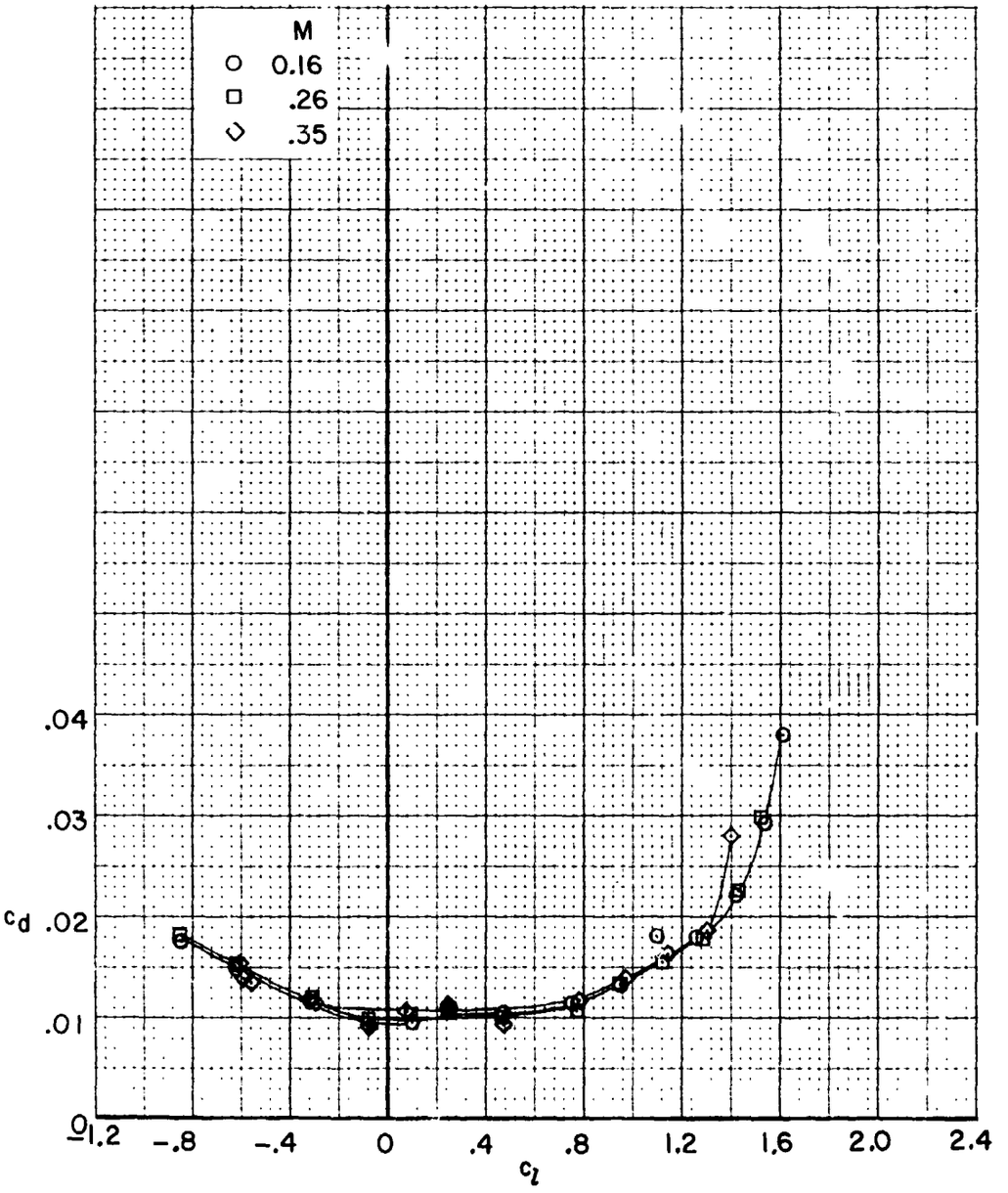

(b) c_d as a function of c_l.

Figure 16.- Concluded.

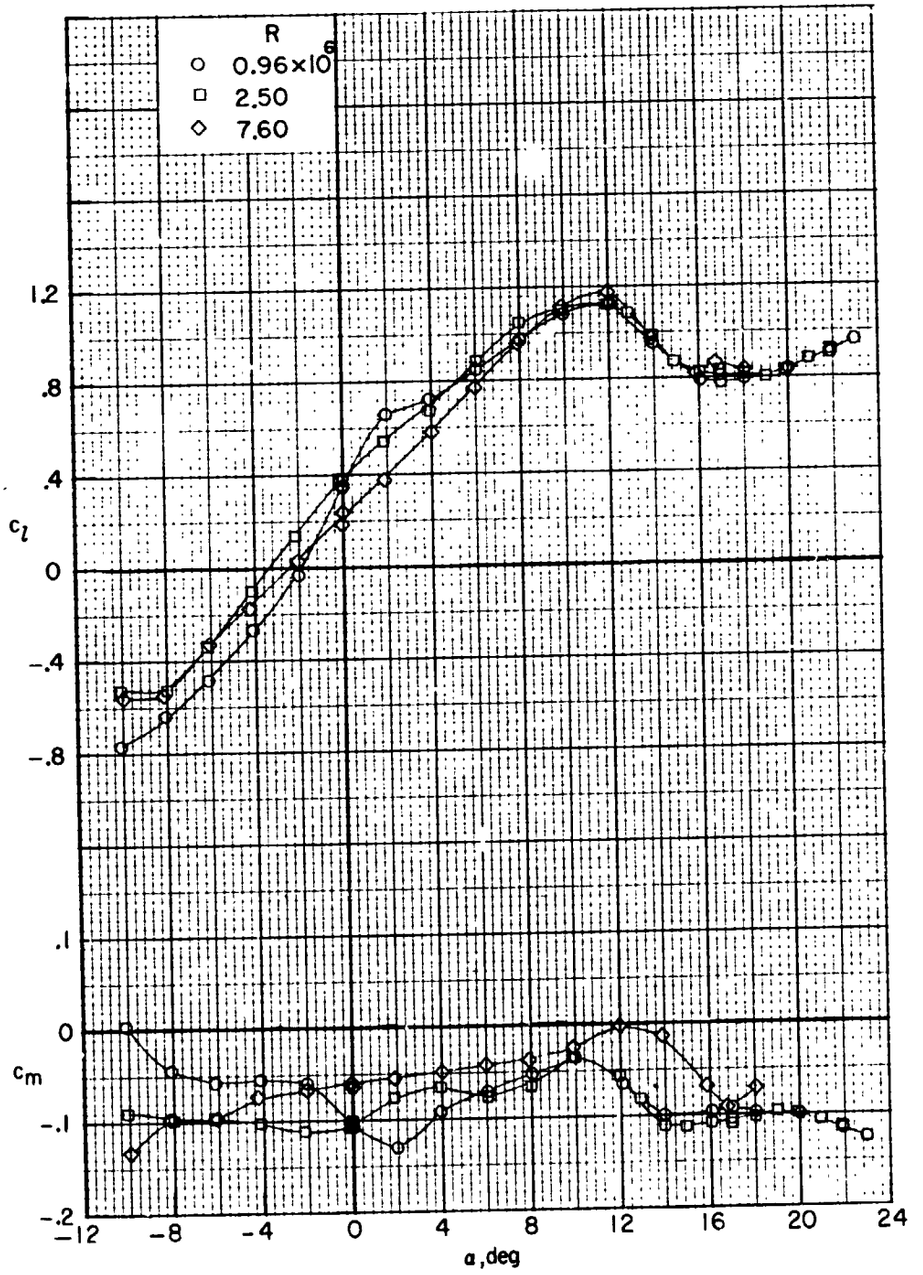

(a) c_l and c_m as a function of α.

Figure 17.- Effect of Reynolds number on section characteristics for 12-percent-thick airfoil with trailing edge forward. M = 0.26; smooth model.

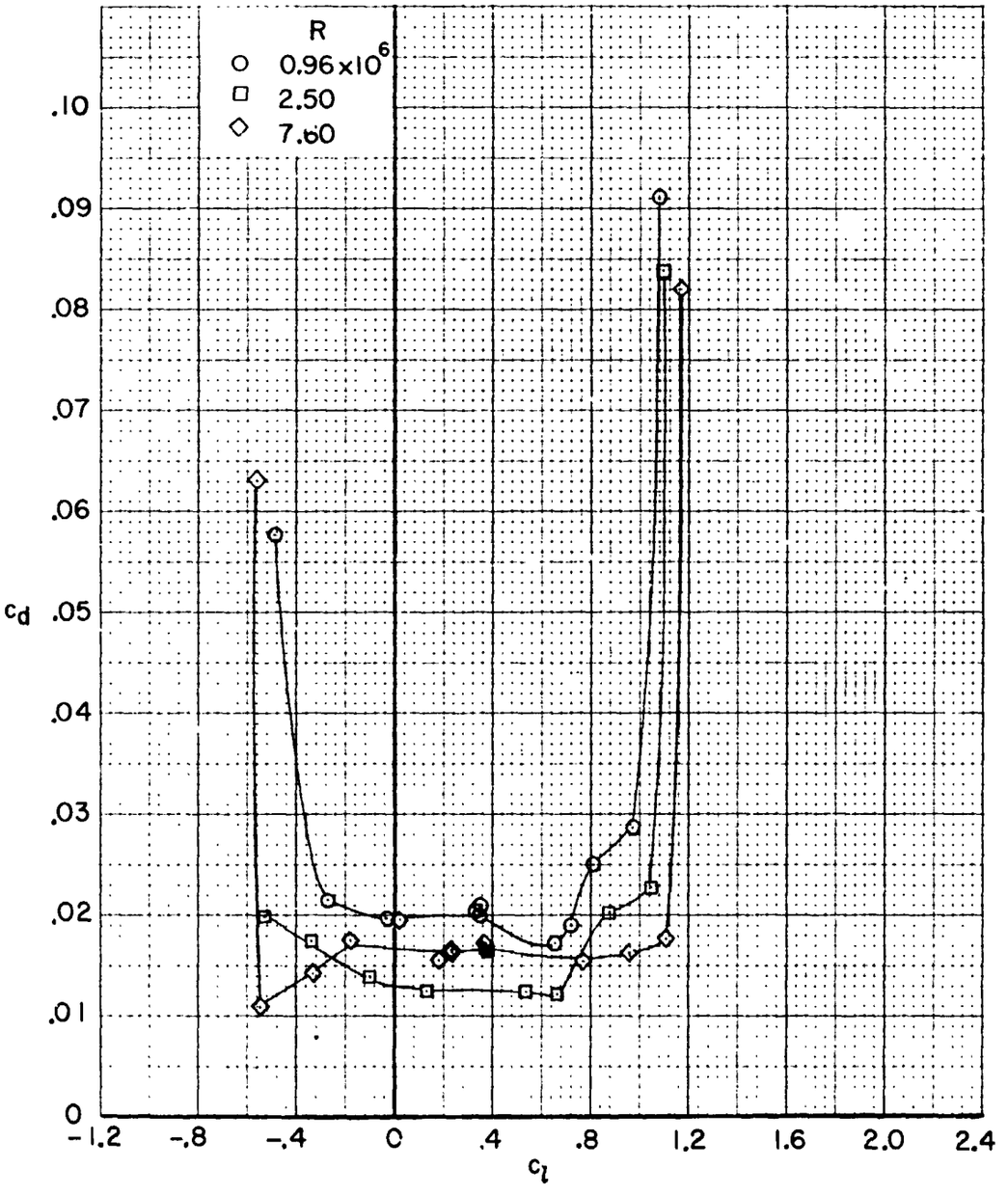

(b) c_d as a function of c_l.

Figure 17.- Concluded.

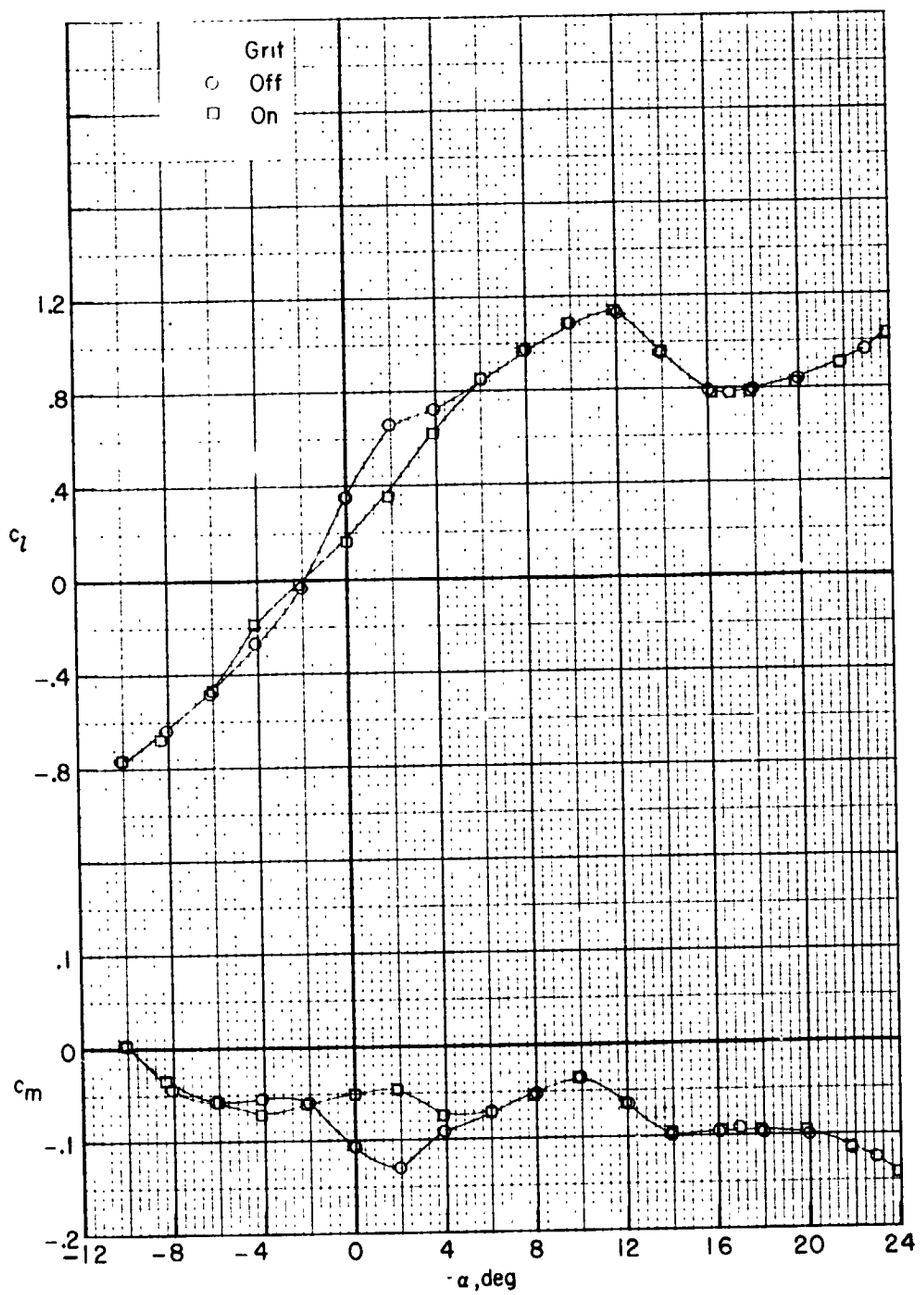

(a) $R = 0.96 \times 10^6$.

Figure 18.- Effect of roughness on section characteristics for 12-percent-thick airfoil with trailing edge forward. Grit located at 0.05c; M = 0.26.

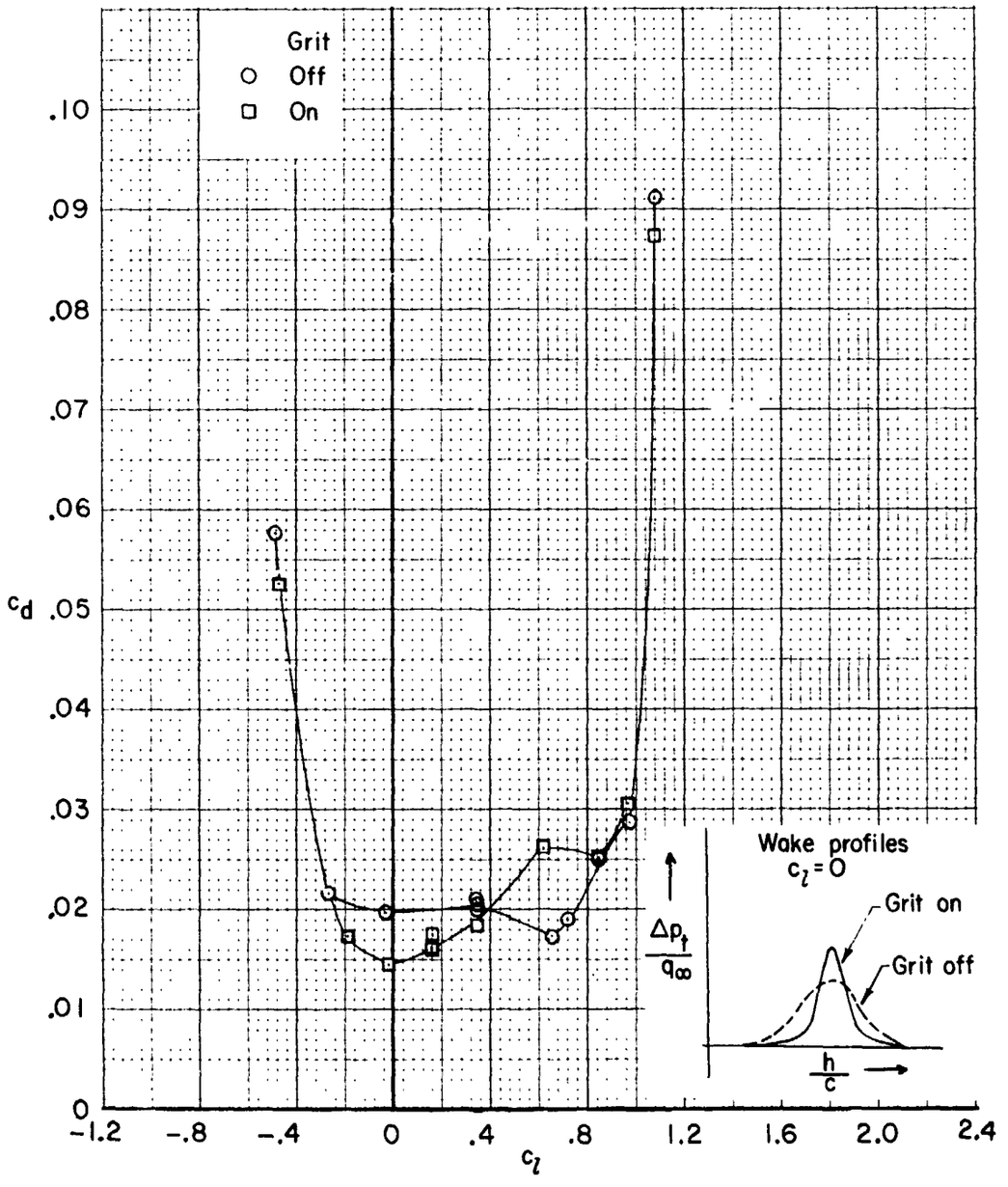

(a) R = 0.96×10^6. Concluded.

Figure 18.- Continued.

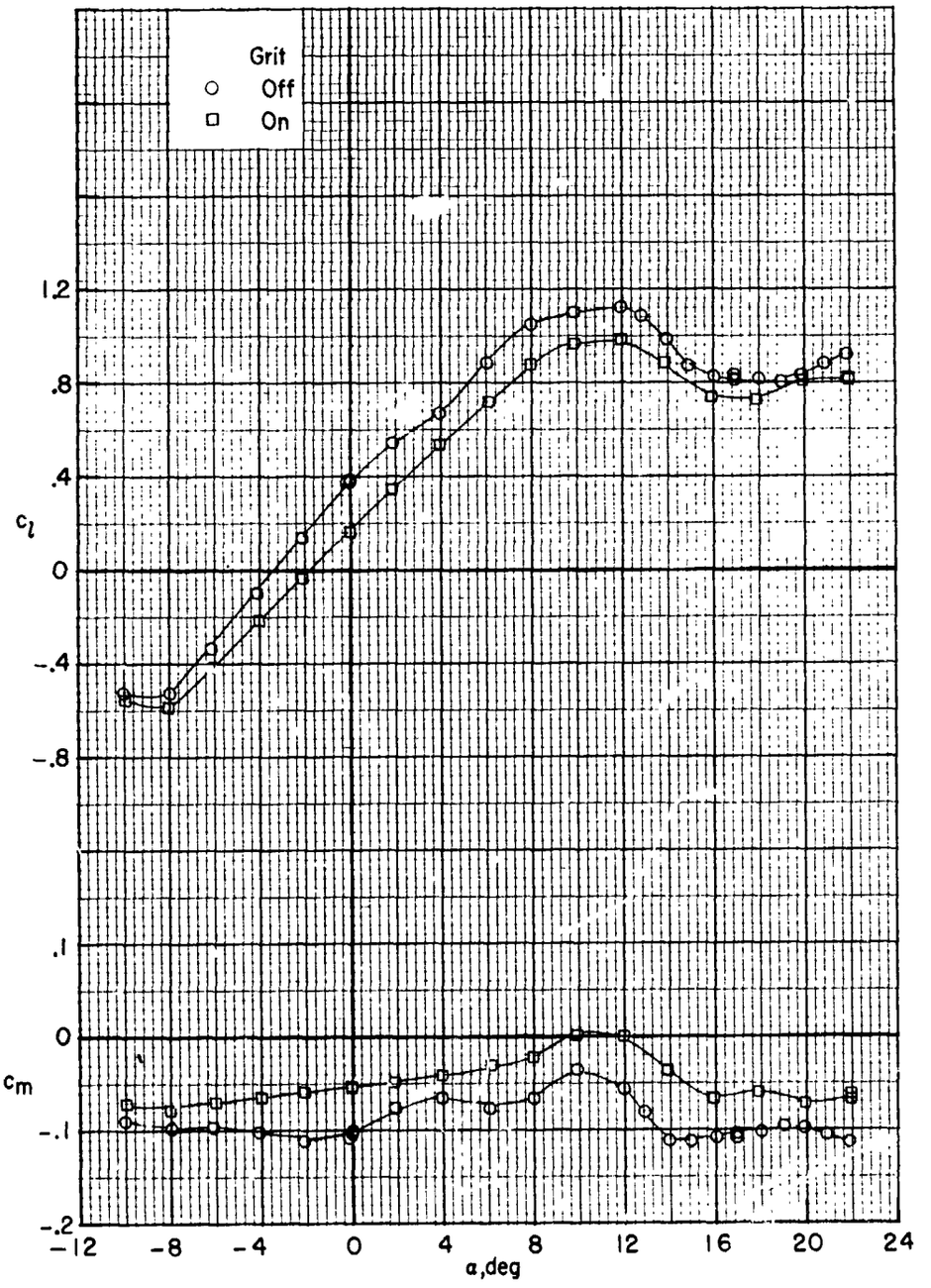

(b) $R = 2.50 \times 10^6$.

Figure 18.- Continued.

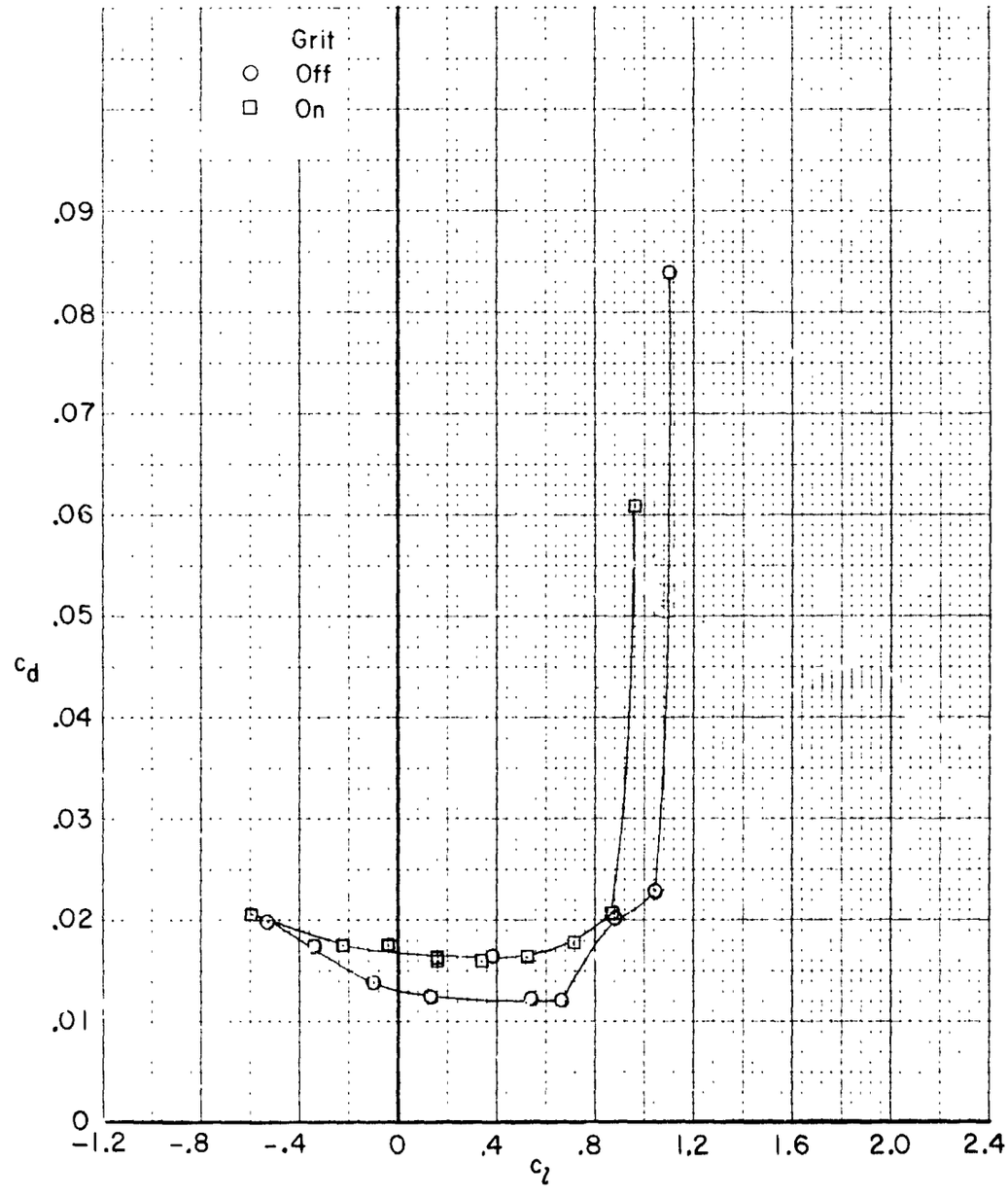

(b) $R = 2.50 \times 10^6$. Concluded.

Figure 18.- Continued.

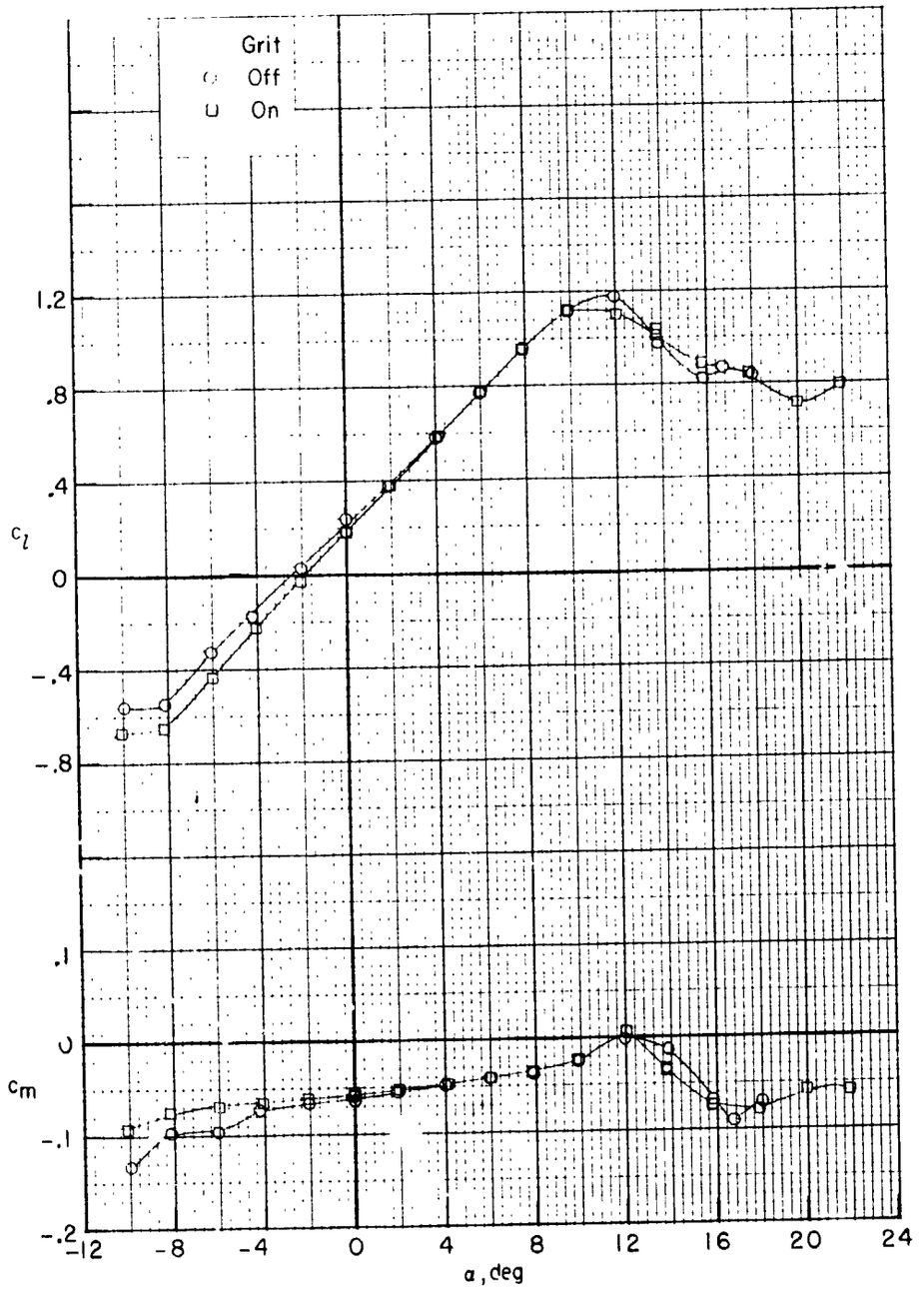

(c) $R = 7.60 \times 10^6$.

Figure 18.- Continued.

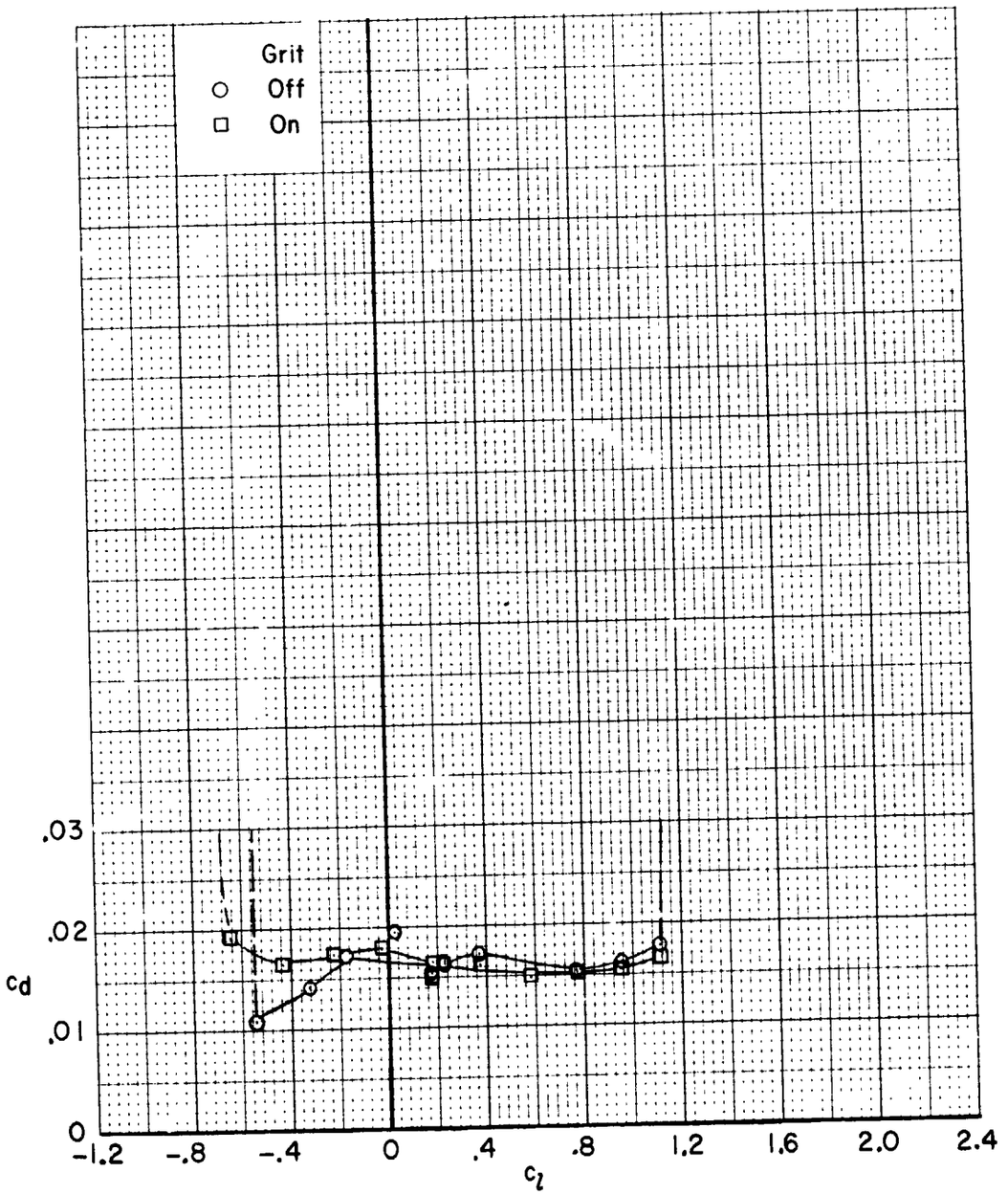

(c) R = 7.60×10^6. Concluded.

Figure 18.- Concluded.

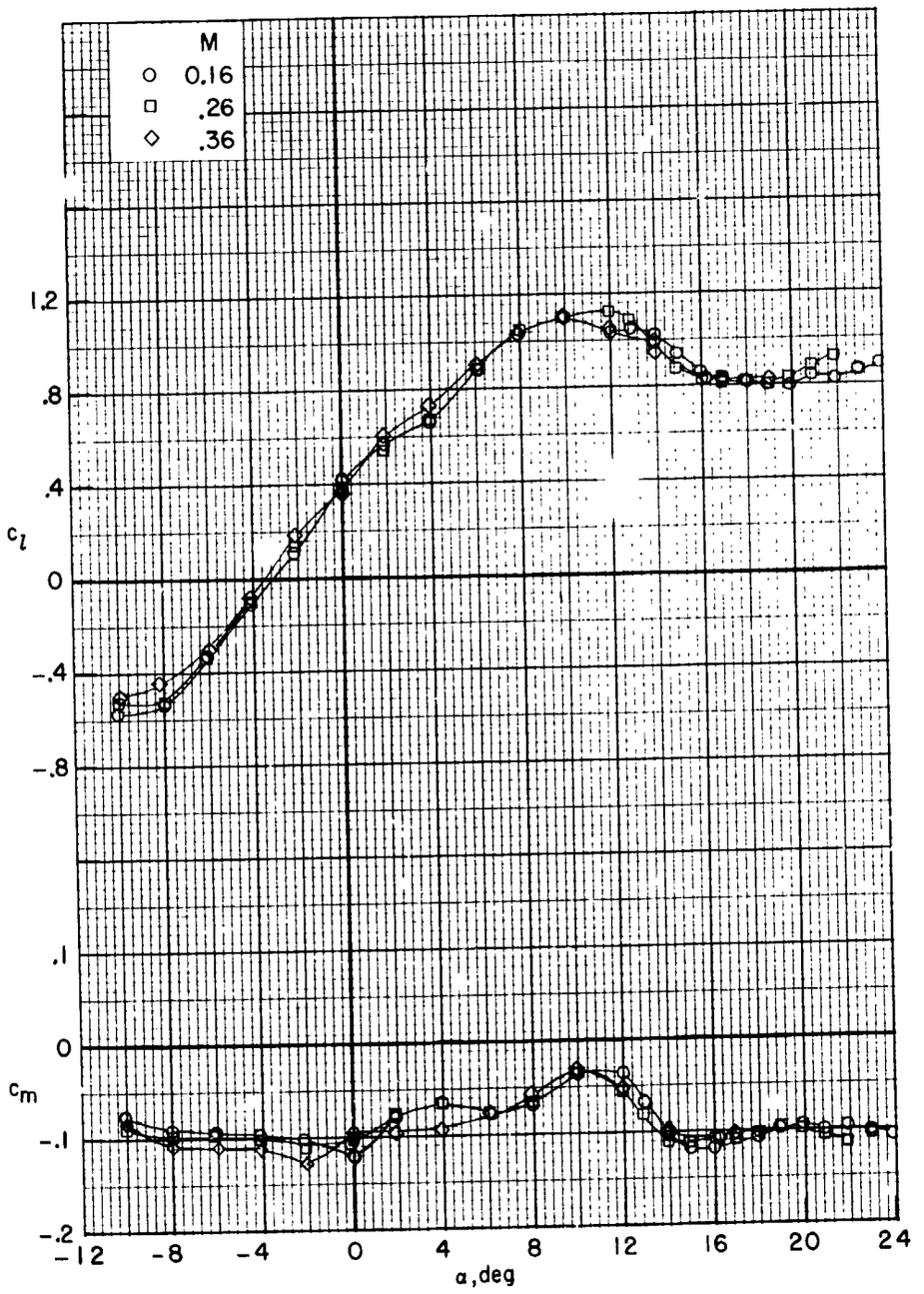

(a) c_l and c_m as a function of α.

Figure 19.- Effect of Mach number on section characteristics for 12-percent-thick airfoil with trailing edge forward. $R \approx 2.50 \times 10^6$; smooth model.

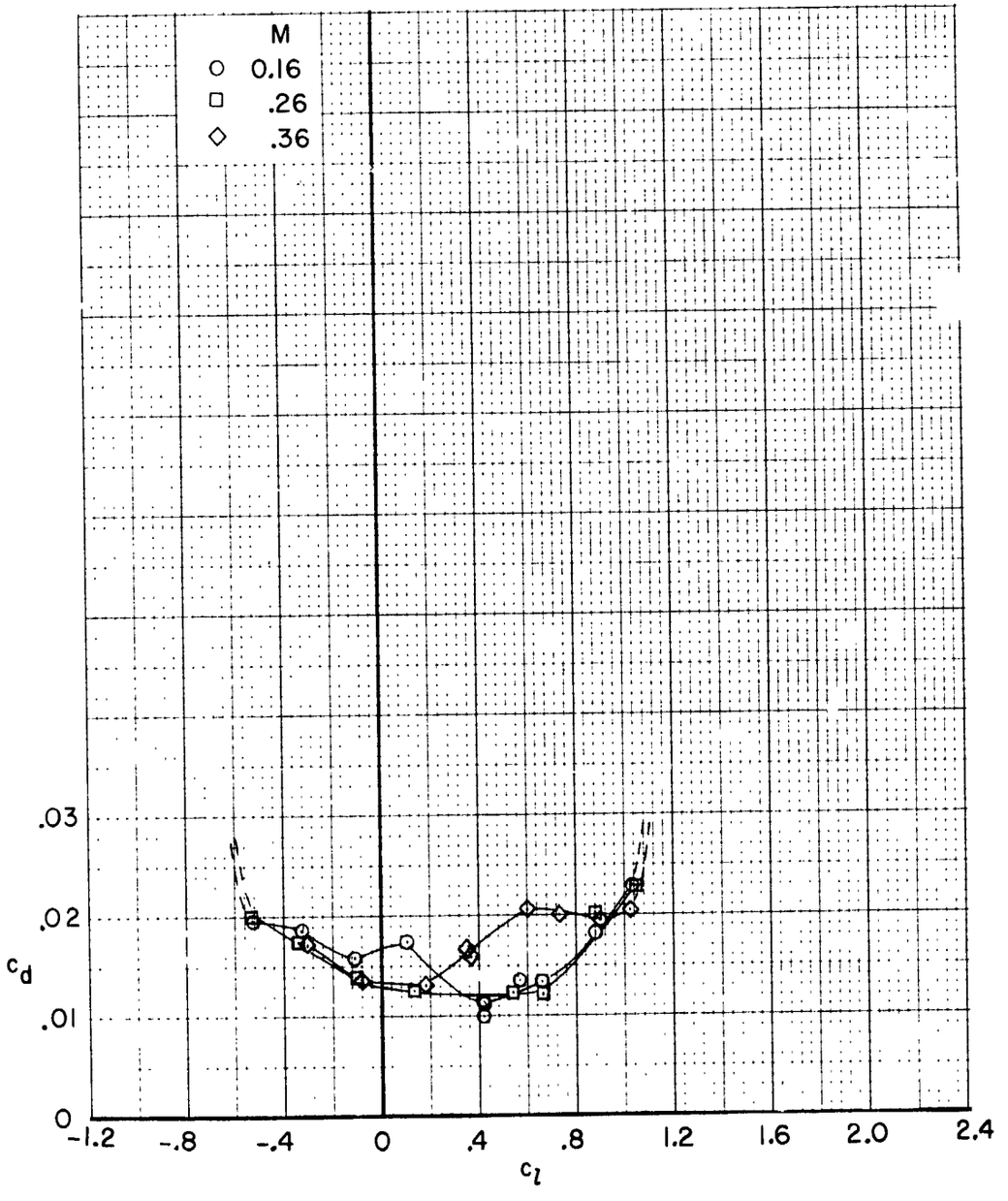

(b) c_d as a function of c_l.

Figure 19.- Concluded.

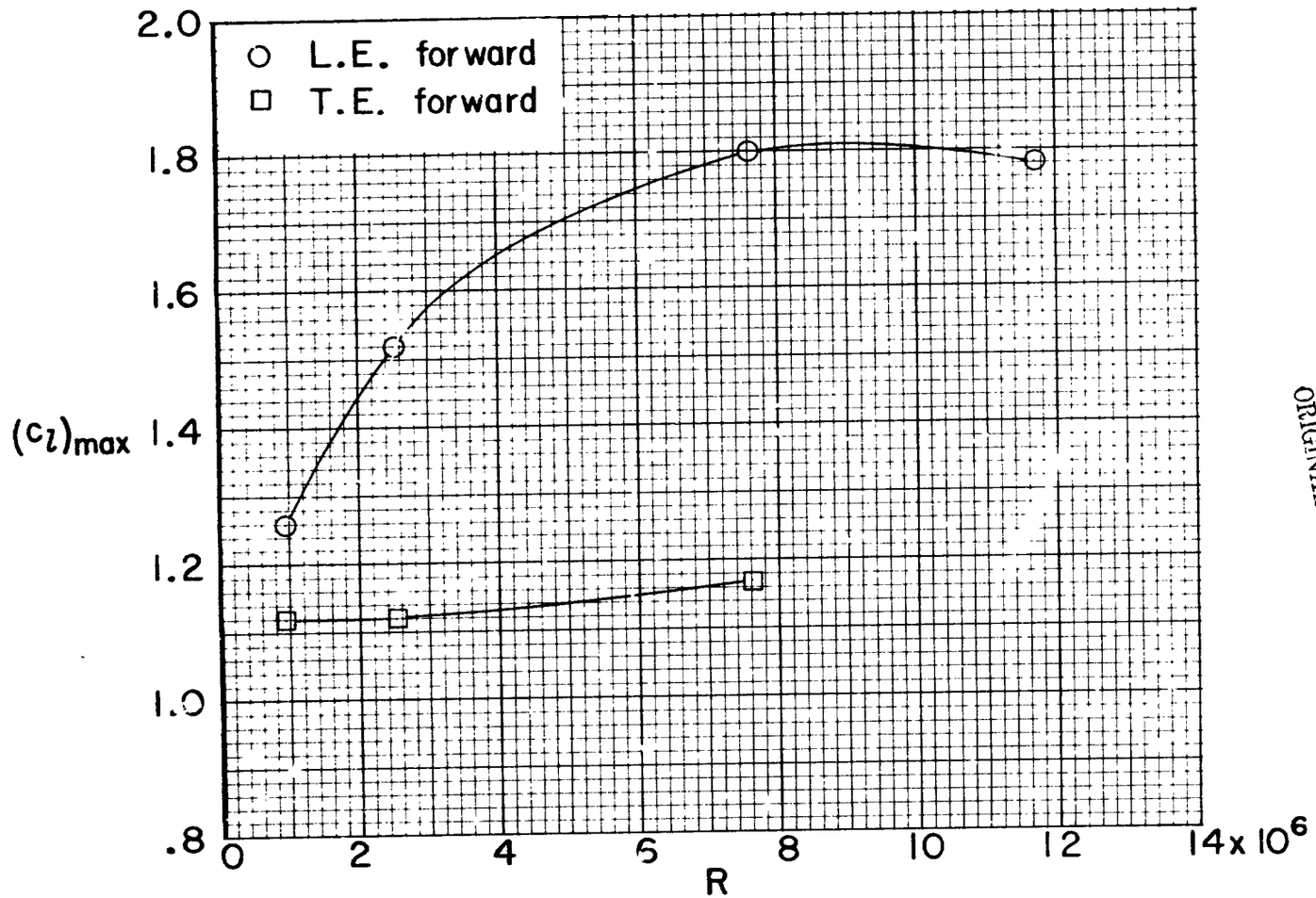

Figure 20.- Variation of maximum section lift coefficient with Reynolds number for 12-percent-thick airfoil. M = 0.26; smooth model.

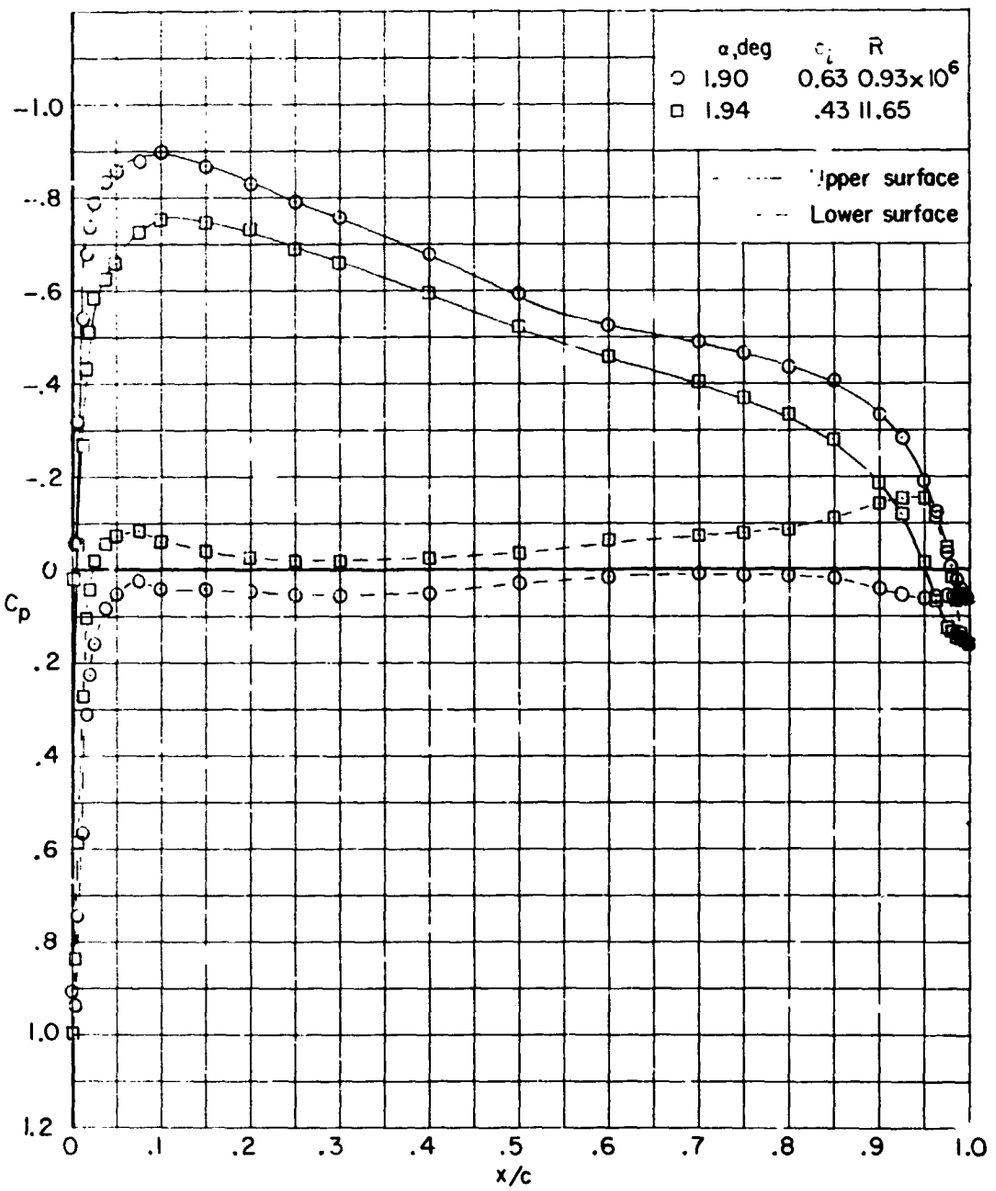

(a) Low angle of attack.

Figure 21.- Effect of Reynolds number on pressure distributions for 12-percent-thick airfoil with leading edge forward. M = 0.26; smooth model.

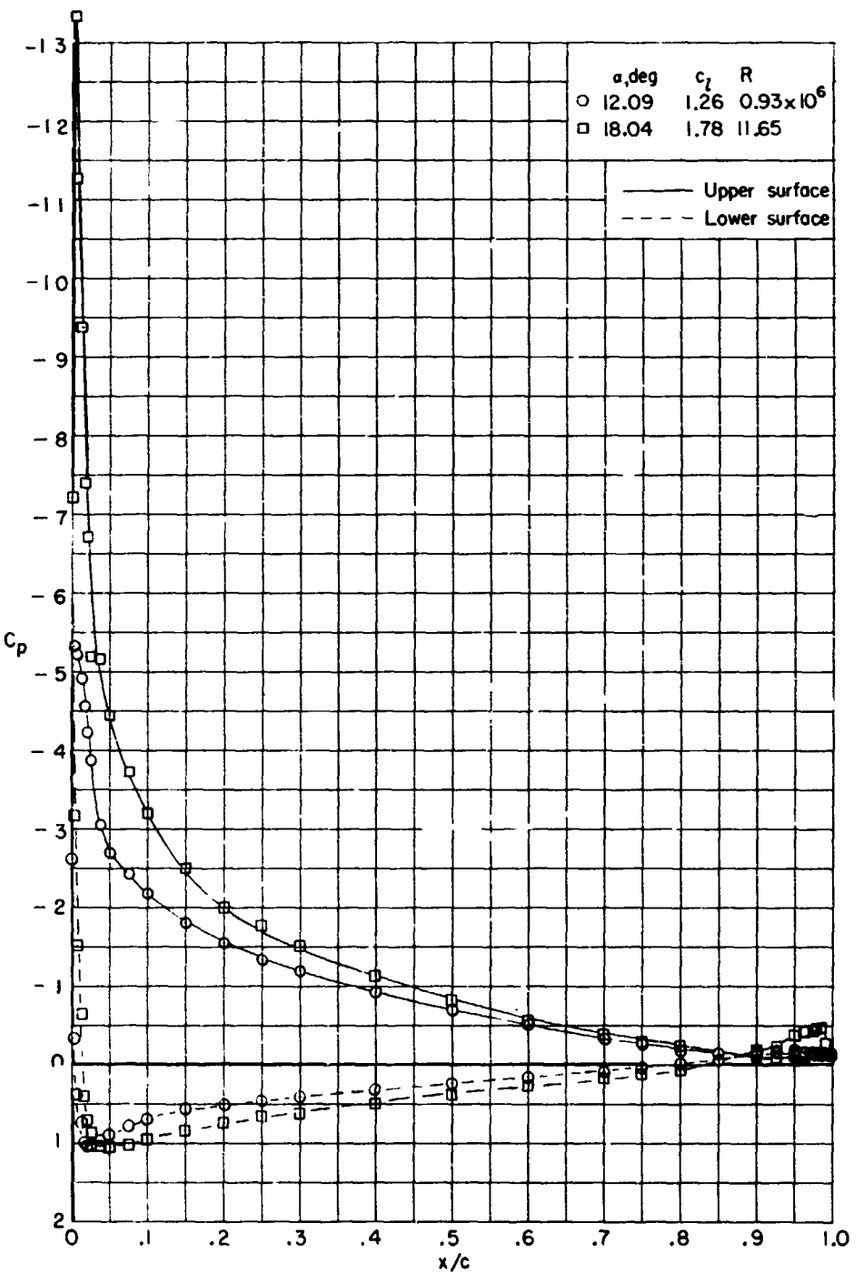

(b) High angle of attack.

Figure 21.- Concluded.

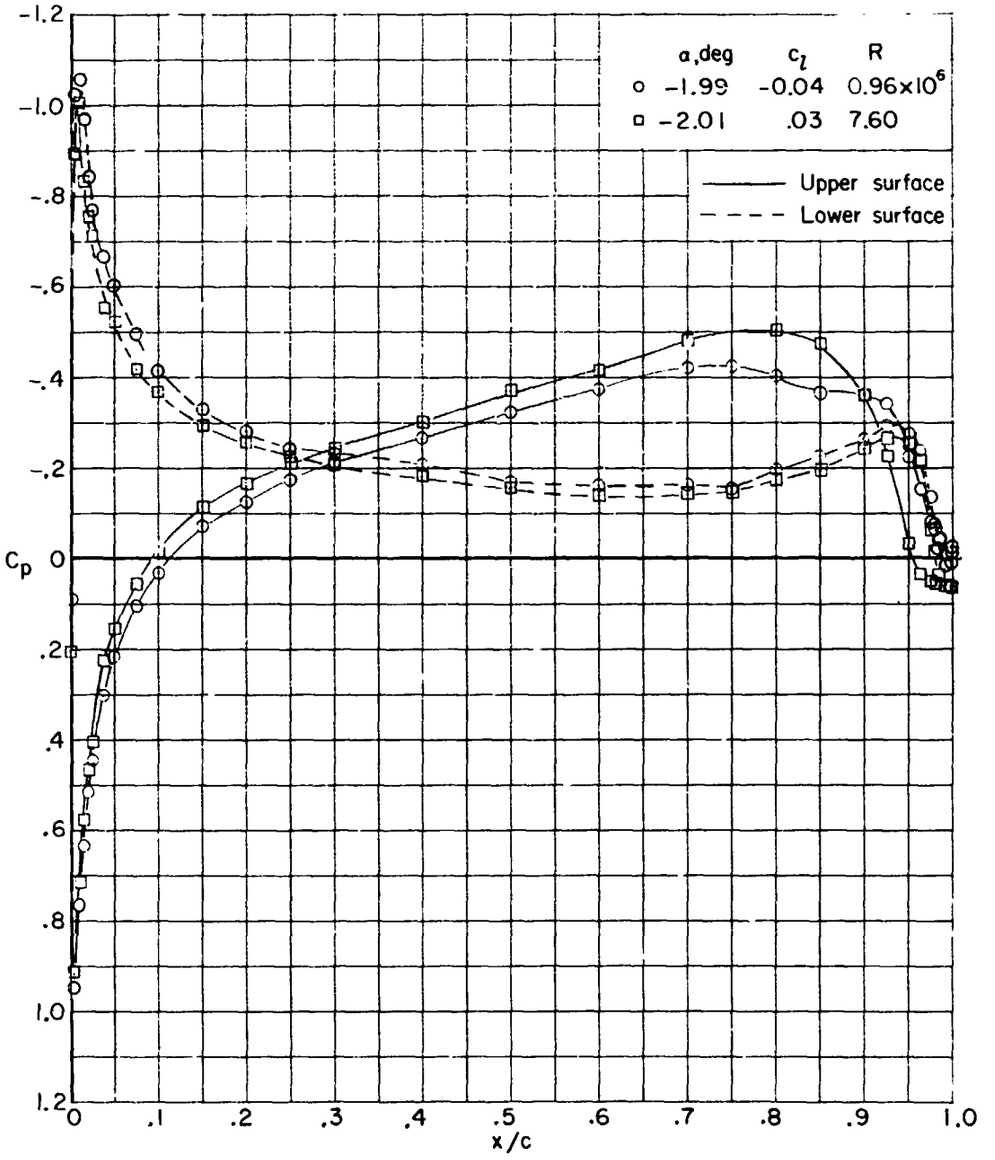

(a) $\alpha \approx -2^{\circ}$.

Figure 22.- Effect of Reynolds number on pressure distributions for 12-percent-thick airfoil with trailing edge forward. M = 0.26; smooth model.

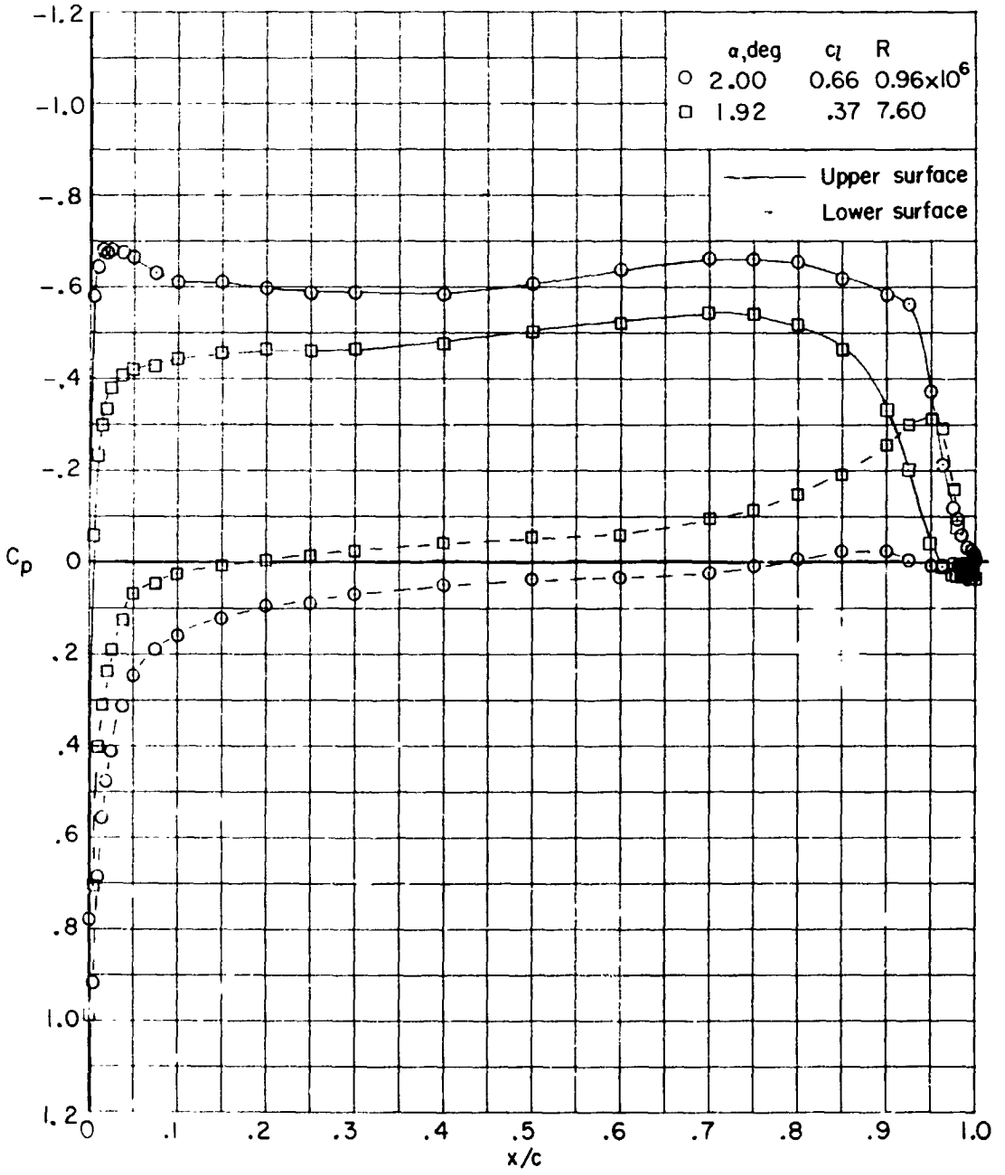

(b) $\alpha \approx 2^{o}$.

Figure 22.- Continued.

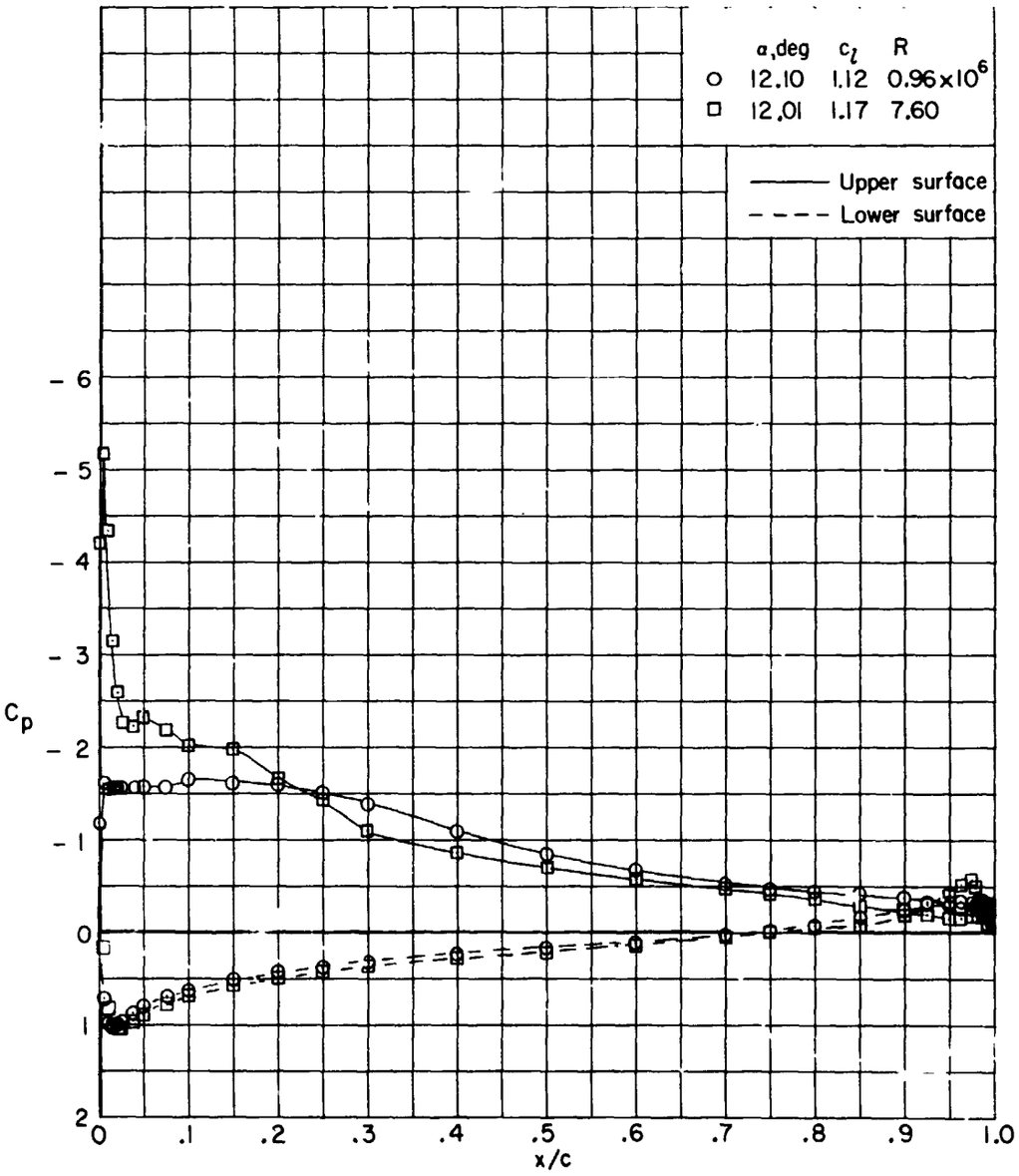

(c) $\alpha \approx 12^{o}$.

Figure 22.- Concluded.

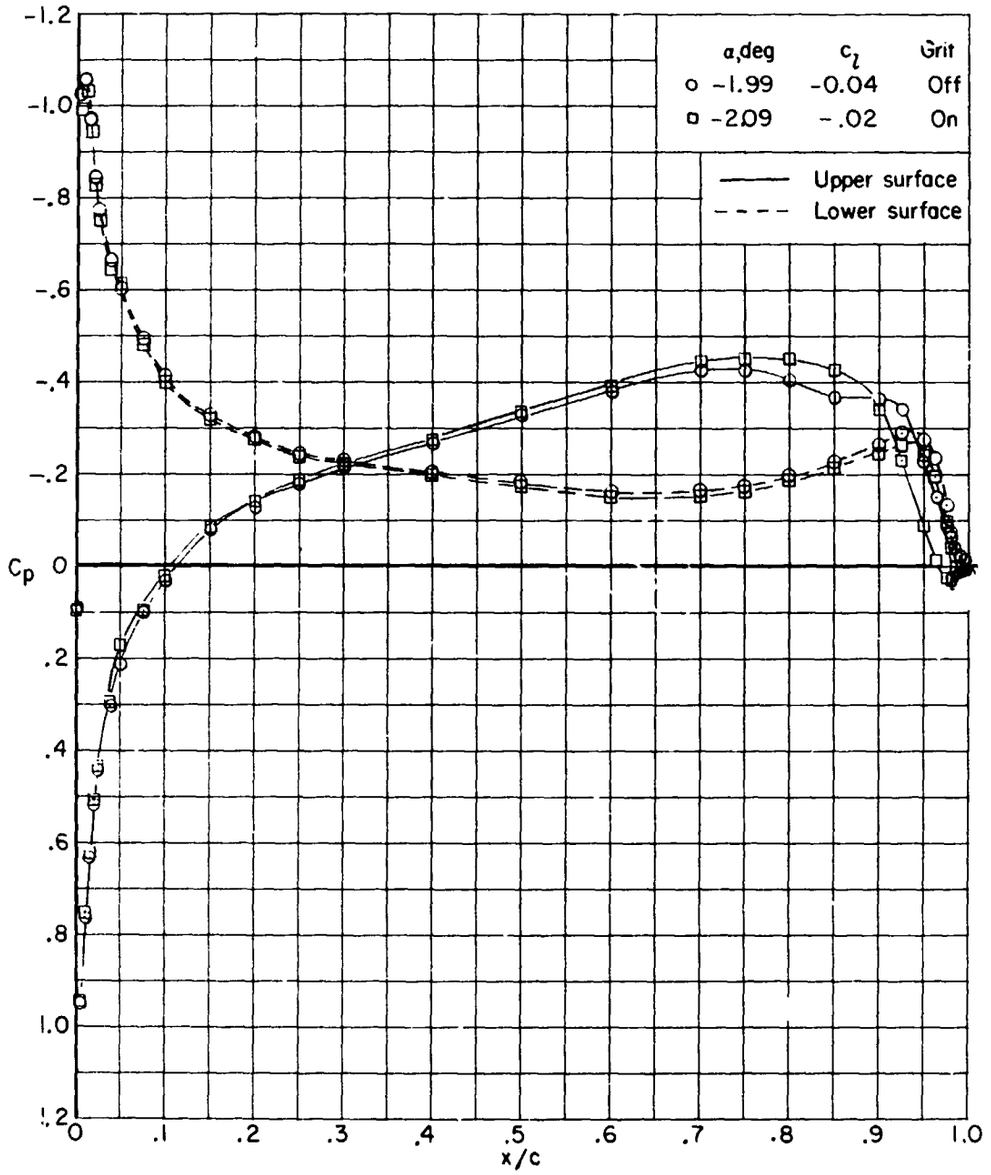

Figure 23.- Effect of roughness on pressure distributions for 12-percent-thick airfoil with trailing edge forward. $R = 0.96 \times 10^6$; grit located at 0.05c; M = 0.26.

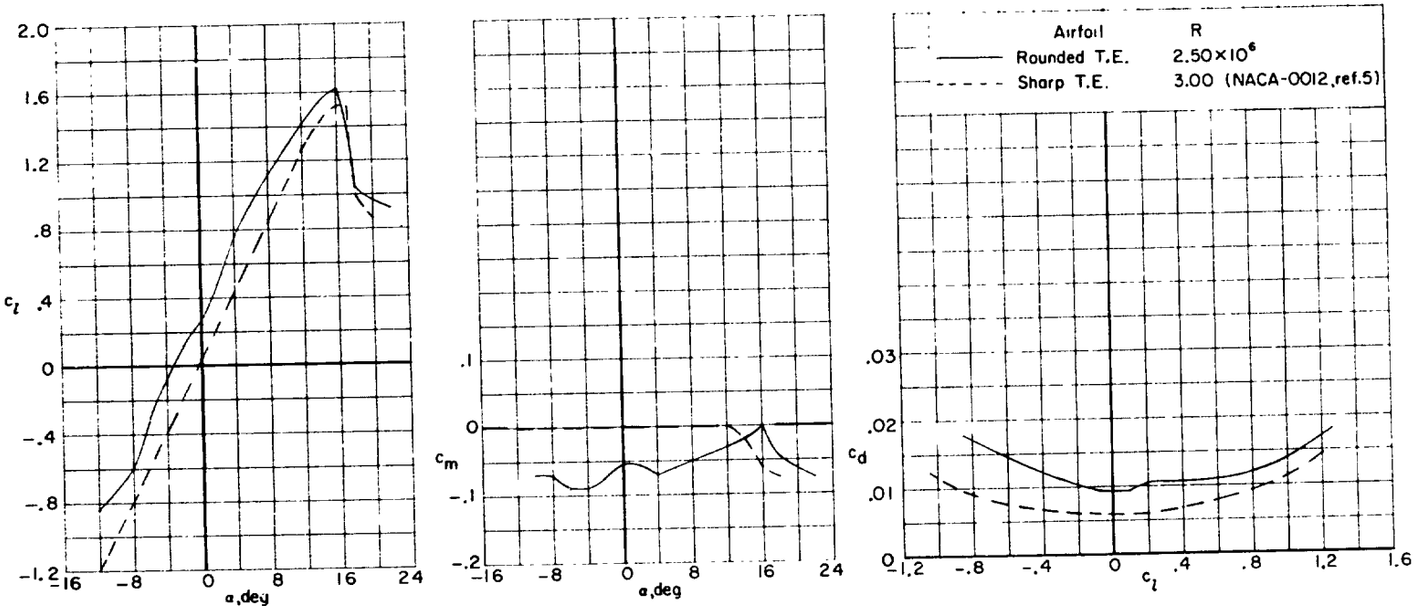

Figure 24.- 12-percent-thick airfoil section. Rounded and sharp trailing edges; forward flow; smooth model; $M \approx 0.16$.

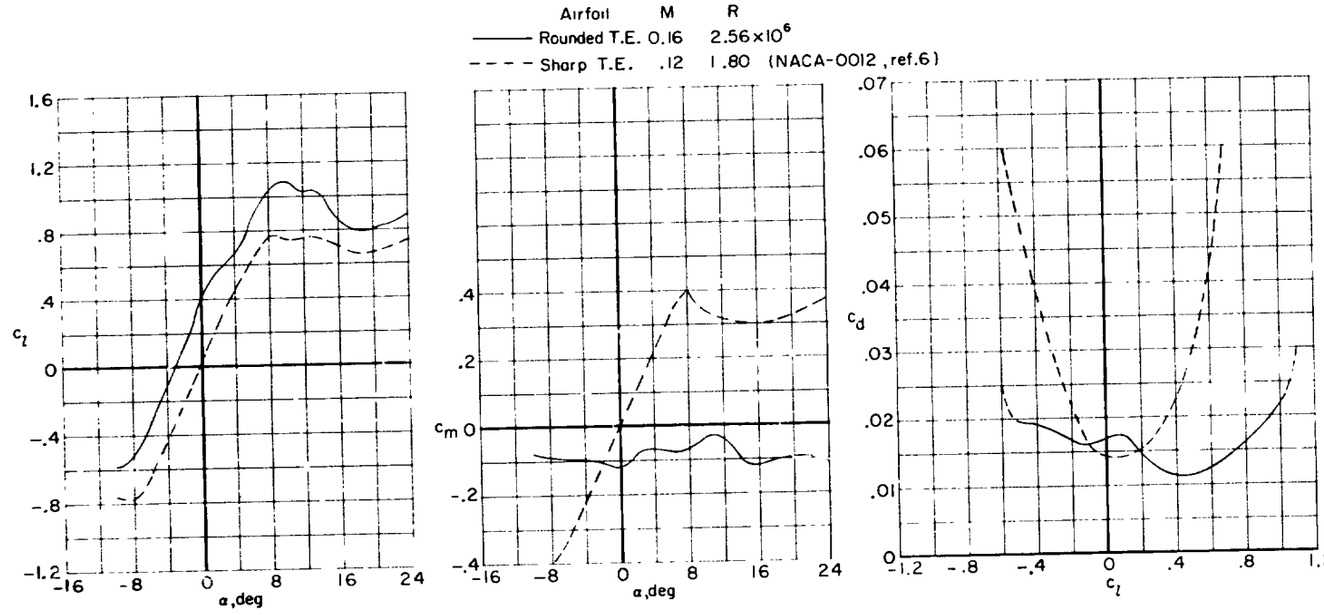

Figure 25.- 12-percent-thick airfoil section. Rounded and sharp trailing edges; reverse flow; smooth model.

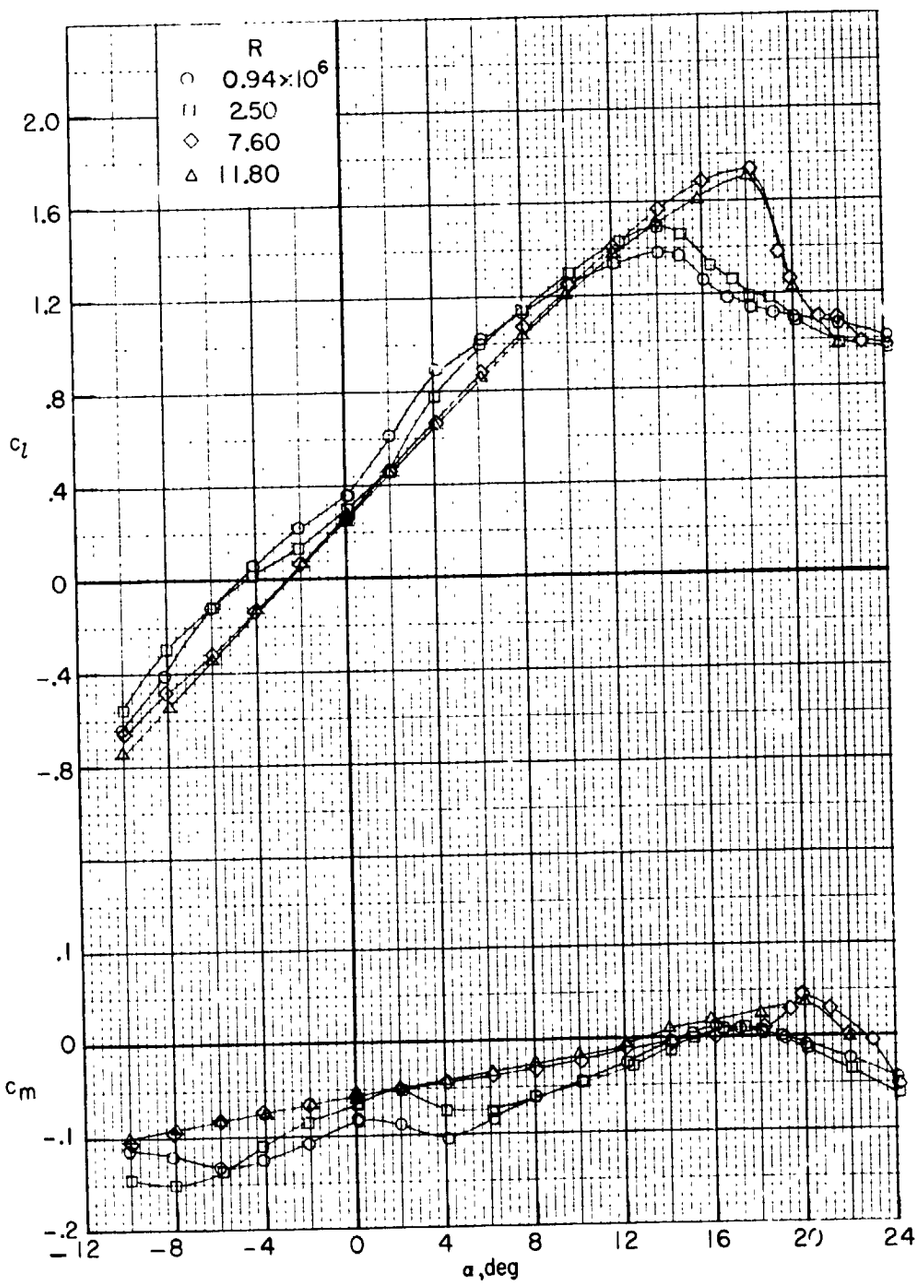

(a) c_l and c_m as a function of α.

Figure 26.- Effect of Reynolds number on section characteristics for 18-percent-thick airfoil with leading edge forward. M = 0.26; smooth model.

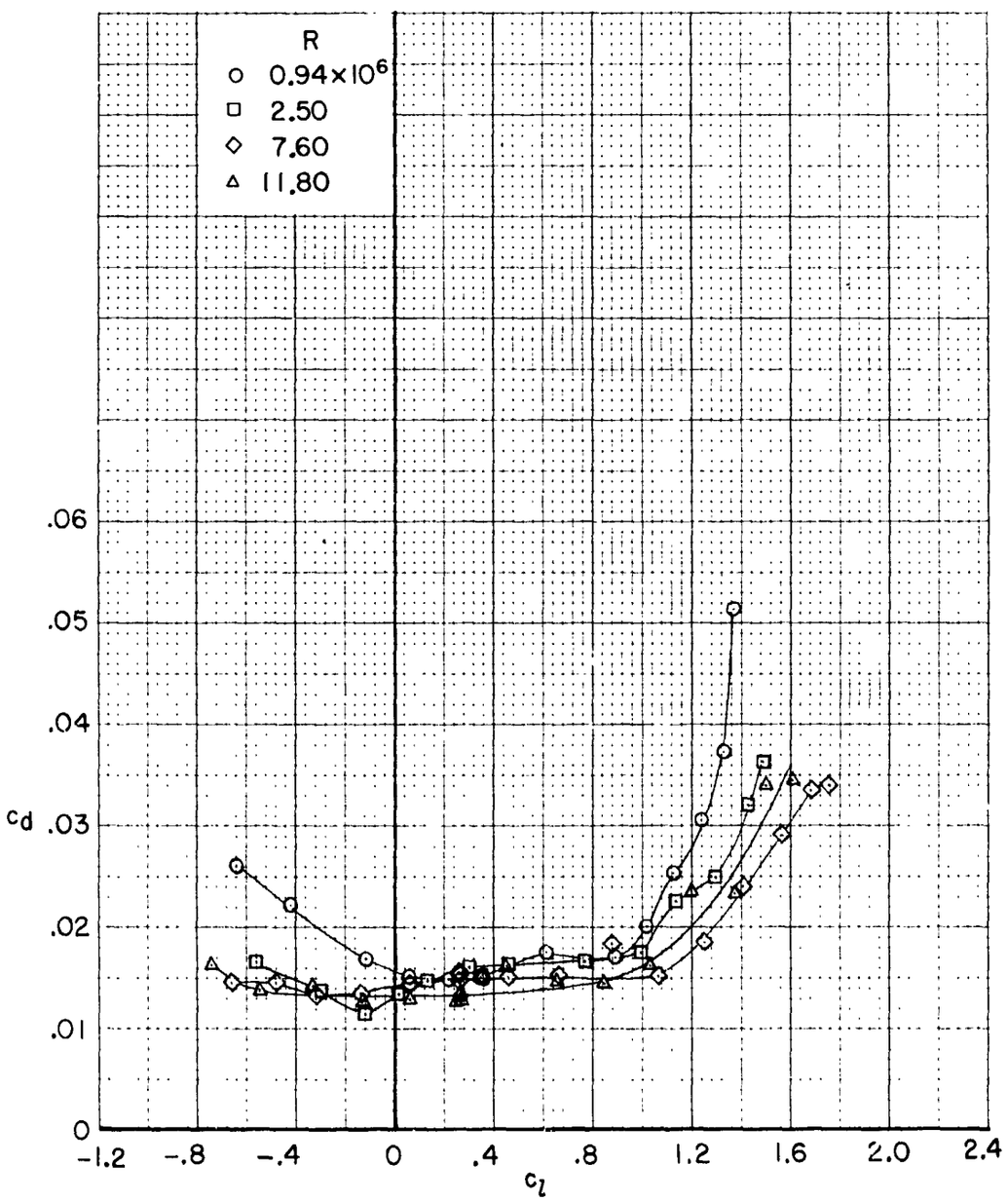

(b) c_d as a function of c_l.

Figure 26.- Concluded.

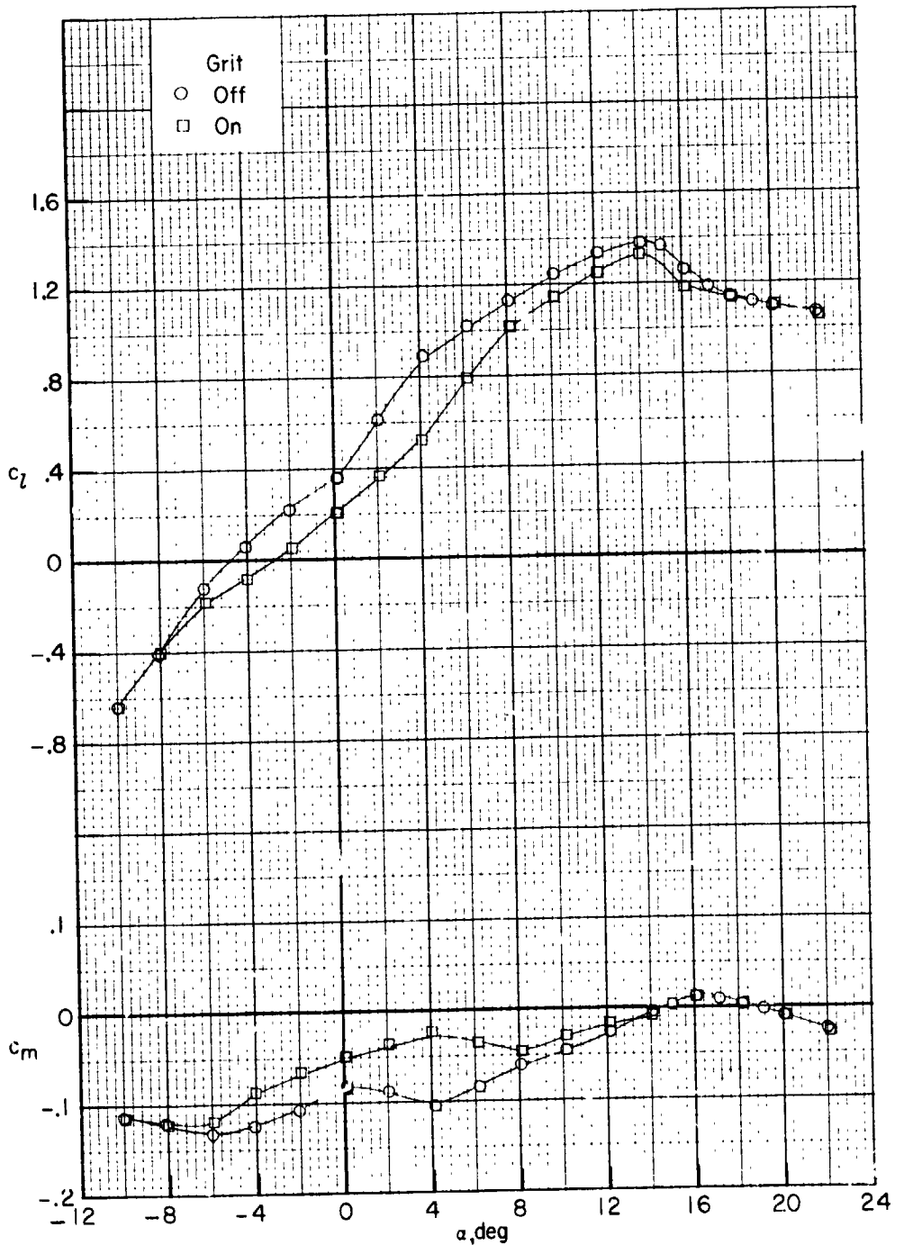

(a) $R = 0.94 \times 10^6$.

Figure 27.- Effect of roughness on section characteristics for 18-percent-thick airfoil with leading edge forward. Grit located at 0.05c; M = 0.26.

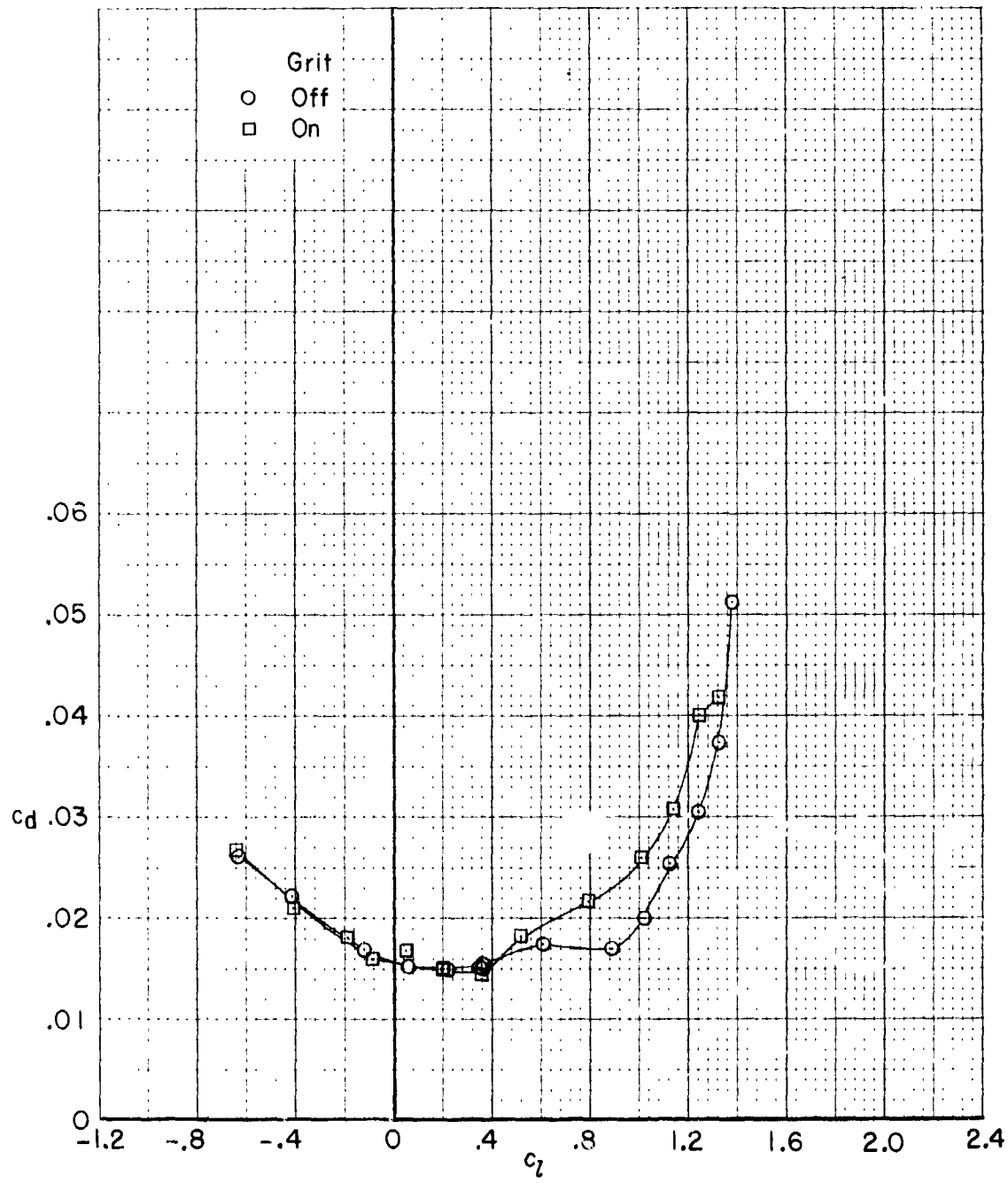

(a) R = 0.94×10^6. Concluded.

Figure 27.- Continued.

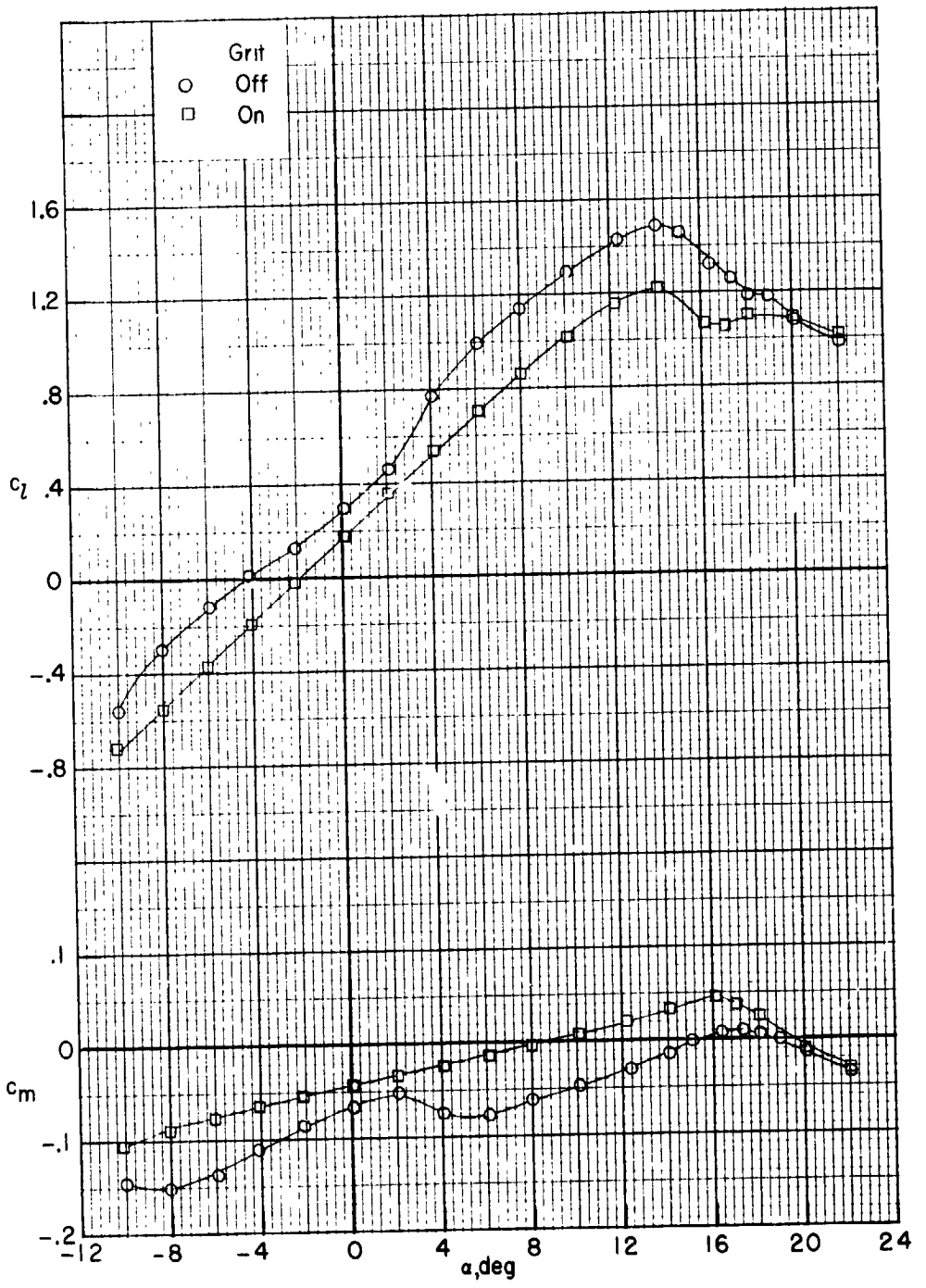

(b) $R = 2.50 \times 10^6$.

Figure 27.- Continued.

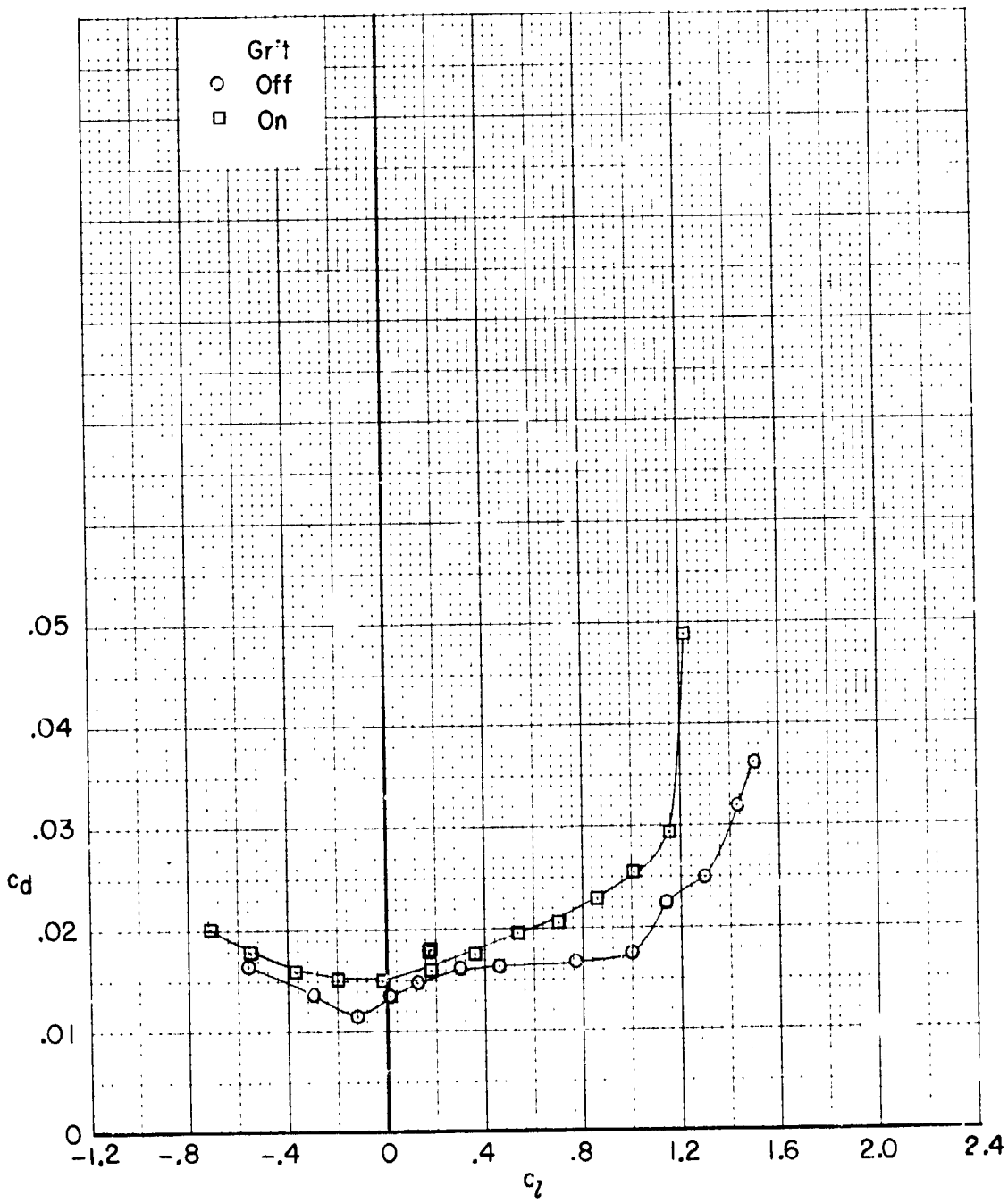

(b) $R = 2.50 \times 10^6$. Concluded.

Figure 27.- Concluded.

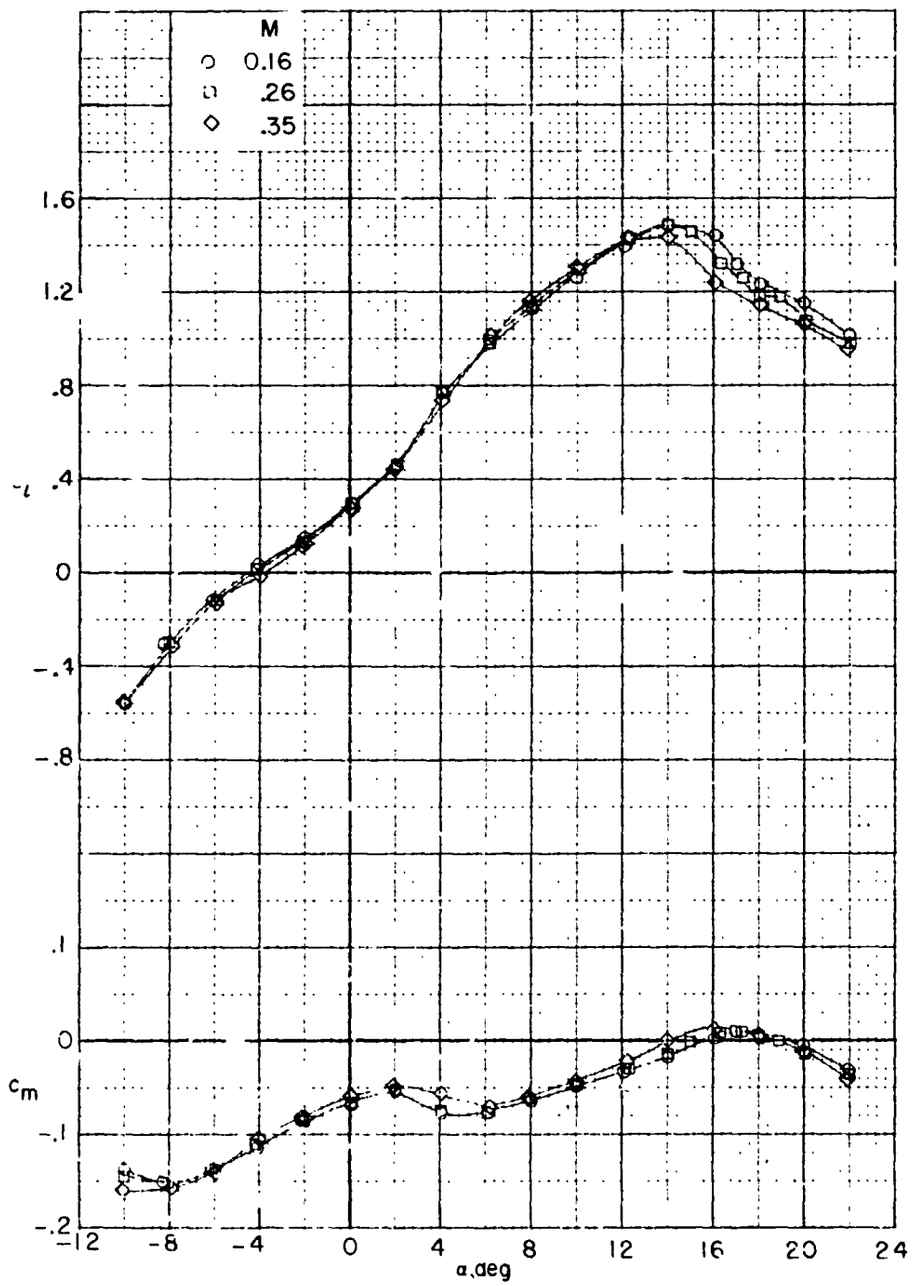

(a) c_l and c_m as a function of α.

Figure 28.- Effect of Mach number on section characteristics for 18-percent-thick airfoil with leading edge forward. $R = 2.50 \times 10^6$; smooth model.

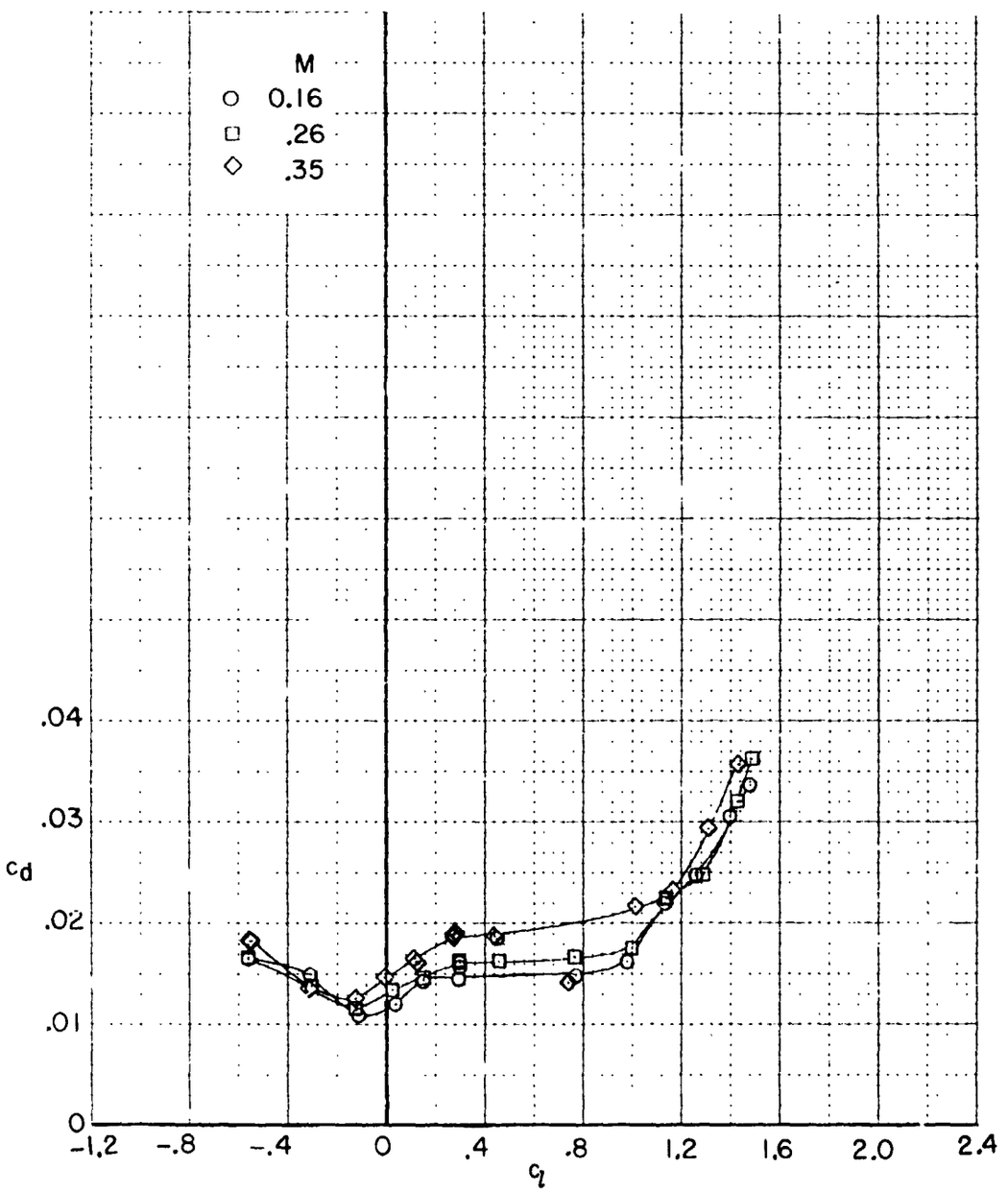

(b) c_d as a function of c_l.

Figure 28.- Concluded.

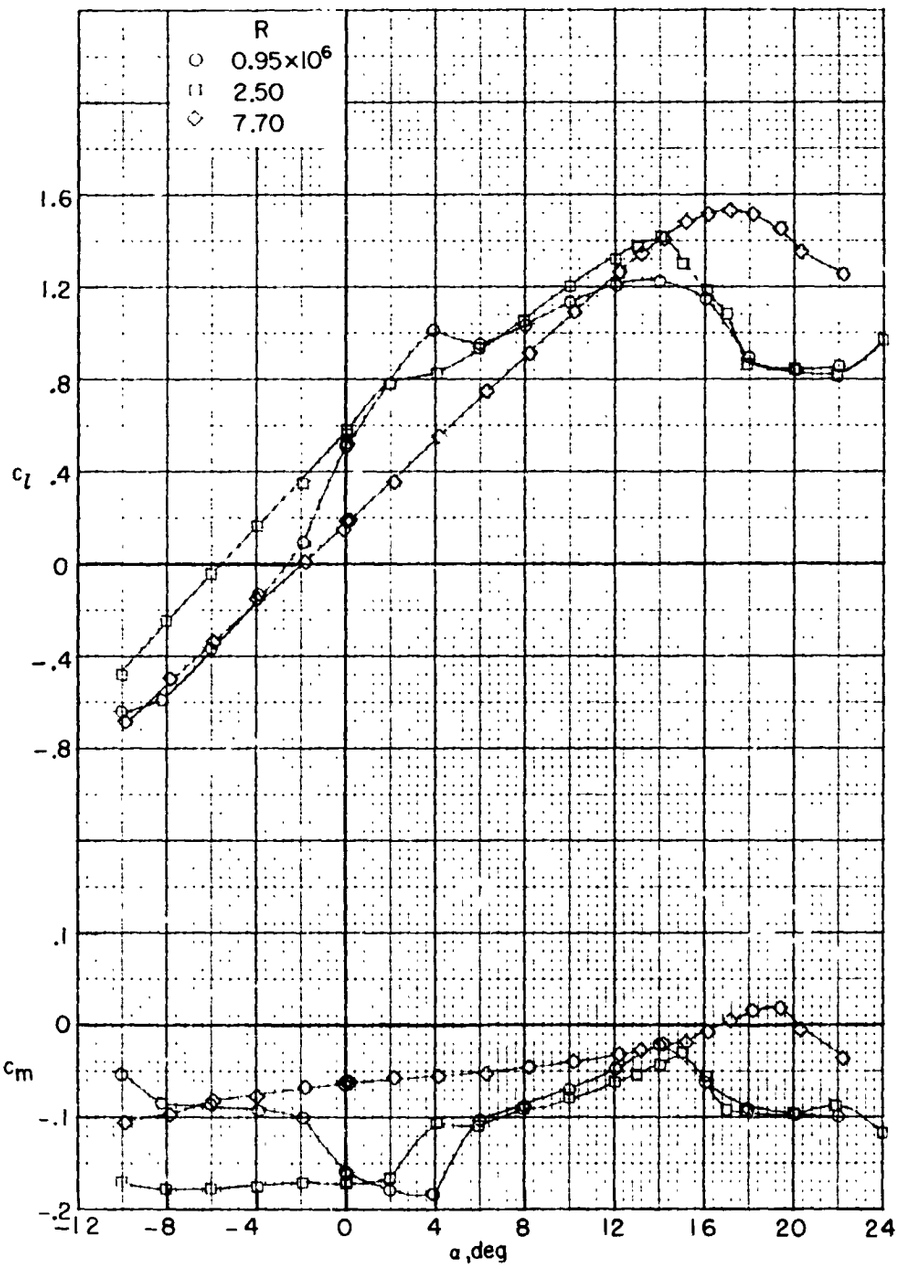

(a) c_l and c_m as a function of α.

Figure 29.- Effect of Reynolds number on section characteristics for 18-percent-thick airfoil with trailing edge forward. M = 0.26; smooth model.

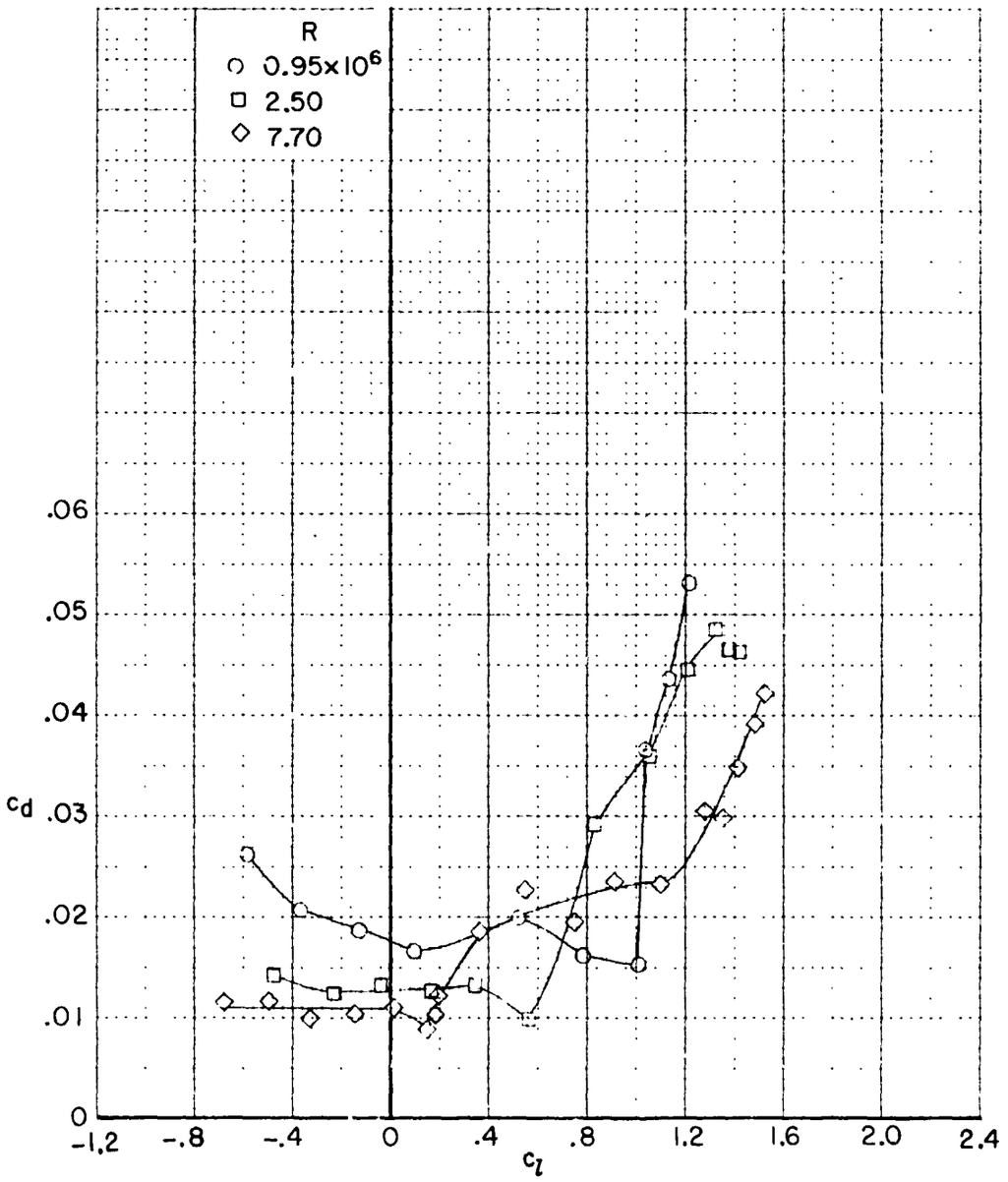

(b) c_d as a function of c_l.

Figure 29.- Concluded.

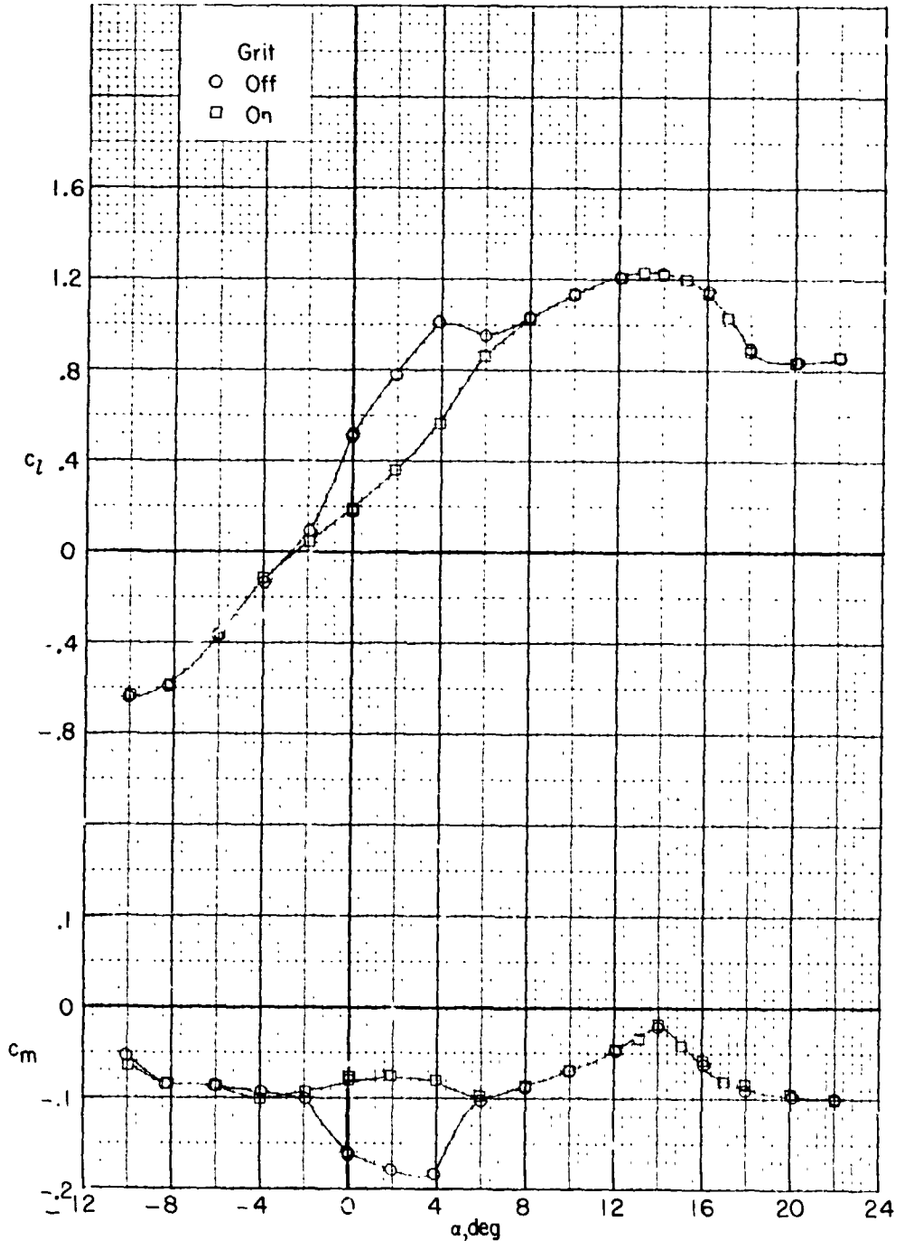

(a) $R = 0.95 \times 10^6$.

Figure 30.- Effect of roughness on section characteristics for 18-percent-thick airfoil with trailing edge forward. Grit located at 0.05c; M = 0.26.

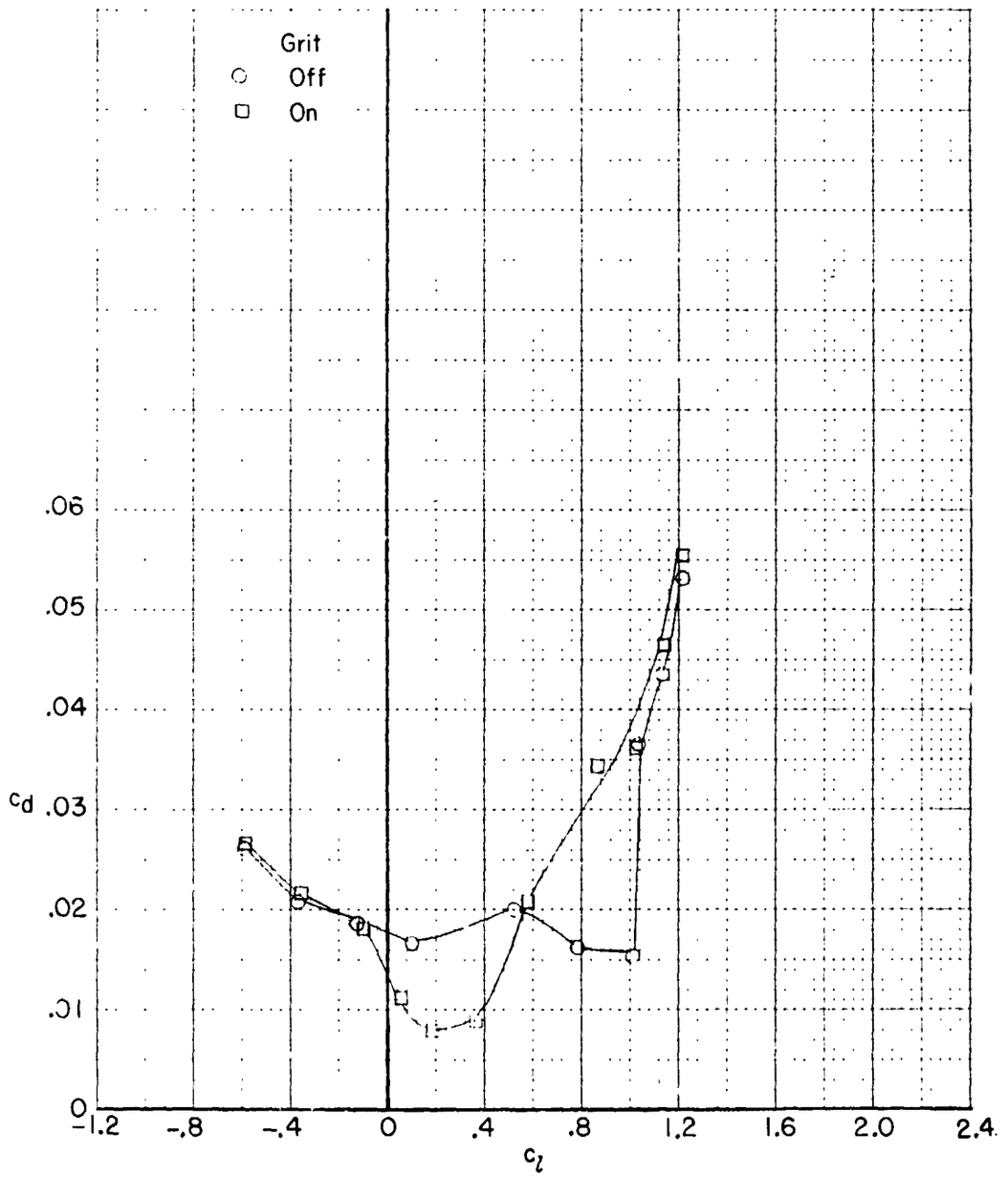

(a) R = 0.95×10^6. Concluded.

Figure 30.- Continued.

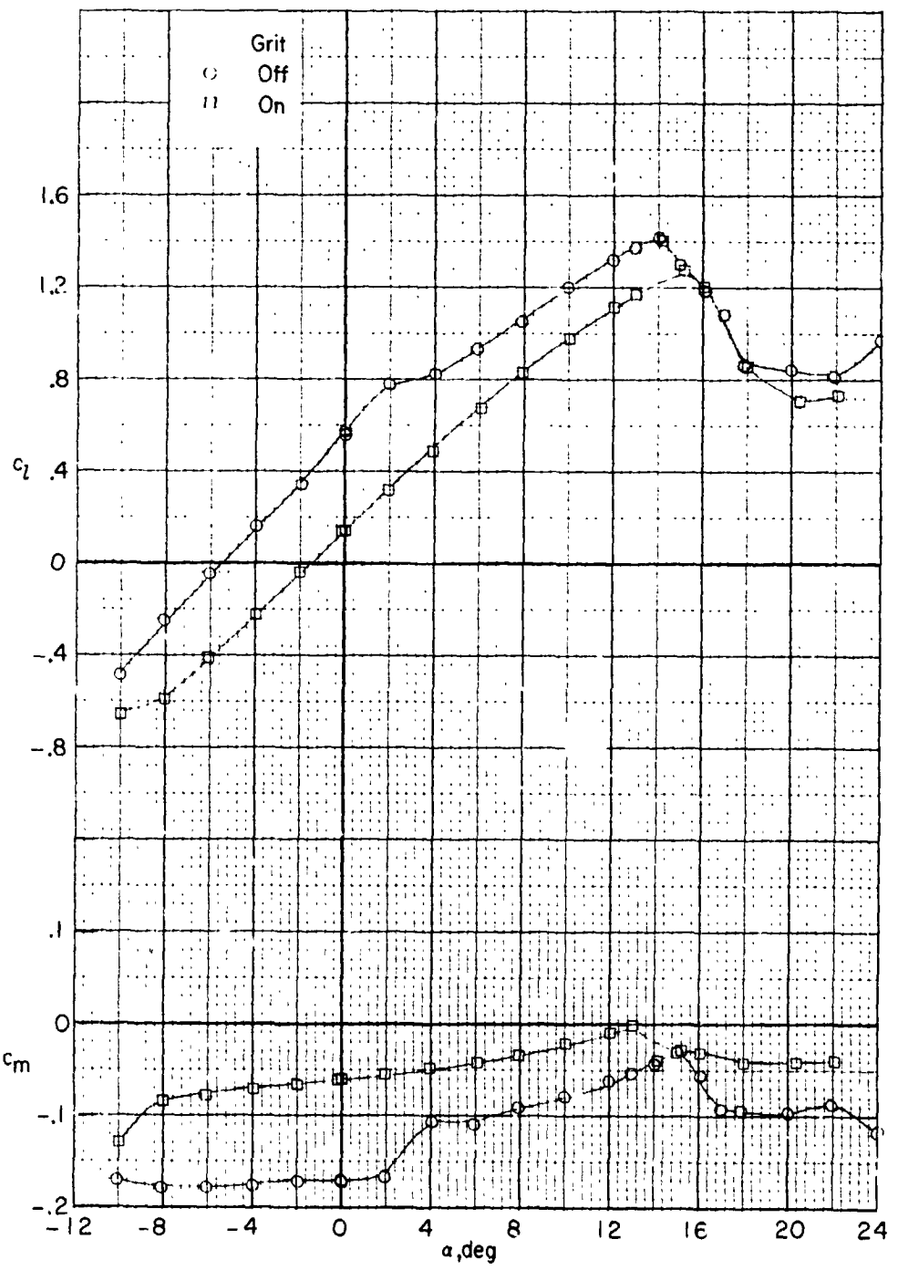

(b) $R = 2.50 \times 10^6$.

Figure 30.- Continued.

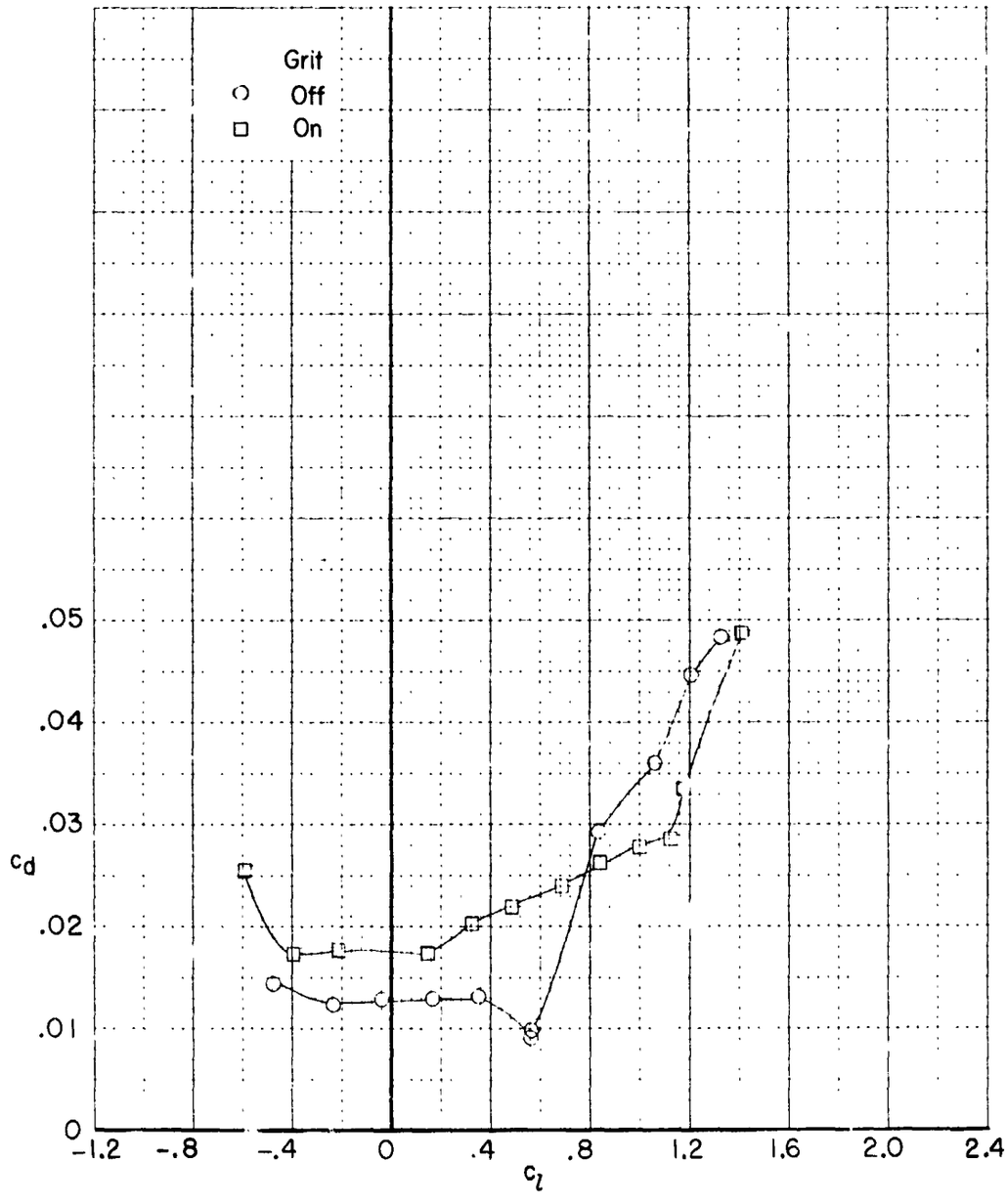

(b) R = 2.50×10^6. Concluded.

Figure 30.- Continued.

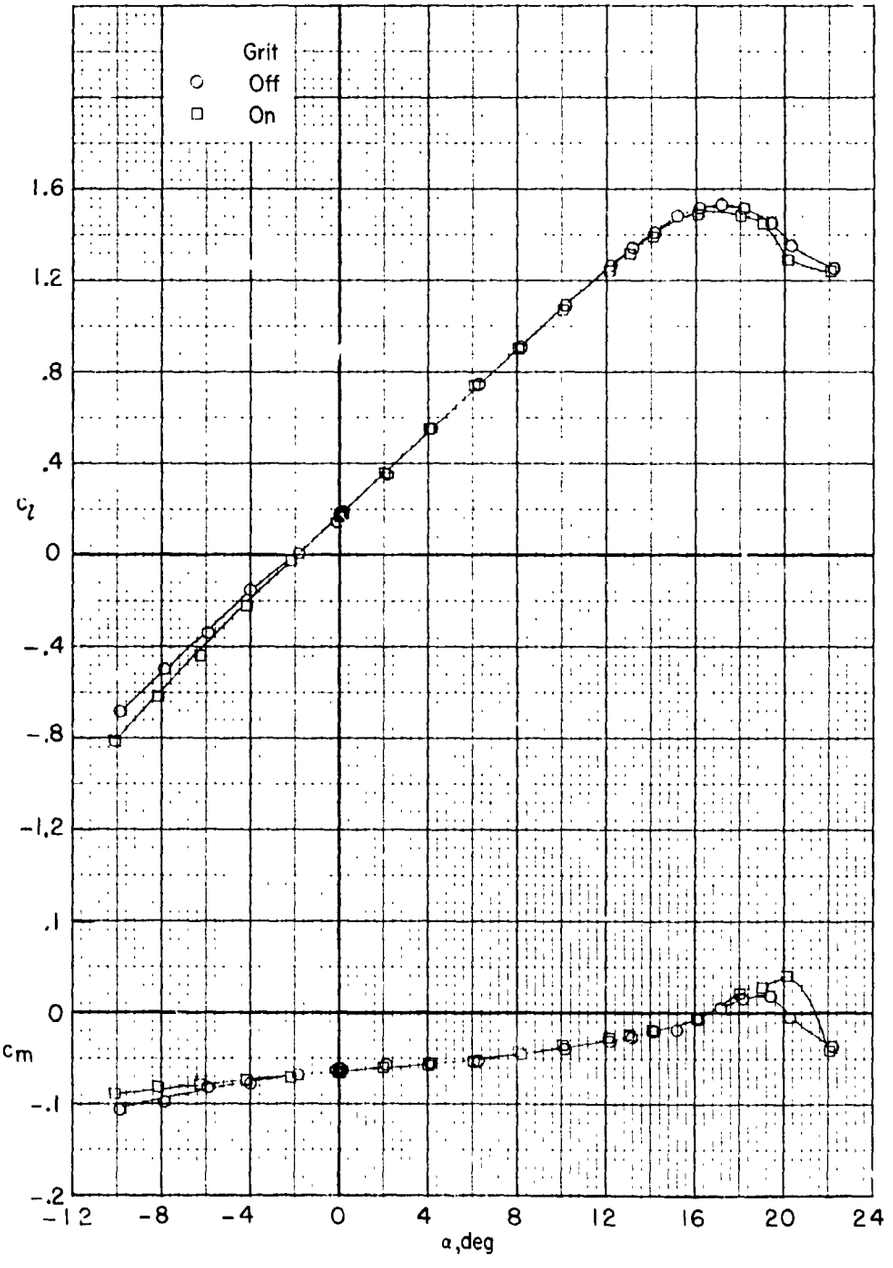

(c) R = 7.70×10^6.

Figure 30.- Continued.

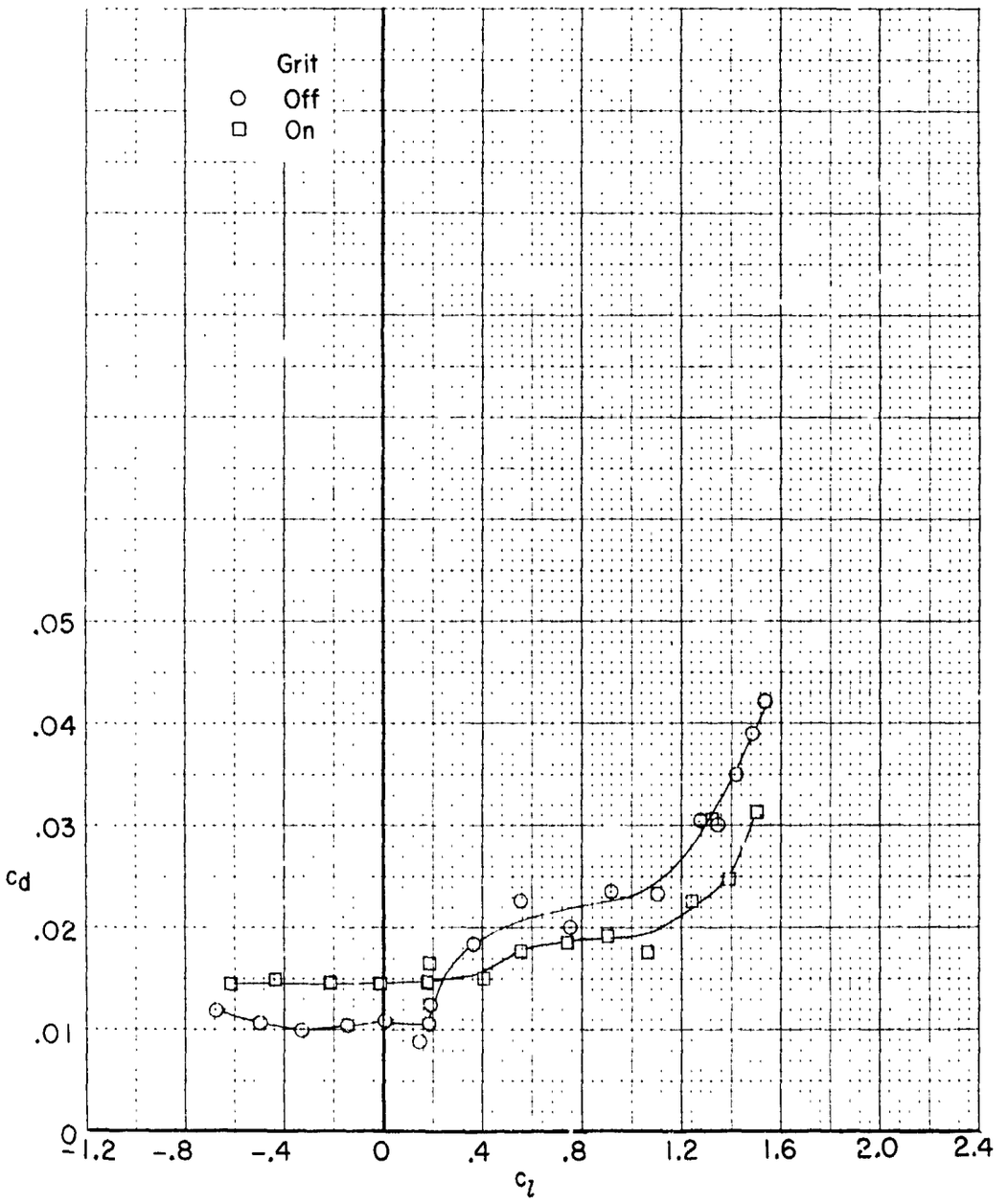

(c) R = 7.70×10^6. Concluded.

Figure 30.- Concluded.

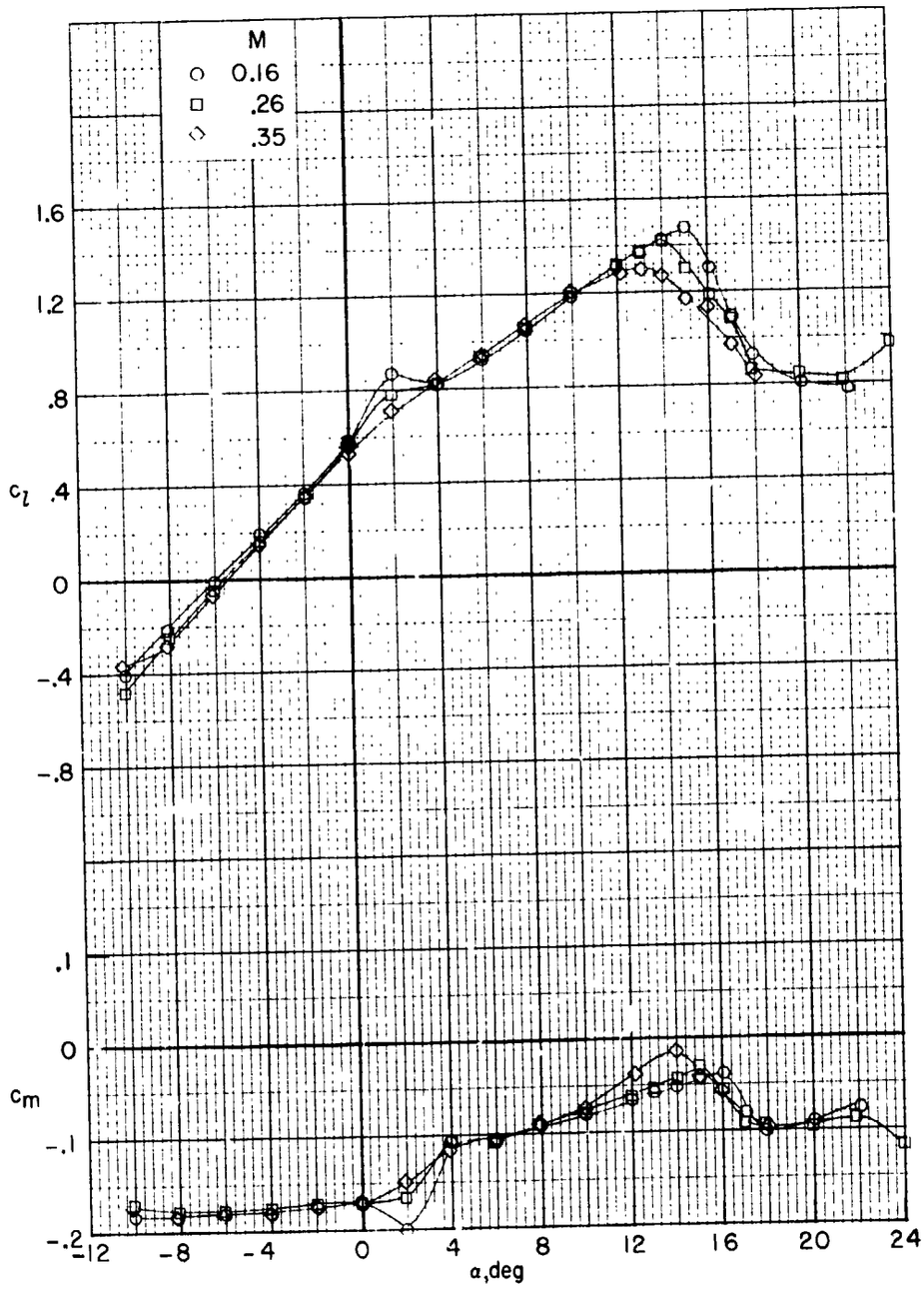

(a) c_l and c_m as a function of α.

Figure 31.- Effect of Mach number on section characteristics for 18-percent-thick airfoil with trailing edge forward. R = 2.50×10^6; smooth model.

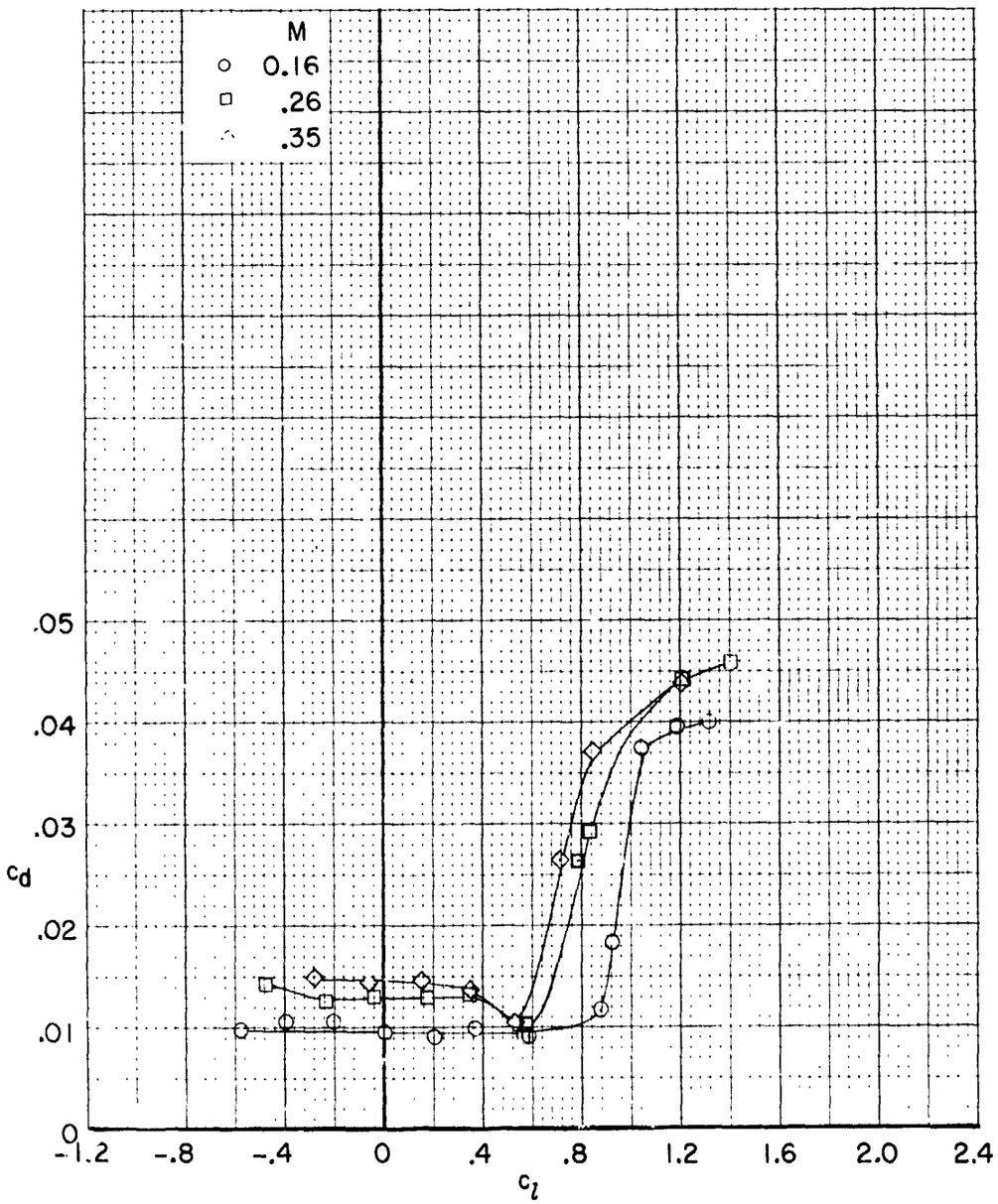

(b) c_d as a function of c_l.

Figure 31.- Concluded.

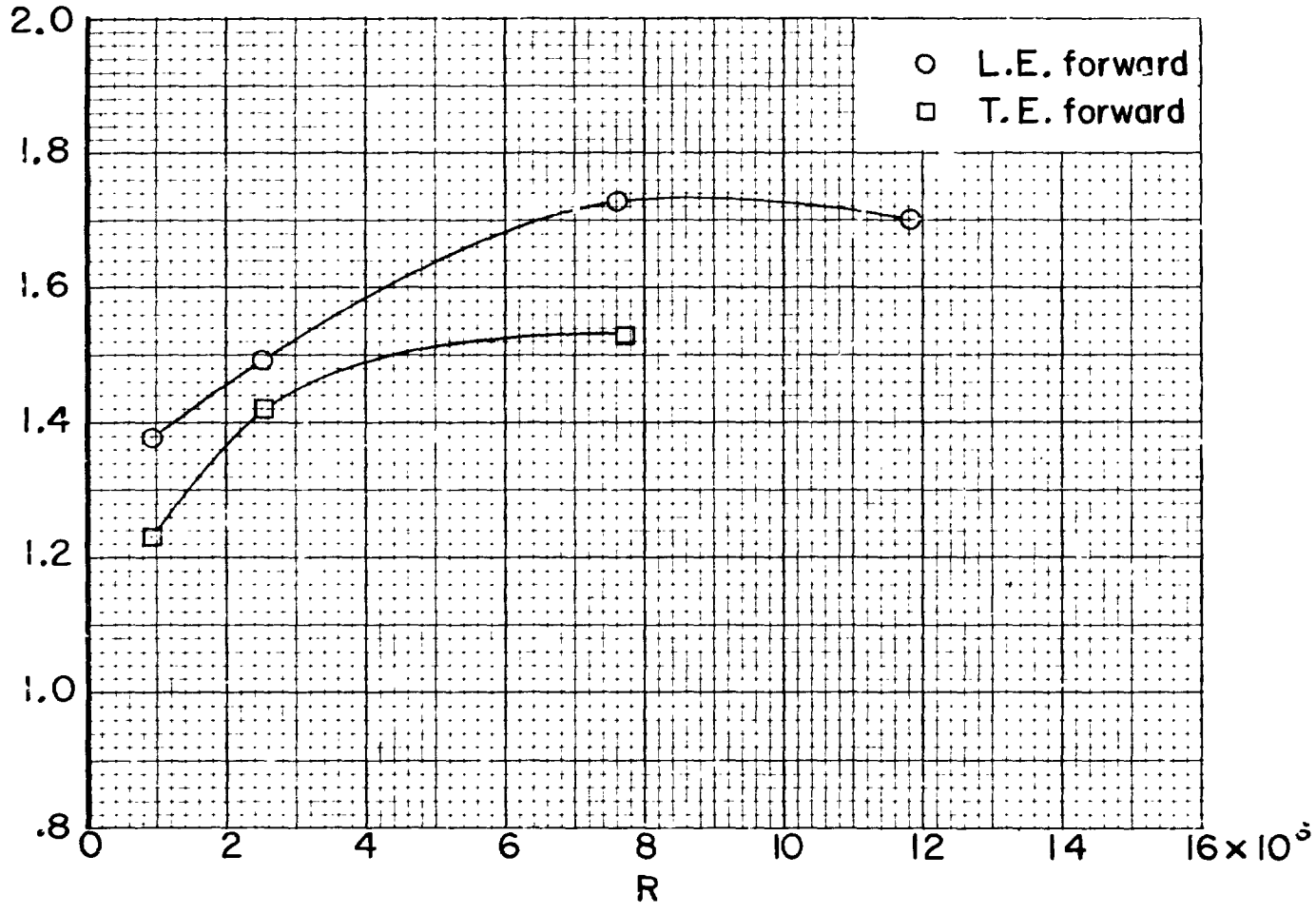

Figure 32.- Variation of maximum section lift coefficient with Reynolds number for 18-percent-thick airfoil. M = 0.26; smooth model.

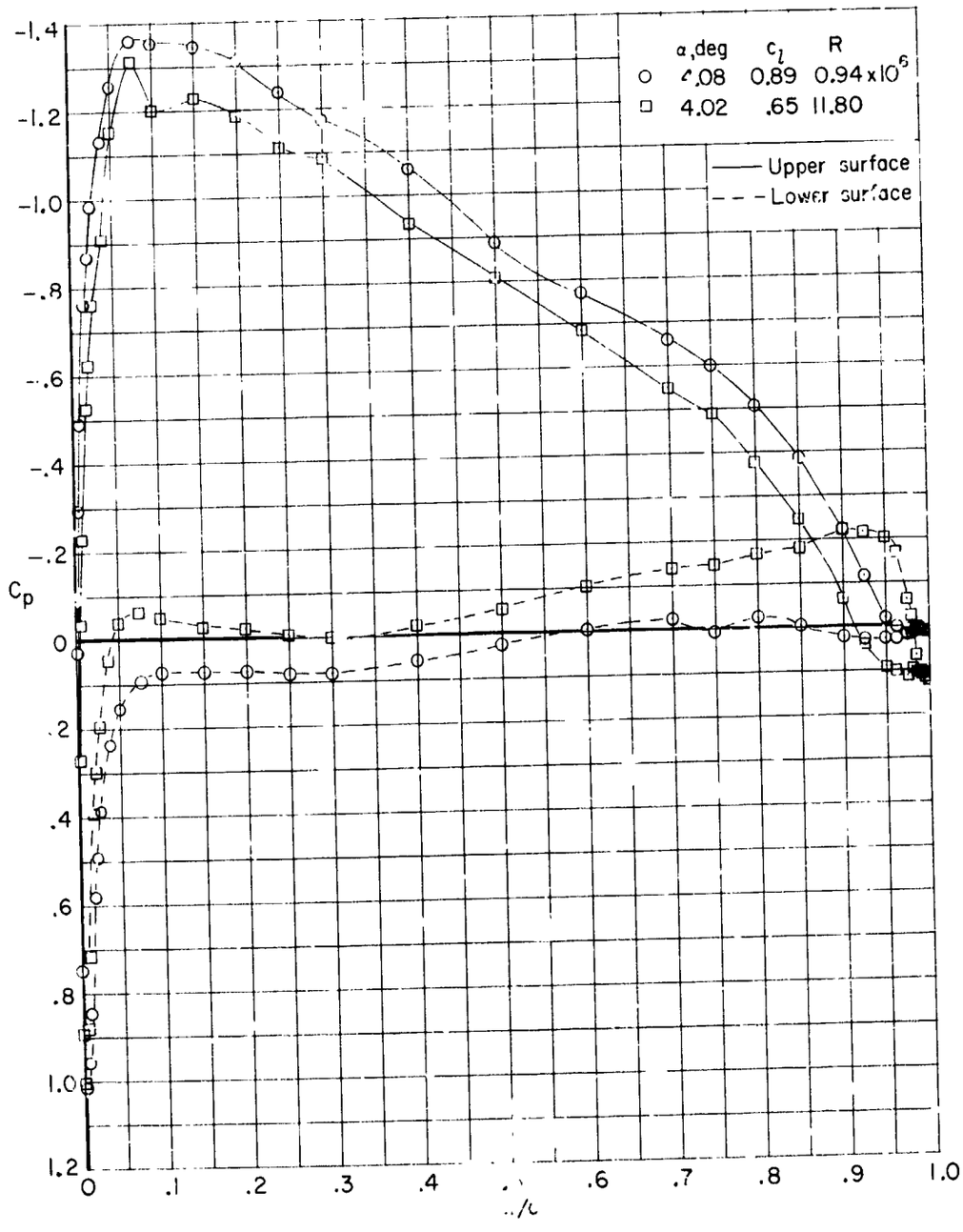

(a) Low angle of attack.

Figure 33.- Effect of Reynolds number on pressure distributions for 18-percent-thick airfoil with leading edge forward. M = 0.26; smooth model.

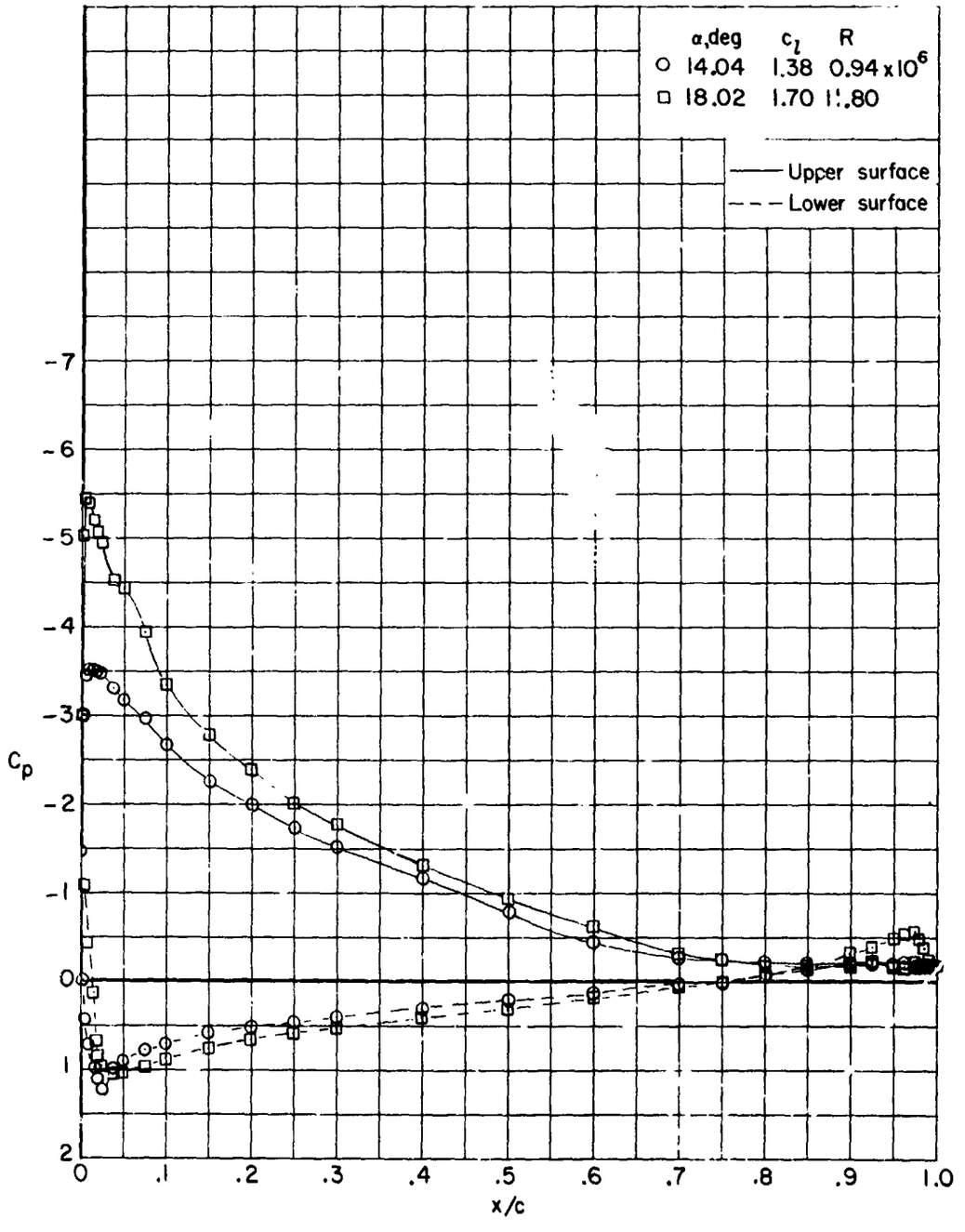

(b) High angle of attack.

Figure 33.- Concluded.

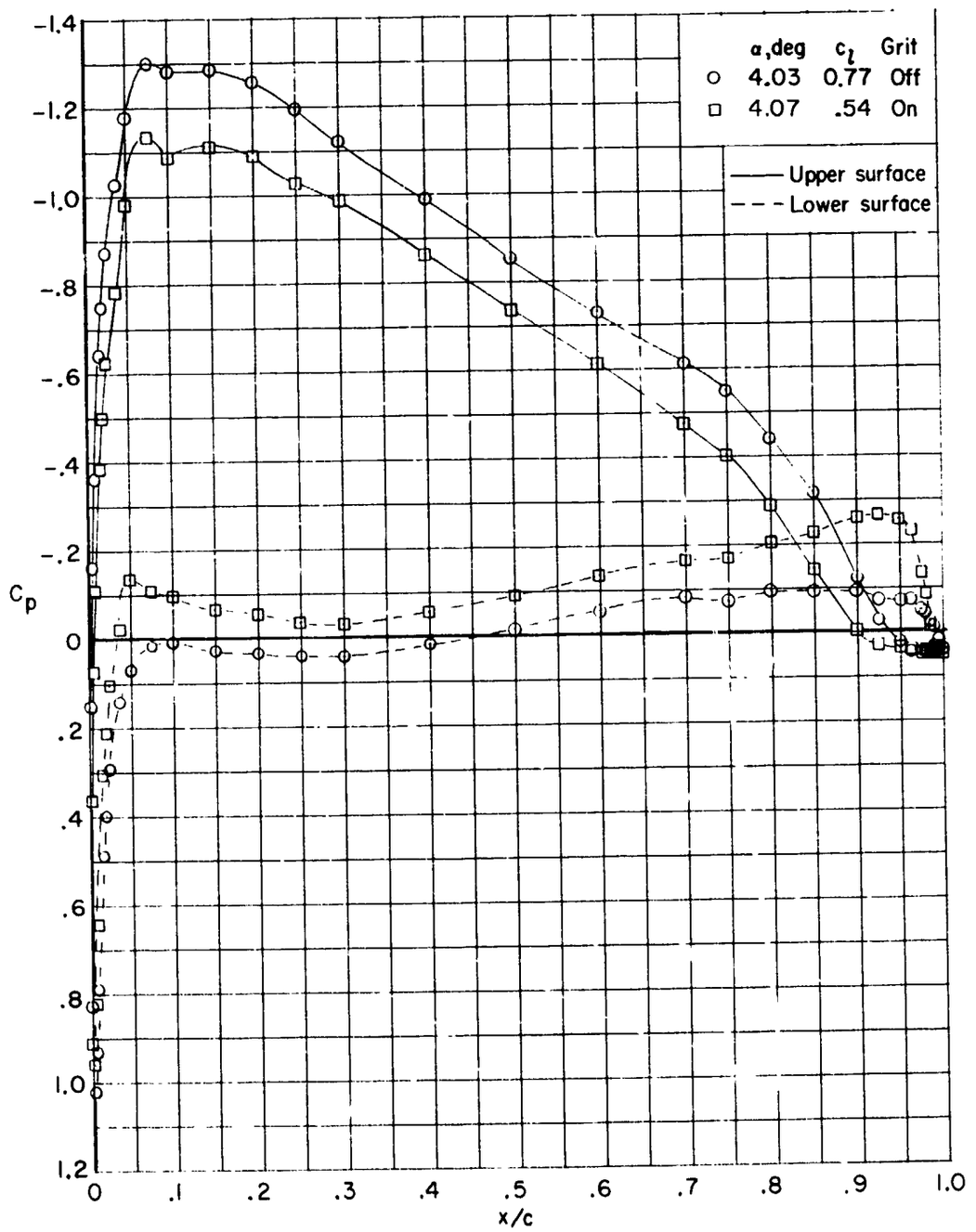

(a) Low angle of attack.

Figure 34.- Effect of roughness on pressure distributions for an 18-percent-thick airfoil with leading edge forward. $R = 2.50 \times 10^6$; grit located at 0.05c; M = 0.26.

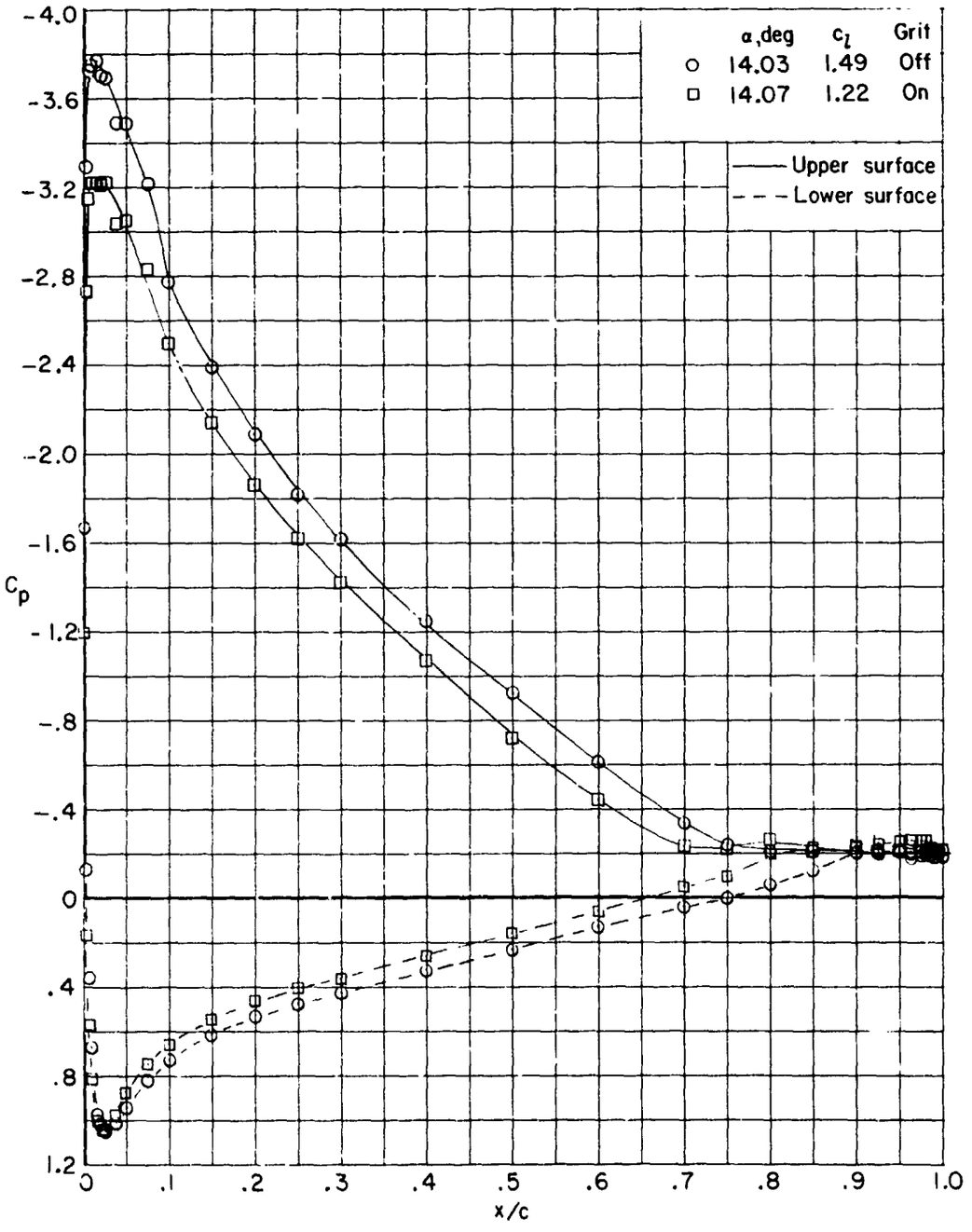

(b) High angle of attack.

Figure 34.- Concluded.

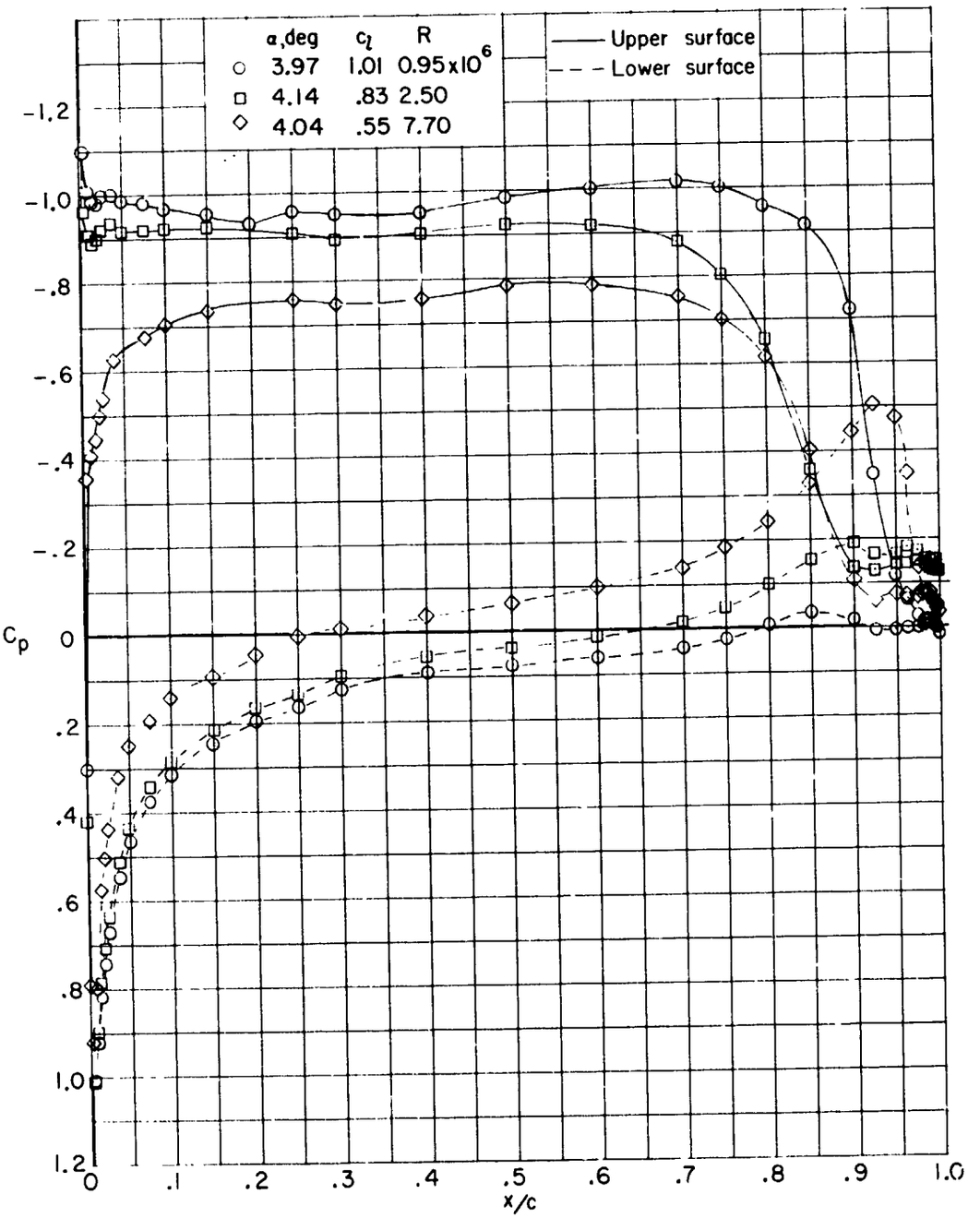

(a) Low angle of attack.

Figure 35.- Effect of Reynolds number on the pressure distributions for 18-percent-thick airfoil with trailing edge forward. M = 0.26; smooth model.

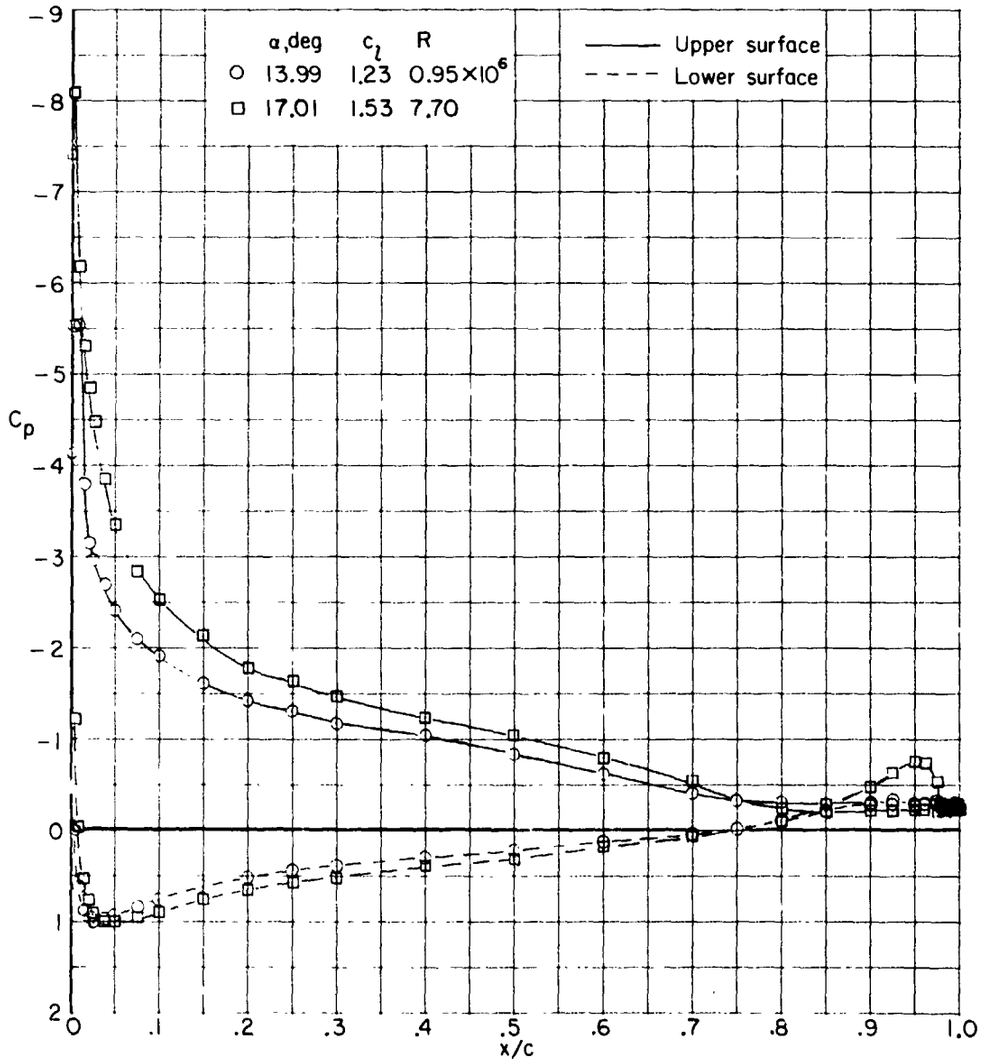

(b) High angle of attack.

Figure 35.- Concluded.

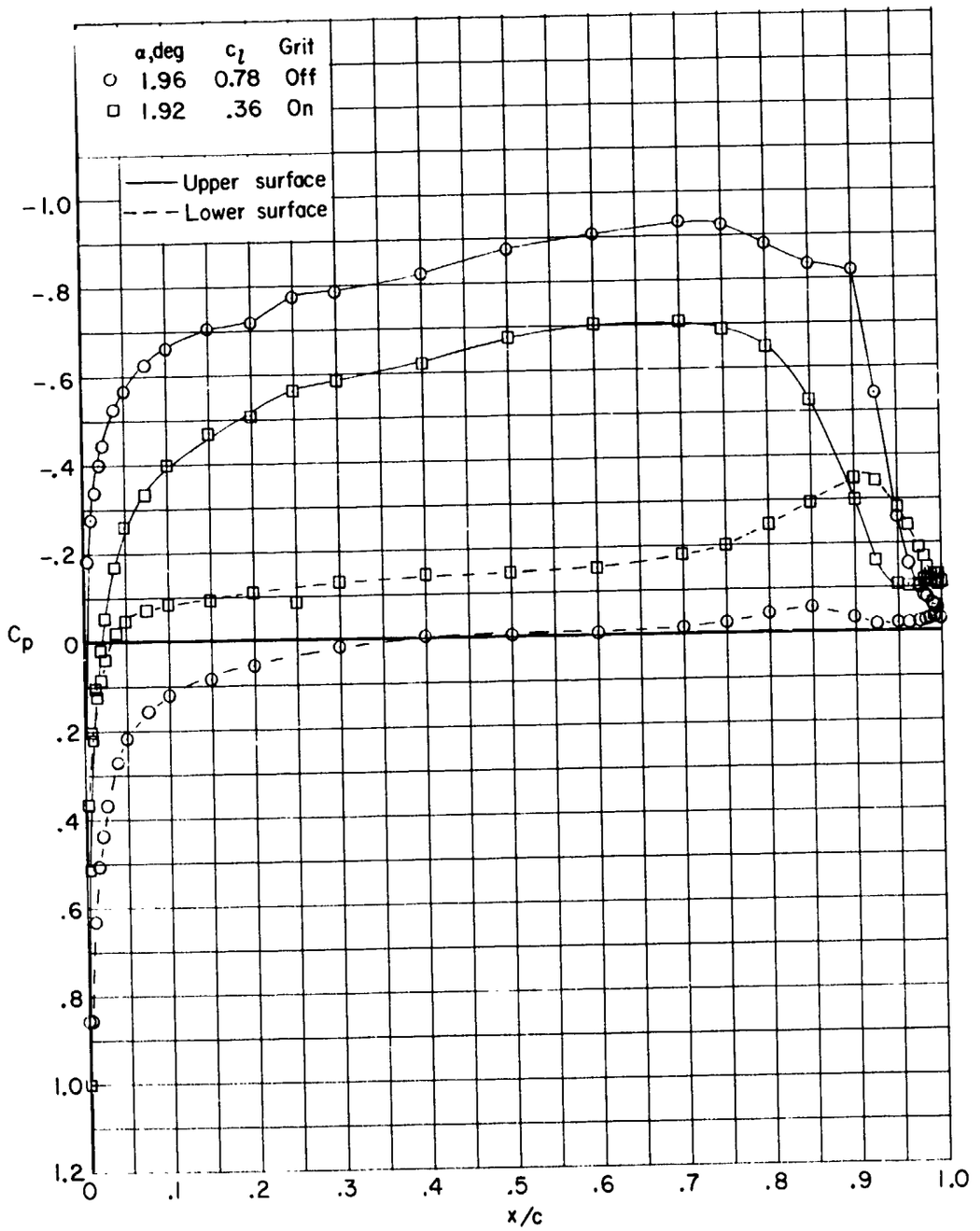

(a) Low angle of attack.

Figure 36.- Effect of roughness on pressure distributions for 18-percent-thick airfoil with trailing edge forward. $R = 0.95 \times 10^6$; grit located at 0.05c; $M = 0.26$.

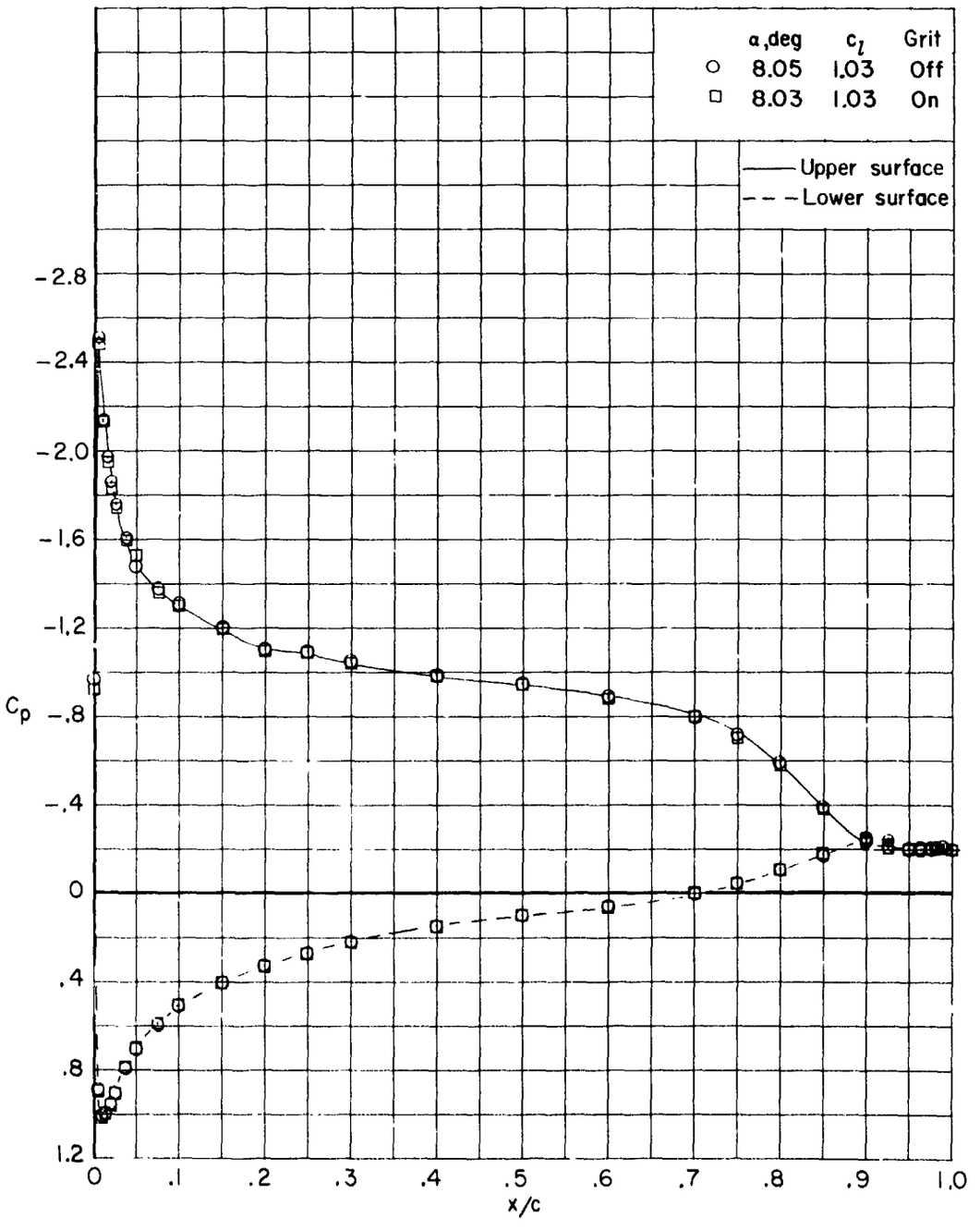

(b) High angle of attack.

Figure 36.- Concluded.

NASA-Langley, 1974 L-9327